

**The Genetic Analysis of Autophagy-Dependent Caspase
Activation in *Drosophila melanogaster***

By

Stephanie McMillan

A thesis
presented to the University of Waterloo
in fulfillment of the
thesis requirement for the degree of
Master of Science
in
Biology

Waterloo, Ontario, Canada, 2009
©Stephanie McMillan 2009

I hereby declare that I am the sole author of this thesis. This is a true copy of the thesis, including any required final revisions, as accepted by my examiners.

I understand that my thesis may be made electronically available to the public.

Abstract

During *Drosophila melanogaster* pupation, groups of undifferentiated adult cells proliferate and undergo regulated cell shape changes, while larval tissues are eliminated by programmed cell death (PCD). PCD is most commonly associated with apoptosis; however, a growing body of evidence suggests that autophagic cell death represents an alternative form of PCD. In some contexts autophagy can induce caspase-dependent PCD, but the regulatory pathways that link autophagy and apoptosis remain poorly understood. The overexpression of *Atg1^{6B}* induces autophagy-dependent caspase activation in the larval epidermis, and presumptive adult tissues. Also, the overexpression of *Atg1^{6B}*, in tissues specified by *pnrGAL4*, results in an adult cuticular phenotype that cannot be directly attributed to caspase activity. However, altering the level of *Atg1^{6B}* expression can modulate the adult cuticular phenotype. Therefore, the adult cuticular phenotype was used in a broad based genome-wide screen for dose-dependent modifiers of the regulation of autophagy. To date, 399 chromosomal deficiencies, representing approximately 92% of the 2nd and 3rd chromosomes, and 25 duplications have been tested. Consequently, 42 deficiencies have been identified as dominant enhancers of the *Atg1^{6B}* overexpression phenotype, 24 deficiencies have been identified as dominant modifiers, and 13 deficiencies have been identified as dominant suppressors. Further genetic analysis of these interacting deficiencies was carried out to initiate the process of identifying individual loci associated with the dose-sensitive modification of the *Atg1^{6B}* overexpression phenotype. It is hoped that the identification of these genes will elucidate the genetic pathways regulating autophagy and the autophagic induction of caspase activity.

Acknowledgments

I would like to express my profound gratitude to my supervisor, Dr. Bruce H. Reed, for his supervision, encouragement, and useful suggestions throughout my project. Bruce's extensive knowledge and guidance enabled me to complete my work successfully. Thank you for allowing me to be a part of your lab; it has been a great 4 years. I am also highly thankful to my committee members, Dr. Bernard Duncker and Dr. Niels Bols for their valuable suggestions throughout this study.

I would also like to thank past and present members of the Reed Lab. In particular, I would like to thank Roopali Chaudhary for her "mind-blasting" friendship and making me laugh during those stressful times. I would also like to thank Nilufar Mohseni for her friendship and advice.

I am as ever, especially indebted to my parents, Neil and Kathryn McMillan, for their love, support, and financial assistance throughout my studies. Also, I would like to thank my sister, Victoria McMillan, for making me laugh during times of frustration. Finally, I would like to express a big "Thank-you" to Paul McKay for his love and support.

Table of Contents

List of Figures	viii
List of Tables	x
List of Abbreviations	xi
Chapter 1. Introduction	1
1.1 Programmed Cell Death	1
1.1.1 Apoptosis	1
1.1.2 Autophagy	3
1.1.2.1 The Process of Autophagosome Formation: An Overview.....	4
1.1.2.2 Atg1 Is A Key Regulator of Autophagy.....	5
1.1.2.3 Autophagy and Cell Survival.	6
1.1.2.4 Autophagic Cell Death.....	7
1.1.2.5 Autophagy-Dependent Caspase Activity	10
1.1.2.6 Interpretation: Autophagic Cell Death and Autophagy-Dependent Caspase Activation	12
1.1.2.7 Why Study Autophagy in <i>Drosophila melanogaster</i> ?	12
1.2 Main Experimental Objectives:	13
Chapter 2. Materials and Methods	14
2.1 Fly Strains and Handling	15
2.2 GAL4-UAS Inducible Gene Expression System	15
2.3 GAL80	16
2.3.1 GAL80 ^{ts}	16
2.3.2 GAL80 ^{ts} Experiment	16
2.4 Embryo Collection	17
2.5 Dechoriation	17
2.6 LysoTracker Staining	17
2.7 Live Imaging	18

2.7.1 Confocal Live Imaging.....	18
2.7.2 Stereomicroscopic Live Imaging:	18
2.8 Scanning Electron Microscopy.....	19
2.9 Screen for Chromosomal Regions that Dominantly Interact with <i>Atg1^{6B}</i>	20
2.10 Screen for loci that dominantly interact with <i>Atg1^{6B}</i>	20
2.11 Confirmation of Genetic Interactions <i>BsgRNAi⁴³³⁰⁷</i> and <i>EP(3)3614</i>	21
2.12 Wing Disc Dissection	22
Chapter 3. Methodologies For Evaluating Autophagy and Caspase Activity	23
3.1 PCD in the AS: Using LysoTracker To Evaluate Autophagy	24
3.1.1 LysoTracker: Visualizing Autophagy In The AS Of Control Embryos	24
3.1.2 LysoTracker: Visualizing Autophagy In Apoptotic Defective Backgrounds.....	28
3.1.3 LysoTracker: <i>Atg1</i> Overexpression Results In Increased Autophagy In The AS	34
3.1.4 LysoTracker: Constitutive Activation of $\Delta\alpha$ InR Decreases Autophagy In The AS.	34
3.2 Evaluating Caspase-Activity in Live Tissues Throughout Development	40
3.2.1 Evaluating Caspase Activity In The AS During Embryogenesis.....	40
3.2.2 Evaluating Caspase Activity In The Dorsal Third Instar Larval Epidermis	44
3.2.3 Apoliner: Evaluating Caspase Activity In The Third Instar Imaginal Wing Disc ..	48
3.3 mCherry: Evaluating Autophagy in Wing Discs Overexpressing <i>Atg1^{6B}</i>	49
3.4 Autophagy-Dependent Caspase Activation in Adult Cuticular Structures	54
3.5 Evaluating Autophagy Dependent Caspase-Activity during Metamorphosis.....	60
3.5.1 Autophagy-Activated Apoptosis During Pharate Adult Formation	60
Chapter 4. Genetic Screen	65
4.1 Genetic Screen for Chromosomal Regions that Dominantly Interact with <i>Atg1^{6B}</i>	67
4.2 Target Interacting Regions that dominantly interact with <i>Atg1^{6B}</i>	91
4.3 Screen For Loci That Dominantly Interact With <i>Atg1^{6B}</i>	93
Chapter 5. Discussion.....	98
5.1 Evaluating Autophagy Dependent Caspase Activation in the AS	99
5.2 Autophagy Dependent Caspase Activation In the Third Instar Wing Disc and Larval Epidermis.....	101

5.3 Stereomicroscopic Live Imaging and Scanning Electron Microscopy: Analyzing Cell Death During Metamorphosis	102
5.4 Genetic Screen	105
Conclusion.....	107
Chapter 6. Future Directions	108
6.1 Caspase-Activation and Autophagosome Formation In The Wing Disc.....	109
6.2 Candidate Deficiencies and Loci Within Targeted Interacting Regions.....	110
Appendices	111
Appendix A. General Background	111
A.1 The <i>Drosophila</i> Life Cycle.....	112
A.2 The Amnioserosa - Embryogenesis	115
A.3 Thorax Closure	117
A.4 Abdomen Development	121
Appendix B. Crossing Schemes.....	123
Appendix C. GAL80 ^{ts} Experiment.....	130
C.1 Gal80 ^{ts} : Evaluation of <i>Atg1</i> ^{6B} Overexpression During Development	132
C.2 Evaluation of <i>Atg1</i> Overexpression During Development using GAL80 ^{ts}	136
C.3 Increasing the Resolution of the GAL80 ^{ts} Experiment	137
Appendix D. Stocks Used in Genetic Screen.....	140
Appendix E. Letters of Copyright Permission	163
References	166

List of Figures

Figure 1.1: The Apoptosis PCD Pathway in <i>Drosophila melanogaster</i>	2
Figure 1.2: Steps In The Formation Of The Autophagosome and Autolysosome	4
Figure 1.3: Nutrient and Developmental Control of Autophagy.....	6
Figure 1.4: Model Diagram Of Autophagic Cell Death	8
Figure 1.5: Model Diagram Of Autophagy-Dependent Caspase Activation	10
Figure 3.1: Confocal Micrographs: LysoTracker Stained Control Embryos.....	26
Figure 3.2: Confocal Micrographs: LysoTracker Stained Caspase-Inhibited Embryos.....	30
Figure 3.3: Confocal Micrographs: LysoTracker Stained <i>HRG</i> Deficient Embryo	32
Figure 3.4: Confocal Micrographs: LysoTracker Stained <i>Atg1^{6B}</i> Overexpressing Embryo.....	36
Figure 3.5: Confocal Micrographs: LysoTracker Stained $\Delta\alpha InR$ Expressing Embryo	38
Figure 3.6: Confocal Timelapse Imaging: Embryos Expressing <i>Apoliner</i> in the AS	42
Figure 3.7: Stereomicroscopic Images: Larvae expressing <i>UAS-Apoliner</i> & <i>UAS-GFP^{nls}</i>	46
Figure 3.8: Confocal Micrographs: Wing Discs Expressing <i>UAS-Apoliner</i>	50
Figure 3.9: Confocal Micrographs: Wing Discs Expressing <i>UAS-mCherry-DrAtg8a</i>	52
Figure 3.10: Scanning Electron Micrographs: Control Adult cuticular Structures	56
Figure 3.11: Scanning Electron Micrographs: Adult cuticular Structures	58
Figure 3.12: Stereomicroscopic Live Imaging Of Four <i>Drosophila</i> Pupae	63
Figure 4.1: Diagram defining the term "Interacting Regions"	70
Figure 4.2: 2L Deficiency and Duplication Map.....	73
Figure 4.3: 2R Deficiency and Duplication Map	75
Figure 4.4: 3L Deficiency and Duplication Map.....	77
Figure 4.5: 3R Deficiency and Duplication Map	79

Figure 4.6: Stereomicroscopic Imaging of *Drosophila* expressing *UAS-BsgRNAi*⁴³³⁰⁷ 89

Figure A.1: The Life Cycle of *Drosophila melanogaster*. 113

Figure A.2: Dorsal Closure During Embryogenesis..... 116

Figure A.3: Thorax Closure..... 119

Figure A.4: Abdomen Development 122

Figure B.1: Crossing Scheme: *pnrGal4* + *UAS-GFP^{nl5}/TM3,Sb* Stock 125

Figure B.2: Crossing Scheme: *pnrGAL4+UAS-Atg1^{6B}/TM6,Tb, [GAL80]* Stock..... 127

Figure B.3: Crossing scheme *pnrGAL4* + *UAS-Atg1^{6B}* + *UAS-Apoliner/TM6[GAL80],Tb* and *pnrGal4+UAS-Apoliner/TM3,Sb* Stocks..... 129

Figure C.1: Summary Tables: GAL80(ts) Experiment 134

Figure C.2: Summary Diagram: The Future GAL80(ts) Experiment 138

List of Tables

Table 4.1: Criteria For The Classification Of Phenotypes During The Genetic Screen.....	69
Table 4.2: Summary Table Illustrating The Results Of The Genetic Screen.	72
Table 4.3: Strong Suppressors Identified In The Genetic Screen.....	81
Table 4.4: Moderate Suppressors Identified In The Genetic Screen.	82
Table 4.5: Strong Enhancers Identified In The Genetic Screen	83
Table 4.6: Moderate Enhancers Identified In The Genetic Screen.....	84
Table 4.7: Undefined Modifiers Identified In The Genetic Screen	85
Table 4.8: Target Interacting Regions and Associated Information.....	92
Table 4.9: Alleles Of Candidate Genes Tested In The Genetic Screen.....	95
Table D.1: Deficiency (2L) Stocks	141
Table D.2: Deficiency (2R) Stocks.....	147
Table D.3: Deficiency (3L) Stocks	151
Table D.4: Deficiency (3R) Stocks.....	156
Table D.5: Duplications Located On The 2 nd Chromosome.....	161
Table D.6: Duplications Located On The 3 rd Chromosome	162

List of Abbreviations

2L	Left arm of the Second Chromosome
2R	Right arm of the Second Chromosome
3L	Left arm of the Third Chromosome
3R	Right arm of the Third Chromosome
AEL	After Egg Lay
Akt/PKB	Protein Kinase B
Apc	Adenomatous polyposis coli protein
AS	Amnioserosa
<i>Atg</i>	Autophagy Genes
<i>Bsg</i>	<i>Basigin</i>
DC	Dorsal Closure
<i>DIAP</i>	<i>Drosophila Inhibitor of Apoptosis Protein</i>
<i>Df</i>	<i>Deficiency or Single Chromosomal Deletion</i>
<i>Dp</i>	<i>Duplication</i>
<i>dpp</i>	<i>decapentaplegic</i>
<i>EcR</i>	<i>Ecdysone Receptor</i>
EN	Enhancer
GFP	Green Fluorescent Protein
<i>HGR</i>	<i>Head involution defective, grim, reaper</i>
HI	Haplo-Insufficient

<i>Hid</i>	<i>Head Involution Defective</i>
IAP	Inhibitor of Apoptosis Protein
$\Delta\alpha$INR	<i>Activated Insulin Receptor</i>
<i>InR</i>	<i>Insulin Receptor</i>
LC3	Light chain 3
UM	Undefined Modifier
mCD8	Myristoylated CD8 protein
PCD	Programmed Cell Death
PI3K	Phosphoinositide 3-Kinase
<i>pnr</i>	<i>pannier</i>
RFP	Red Fluorescent Protein
<i>rpr</i>	<i>reaper</i>
SEM	Scanning Electron Microscopy
SU	Suppressor
TEM	Transmission Electron Microscopy
<i>TOR</i>	<i>Target Of Rapamycin</i>
UAS	Upstream Activating Sequences

Chapter 1. Introduction

1.1 Programmed Cell Death

Cell death can be divided into two categories: Programmed Cell Death (PCD) and Necrosis. Necrosis is an uncontrolled form of cell death that results when cells are accidentally injured by mechanical damage, exposure to toxins, or pathogenic infection (Van Cruchten and Van Den Broeck, 2002). In contrast, PCD is a genetically regulated process that is frequently used to remove superfluous cells and tissues during animal development (Mohseni *et al.*, 2009). Furthermore, PCD is controlled through three distinct PCD initiating pathways: apoptosis, autophagy, and non-lysosomal cell death (Luo *et al.*, 2007). Typically, apoptotic and autophagic cell morphologies are observed in cells that are destined to die during development. In contrast, non-lysosomal cell death is rarely observed during development, and is identified by swollen organelles and the lysosome-independent formation of ‘empty spaces’ in the cytoplasm (Baehrecke, 2005).

1.1.1 Apoptosis

Apoptosis, the most recognized form of PCD, is often described as a “suicide” program that, when activated, leads to the death of individual cells by caspases, a family of site specific proteases (Alberts *et al.*, 2008). Apoptosis, or caspases, can be activated in two distinct ways: extrinsically and intrinsically. The extrinsic pathway is activated by the binding of extracellular signal proteins to death receptors on the surface of the cell, whereas the intrinsic pathway is triggered by signals from inside the cell in response to a loss of inner mitochondrial membrane potential. Two groups of caspases are activated in response to the extrinsic and intrinsic pathways: the initiator caspases and the executioner caspases. The first

caspases to be activated in response to the extrinsic and intrinsic pathways are the initiator caspases. Upon activation, the initiator caspases cleave and activate many downstream executioner caspases, resulting in a proteolytic caspase cascade (Alberts *et al.*, 2008). Ultimately, this proteolytic cascade results in the cleavage of various protein substrates by executioner caspases, which results in a characteristic morphology that includes: cell shrinkage, nuclear fragmentation, cytoskeleton collapse, and membrane blebbing (Alberts *et al.*, 2008). Also, the cell membrane of an apoptotic cell changes its chemical composition through the exposure of phosphatidylserine on the outer leaflet of the lipid bilayer, signaling neighboring cells or macrophages to engulf the apoptotic corpse (Baehrecke, 2005).

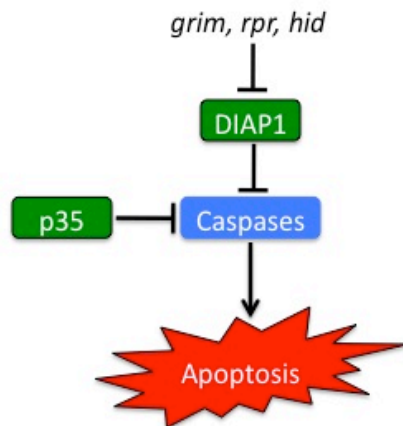


Figure 1.1: The apoptosis PCD Pathway in *Drosophila melanogaster*. Normally, the *H99* genes: *grim*, *reaper* and *hid* inhibit DIAPs. The inhibition of DIAPs allows the activation of caspases. Caspase activation results in apoptosis. *p35* inhibits caspases, preventing apoptosis. Proteins in green inhibit apoptosis. Proteins in blue stimulate apoptosis.

To prevent the inappropriate activation of caspases and subsequently apoptosis, cells possess Inhibitor of Apoptosis Proteins (IAPs). Normally, IAPs bind to and inhibit inappropriately activated caspases, preventing the proteolytic cascade that would ultimately result in a cell's demise. In *Drosophila*, IAPs (DIAPs) are targeted for proteolytic degradation during an apoptotic response by the products of the so-called H99 genes: *head involution defective (hid)*, *grim*, and *reaper (rpr)* (Bangs *et al.*, 2000). The downregulation of DIAPs

allows caspase activation and thereby promotes apoptosis (Figure 1.1). In principle, this highly regulated pathway should prevent the inappropriate activation of apoptosis. Many viruses, however, express genes that target this pathway in order to prevent host cells from entering apoptosis. The baculovirus caspase inhibitor, *p35*, when expressed in *Drosophila*, acts as a suicide inhibitor or “Trojan horse” destroying itself upon irreversibly inactivating caspases (Figure 1.1) (Tschopp *et al.*, 1998).

1.1.2 Autophagy

Unlike apoptosis, which is synonymous with PCD, autophagy represents a catabolic process that functions in many cellular and biological processes (Berry and Baehrecke, 2007). Autophagy occurs as a normal cellular response to starvation, and acts a mechanism for the turnover of organelles and the clearance of protein aggregates (Klionsky and Emr, 2000). Also, autophagy can, in certain contexts, function as a pro-death mechanism (Levine and Yuan, 2005; Tsujimoto and Shimizu, 2005; Mohseni *et al.*, 2009). Given that autophagy is often employed as a cellular response to starvation, and is therefore considered a pro-survival mechanism, the role of autophagy in PCD seems paradoxical (Tsujimoto and Shimizu, 2005). In particular, it is often debated whether autophagy functions as an independent cell death pathway, acts to promote apoptosis, or represents a failed attempt to suppress cell death (Tsujimoto and Shimizu, 2005; Mohseni *et al.*, 2009; Scott *et al.*, 2007; Berry and Baehrecke, 2007).

1.1.2.1 The Process of Autophagosome Formation: An Overview

In response to starvation or other inductive cues, autophagosomes, double membrane vesicles that engulf cytoplasmic elements, are formed (Klionsky, 2004).

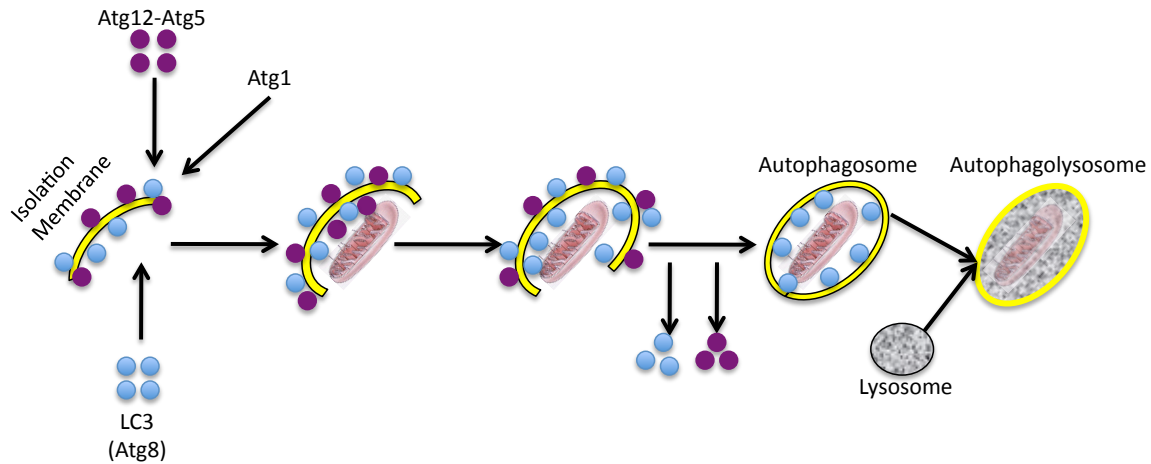


Figure 1.2: Diagram illustrating the various steps in the formation of the autophagosome and autolysosome (Adapted from Pattingre *et al.*, 2008).

The autophagy related proteins, Atg1, Atg5, Atg8, and Atg12 are essential for the formation of autophagosomes. Upon the initiation of autophagy, Atg12 is attached to Atg5, forming the Atg12-Atg5 complex. This complex is required for the localization of Atg8 to the isolation membrane. It is thought that the localization of Atg8 to the isolation membrane contributes to its elongation. As the isolation membrane elongates and closes to form the autophagosome, it sequesters cytoplasm and organelles. Upon autophagosome formation, the Atg12-Atg5 complex is lost from the autophagosomal membrane (Rusten *et al.*, 2004). Afterwards, the autophagosome fuses with a lysosome, resulting in the breakdown of Atg8, the inner autophagosomal membrane, and any sequestered material (Figure 1.2) (Pattingre *et al.*, 2007). Since Atg8 remains associated with the inner autophagosomal membrane until it is

degraded by the lysosome, Atg8 is widely used as a marker of autophagosomes (McPhee and Baehrecke, 2009).

1.1.2.2 Atg1 Is A Key Regulator of Autophagy

Atg1, a conserved serine/threonine-specific protein kinase, appears to be a key regulator of multiple steps in the autophagic process (Scott *et al.*, 2007). Recent studies have shown that Atg1 is involved in the initiation and execution of autophagosome formation, and the shuttling of proteins into and out of the autophagosomal membranes (Pattingre *et al.*, 2008; Reggiori *et al.*, 2005). Furthermore, it has been shown that Atg1 is a target of the InR/PI3K and TOR signaling pathways (Figure 1.3) (Stephan and Herman, 2006; Scott *et al.*, 2007). The interaction between TOR and Atg1 is particularly interesting since TOR is also a target of Atg1 through a self-reinforcing negative feedback loop (Figure 1.3) (Neufeld, 2007; Neufeld and Baehrecke, 2008). It has been speculated that it is the mutual antagonism between Atg1 and TOR that ultimately regulates autophagy (Neufeld, 2007). Determining the mechanisms regulating autophagy is important since it is speculated that low levels of autophagy can be cytoprotective, whereas high levels of autophagy result in the activation of PCD (Scott *et al.*, 2007). Revealing the substrates of Atg1, which are currently poorly defined, may elucidate the mechanisms involved in controlling the various cellular and biological processes of autophagy.

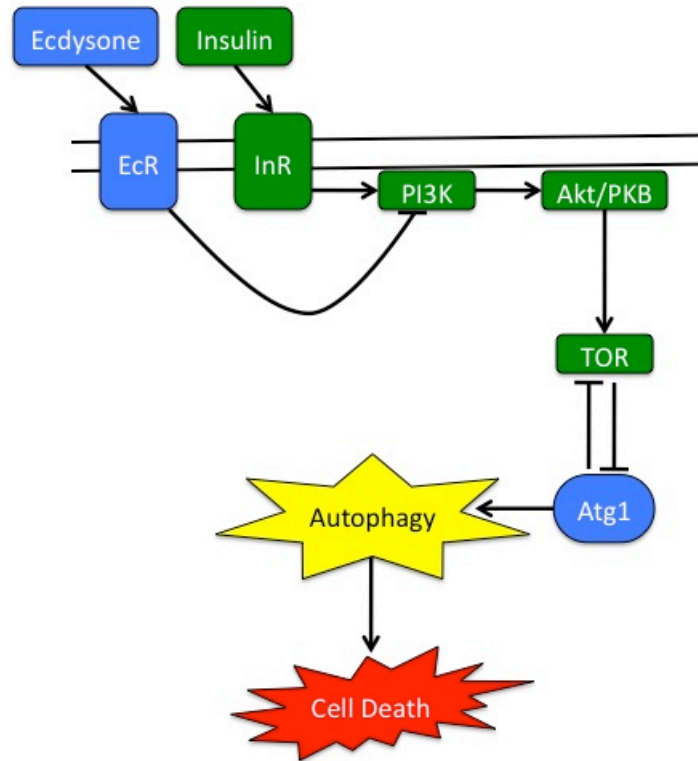


Figure 1.3: Nutritional and developmental control of Autophagy. Upon activation, the insulin receptor (InR) activates phosphatidylinositol-3 kinase (PI3K) which leads to the activation of protein kinase B (PKB)/Akt. An increase in TOR activity results in the inhibition of Atg1 and autophagy levels decrease. Ecdysone Receptor negatively regulates PI3K, resulting in an increase in autophagy. Prolonged increases in autophagy can lead to cell death (Neufeld and Baehrecke, 2008). Proteins and steroids that stimulate autophagy are colored in blue. Proteins that inhibit autophagy are colored in green.

1.1.2.3 Autophagy and Cell Survival

A relationship between cell survival and autophagy has been observed during *Drosophila* development. Normally, when nutrients are plentiful TOR (Target Of Rapamycin) signaling is active, and autophagy proceeds at a basal level. Under these conditions, autophagy functions to maintain homeostasis through the removal of defective or superfluous organelles, and abnormal or damaged proteins (Meléndez and Neufeld, 2008). Conversely, under nutrient limiting conditions, a decrease in the activity of Insulin/PI3K or TOR signaling pathways results in an increase in the level of autophagy. At increased levels, autophagy functions to promote cell survival by supplying the cell with energy and nutrients such as

methylpyruvate, a mitochondrial substrate of the tricarboxylic acid cycle (Lum *et al.*, 2005) and amino acids, building blocks for the synthesis of new proteins (McPhee and Baehrecke 2008). Therefore, a basal level of autophagy is essential to maintain homeostasis and autophagy is upregulated under starvation conditions to promote survival. Since autophagy is a catabolic process, prolonged induction of this process can decrease cell growth and deplete energy and nutrient supplies, ultimately leading to cell death (Neufeld and Baehrecke, 2008; Debnath *et al.*, 2005; Berry and Baehrecke, 2007). Therefore, autophagy can promote cell survival but should be carefully regulated as prolonged autophagic induction can also lead to cell death.

1.1.2.4 Autophagic Cell Death

Autophagic (Type II) cell death describes a form of cell death that results from excessive levels of autophagy and occurs primarily during development when cell death occurs *en masse* (Levine and Yuan, 2005). Sometimes described as “histolysis”, autophagic cell death is distinguished from apoptosis through many of its distinct morphological features. In general, the morphological characteristics of autophagic cell death include, an abundance of autophagosomes and autolysosomes, early organelle degradation, late cytoskeletal disassembly and chromatin condensation, and finally DNA fragmentation (Shimizu *et al.*, 2004; Yu *et al.*, 2004; Levine and Yuan, 2005; Lockshin and Zakeri, 2004). Also, autophagic cell death occurs largely in the absence of macrophages, since dying cells are degraded by their own lysosomal enzymes rather than by phagocytosis (Lee and Baehrecke, 2001; Martin and Baehrecke, 2004).

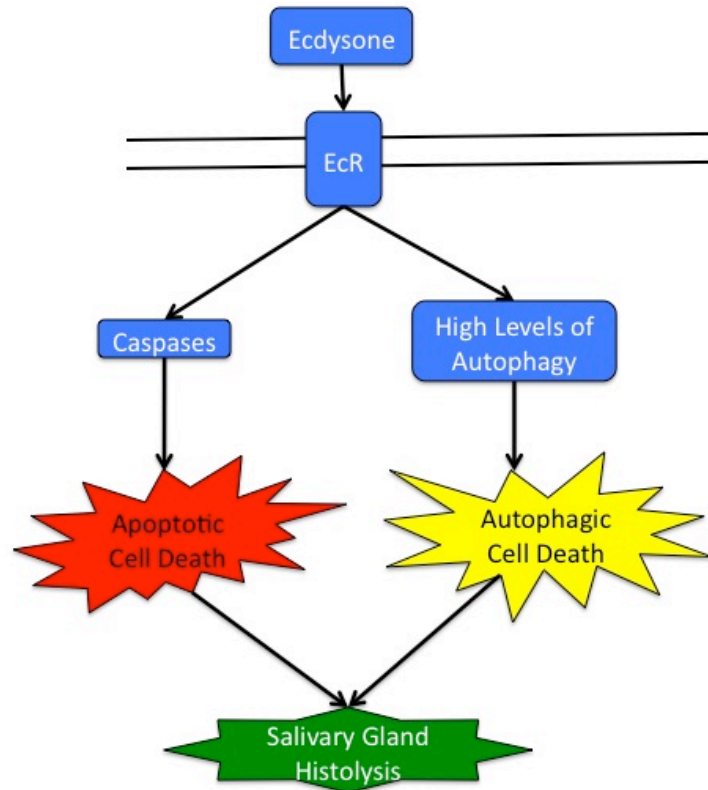


Figure 1.4: Model diagram of autophagic cell death, illustrating the parallel relationship that occurs between autophagy and apoptosis during salivary gland histolysis. Elevated levels of ecdysone result in caspase activation and a dramatic increase in autophagy. Each PCD pathway is activated by ecdysone but act independently to promote salivary gland histolysis.

During metamorphosis, a rise in the steroid hormone 20-hydroxyecdysone (ecdysone) triggers the autophagic destruction of obsolete larval structures. Ecdysone signaling has been found to be involved in larval tissue histolysis through a negative interaction with PI3K (Figure 1.3) (Rusten *et al.*, 2004). The inhibition of the InR/PI3K pathway, through ecdysone signaling, results in the dramatic increase in autophagy and subsequent autophagic degradation of larval tissues (Rusten *et al.*, 2004; Lee and Baehrecke, 2001; Martin and Baehrecke, 2004; Berry and Baehrecke, 2007). Although these larval tissues are largely eliminated by autophagic cell death, some hallmarks of apoptosis have been observed. The observation of both apoptotic and autophagic morphologies indicate that these PCD pathways can act cooperatively during larval tissue histolysis (Berry and Baehrecke, 2007; Scott *et al.*,

2007; Pattingre *et al.*, 2007). In particular, studies of larval salivary gland histolysis have shown that a rise in ecdysone during metamorphosis induces the transcription of *hid* and *rpr*, two of the pro-apoptotic *H99* genes (described in Section 1.1.1)(Jiang *et al.*, 1997; Lee *et al.*, 2000; Yin and Thummel, 2004). Additionally, it has been shown that the complete destruction of *Drosophila* salivary glands requires autophagy and caspase activation (Lee and Baehrecke, 2001). However, the relationship between the apoptotic and autophagic cell death pathways, in this context, is parallel with both pathways acting on salivary gland histolysis independently (Figure 1.4)(Lee and Baehrecke, 2001; Berry and Baehrecke, 2007). In other tissues, the role of autophagy and its relationship with caspase activation can change depending on the organism, cell type, and cell-specific conditions (Baehrecke, 2005).

1.1.2.5 Autophagy-Dependent Caspase Activity

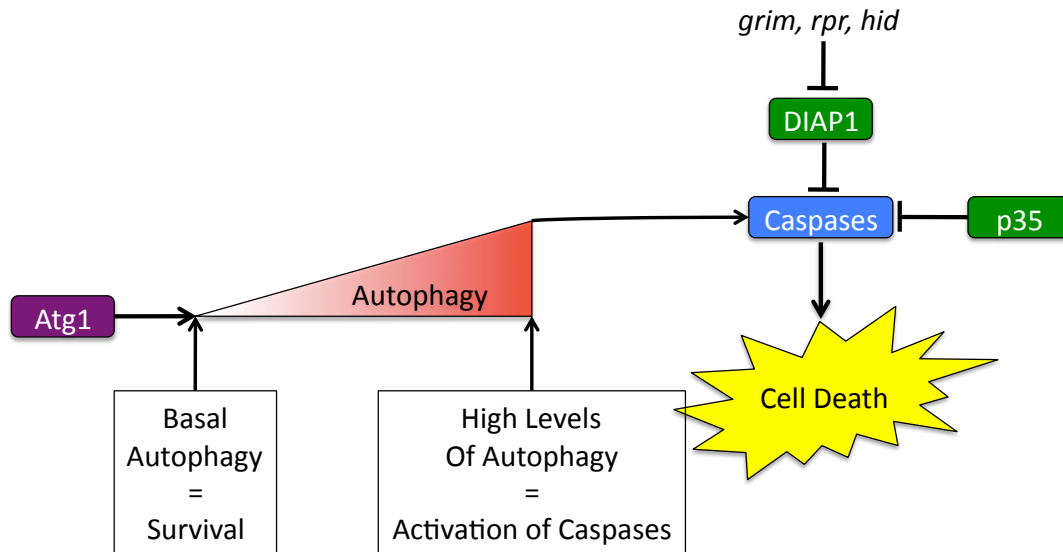


Figure 1.5: Model diagram of autophagy-dependent caspase activation, illustrating that low levels of autophagy promotes cell survival and high levels of autophagy, through the overexpression of *Atg1*, results in autophagy-dependent caspase activity and ultimately cell death. In this model the relationship between caspase activation and autophagy is epistatic.

Recently, “autophagy-dependent caspase activation” was coined as a term to describe a type of caspase-dependent cell death that is induced by high levels of autophagy (Mohseni *et al.*, 2009). Unlike autophagic cell death, which acts as an independent cell death pathway, autophagy-dependent caspase activation employs a single pathway whereby high levels of autophagy act to induce caspases and subsequently apoptosis (Figure 1.5). Although the mechanisms regulating this pathway remain unknown, a recent study has shown the existence of autophagy-dependent caspase activity during *Drosophila* development. An article by Mohseni *et al.*, which includes data from this thesis, illustrates that the upregulation of autophagy in the amnioserosa (AS), an extra-embryonic epithelial tissue, results in a caspase-dependent cell death (2009) (For more information on AS degeneration during dorsal closure (DC) see Appendix A – Section A.2). In this study, it was demonstrated that the complete destruction of the AS requires both autophagy and caspase activation (Mohseni *et al.*, 2009).

Also, it was established that, during the elimination of the AS, autophagy is required for caspase-activation; however, autophagy continues unabated in mutants defective in the activation of apoptosis (Mohseni *et al.*, 2009; Reed Lab Unpublished Data). Together, these results suggest that autophagy acts upstream of caspase-activation during the elimination of the AS (Figure 1.5).

In another study, Scott *et al.*, have demonstrated that the overexpression of *Atg1* in patches of the imaginal wing disc results in the induction of autophagy-dependent caspase-activation (2007) (For more information on the development of the wing disc see Appendix A – Section A.3). This induction of cell death is rescued by an *Atg8* mutant background (Scott *et al.*, 2007), demonstrating the requirement of an intact autophagy pathway for the induction of caspases. This study also reported that the co-expression of *p35* was able to delay the death of *Atg1*-overexpressing patches in the wing-disc (Figure 1.5) (Scott *et al.*, 2007). Similarly, one of the findings reported in this thesis is that an increase in autophagy, through the overexpression of *Atg1* in the proximal area of the wing disc, results in a caspase-mediated cell death, and this cell death can also be rescued by the co-expression of *p35* (Figure 1.5). Together, these results suggest that an increase in autophagy via *Atg1* overexpression, in this context, results in the promotion of cell death directly through caspases rather than autophagy acting as a distinct form of cell death.

1.1.2.6 Interpretation: Autophagic Cell Death and Autophagy-Dependent Caspase Activation

The most parsimonious interpretation of the literature is that the role of autophagy, be it pro-death or pro-survival, is context or tissue dependent. Although it has been shown that nutrient conditions, developmental signaling, and TOR expression levels all regulate autophagy, it is unknown whether these factors may be implicated in the decision to undergo an autophagy-induced cell death (Neufeld and Baehrecke, 2008). Consequently, further research should be conducted to determine what mechanisms are involved in the regulation of both PCD pathways in *Drosophila*.

1.1.2.7 Why Study Autophagy in *Drosophila melanogaster*?

Understanding the regulation of autophagy and its relationship with PCD is important since it is closely associated with human health and disease. For example, various human neurodegenerative diseases including Huntington's chorea, Alzheimer disease, and Parkinson's Syndrome are associated with aggregate-prone proteins (Sarkar *et al.*, 2008). While low levels of autophagy may be beneficial in clearing cells of these pathogenic protein aggregates (Sarkar *et al.*, 2008), high levels of autophagy are thought to induce apoptosis (Klionsky, 2007; Scott *et al.*, 2007; Mohseni *et al.*, 2009). Since increased rates of apoptotic neuronal cell death leads to the progression of these debilitating diseases, a better understanding of the mechanisms regulating autophagy is required before agents that manipulate autophagy, such as rapamycin, are used as a therapy for neurodegenerative disorders (Sarkar *et al.*, 2008),

1.2 Main Experimental Objectives:

The first objective of this study involves the development of an *in vivo* method for the detection of autophagy in the amnioserosa (AS), an extraembryonic membrane, during *Drosophila* embryogenesis. The data presented here demonstrates that the onset and disruptions of autophagy can be detected using the vital dye lysotracker. Also, it has been shown that autophagy proceeds in backgrounds that lack caspase activity.

The second objective is to address the relationship between autophagy and caspase activation. The approach presented here involves the development of an *in vivo* method (Apoliner) for detecting caspase activity. This method is applied to a variety of tissues during *Drosophila* development including the AS, dorsal larval epidermis and presumptive adult tissues (for more information on the developmental events associated with these tissues, see Appendix A). Together, the data here confirms that autophagy can induce caspase activation in the context of the AS, as well as the third instar larval epidermis and wing disc.

It is also presented in this thesis that the overexpression of *Atg1^{6B}* results in an adult cuticular phenotype that is not directly associated with caspase activity. Nonetheless, altering the level of *Atg1^{6B}* expression can modulate this adult cuticular phenotype. The third and last objective is the design and execution of a genetic screen to identify dose-sensitive modifiers associated with the induction of autophagy by ectopic Atg1 kinase expression.

Chapter 2. Materials and Methods

Chapter 2. Materials and Methods

2.1 Fly Strains and Handling

Flies were raised on standard *Drosophila* medium at 25°C unless otherwise stated. Detailed descriptions of the *[UAS-Atg1^{6A}]*, *[UAS-Atg1^{6B}]*, *[LPI-GAL4]*, *[yw⁶⁷]*, *[(UAS-GFPnls)8]*, *[UAS-p35]*, *[UAS-Apoliner]*, *[Yet1; LPI-GAL4]*, *[UAS-p35; UAS-p35]* stocks can be found in Mohseni *et al.*, 2009. Deficiencies, duplications, and mutations utilized in the enhancer and suppressor screen were obtained from Bloomington *Drosophila* Stock Center or Dr. Tony Harris and Dr. Craig Smibert at the University of Toronto. Complete genotype notations for all stocks are available online at FlyBase (<http://flybase.bio.indiana.edu/>). For a complete list of the stocks used in the enhancer and suppressor screen see Appendix D.

2.2 GAL4-UAS Inducible Gene Expression System

The GAL4-UAS inducible gene expression system was used to express a variety of genes at different stages and in different tissues during *Drosophila* development. To express genes of interest using the GAL4-UAS system, a genetic cross is performed between a GAL4 transcription factor bearing stock (the “driver”), and a stock carrying a gene with an upstream activating sequence (UAS)(the “reporter”). In progeny that contain both the driver and reporter, genes of interest are expressed in the tissue specified by the driver (Hartwell *et al.*, 2000). Drivers that were used in the following experiments include the AS-specific *LPI-GAL4* and *pnrGAL4*, a driver that enables ectopic gene expression in a medial-dorsal stripe throughout development. Additionally, this system was used to alter the level of ectopic gene expression throughout development. Increasing the temperature from 25°C to 29°C increases the level of GAL4 expression, while decreasing the temperature from 25°C to 18°C decreases the level of GAL4 expression (Armstrong *et al.*, 2006).

2.3 GAL80

In the GAL4-UAS system, *Gal4* is expressed in a defined set of cells as specified by a tissue-specific enhancer, or other regulating sequences. GAL80 suppresses GAL4 activity by binding to the activation domain of GAL4, inhibiting the ability of GAL4 to bind to the UAS sequences. Expressing *Gal80* with a tubulin promoter results in the global suppression of GAL4 activity (McGuire *et al.*, 2003).

2.3.1 GAL80^{ts}

GAL80^{ts} is a temperature-sensitive version of the previously mentioned GAL80 protein. In this system, the temperature-sensitive GAL80 protein is expressed ubiquitously from the tubulin promoter at 19°C, thereby repressing the transcriptional activity of GAL4. However, GAL80^{ts} is rendered inactive at 30°C, allowing GAL4 to drive the expression of the gene of interest in cells specified by the tissue-specific driver (McGuire *et al.*, 2003).

2.3.2 GAL80^{ts} Experiment

Twenty-four vials, containing *pnrGAL4+UAS-Atg1^{6B}/TM6,Tb[GAL80]* females crossed to *w^{*}; P[tubP-GAL80ts]; TM2/TM6B,Tb^l* males, were set up. In each vial, adults were allowed to mate and lay embryos for 24 hours. After 24 hours, adults were removed and the resulting progeny were allowed to develop. At various time-points during development, each vial was shifted once, either upwards, from 18°C to 29°C, or downwards, from 29°C to 18°C. Once eclosed, the severity of the thoracic cleft and the reduced scutellum phenotype of *[GAL80^{ts}]/+; pnrGAL4+UAS-Atg1/TM2 or TM6B* progeny were evaluated. Any consistent difference (enhancement or suppression of thoracic cleft and reduced scutellum phenotype) was noted (for more information on the life cycle and developmental processes associated with development See Appendix A1-4).

2.4 Embryo Collection

Embryos were collected on juice agar plates in three-hour intervals at 25°C or 29°C using an automated *Drosophila* egg collector (Flymax Scientific Equipment Ltd.). Using PBT (0.1% Triton X-100 in 1x PBS), embryos were washed from the plates, collected in a nylon mesh basket, and washed with a copious amount of PBT and distilled water (Wieschaus and Nusslein-Volhard, 1986).

2.5 Dechoriation

The dechoriation technique varied depending on the experiment. Embryos being prepared for live imaging were dechoriated as follows: embryos were rolled gently on non-toxic sticky tape with forceps. The chorion adheres well to the sticky tape while the vitelline membrane beneath the chorion does not, allowing for the removal of the chorion (Ashburner, 1989). Alternatively, for lysotracker staining, embryos were collected in a nylon mesh basket and placed in 50% bleach, 50% PBT for 3 minutes. After 3 minutes, embryos were washed with copious amounts of water (Wieschaus and Nusslein-Volhard, 1986).

2.6 Lysotracker Staining

10-17-hour old embryos were collected and dechoriated as previously mentioned. Dechoriated embryos were transferred to a glass vial containing a 1:1 mixture of heptane and lysotracker solution (2 μ l of 1mM Lysotracker stock solution in 50mL of 0.7% NaCl Solution). Embryos were then shaken lightly for ten minutes. Afterwards, the aqueous phase (lysotracker solution) of the mixture was removed and replaced with heptane. Embryos were then collected in a nylon mesh filter and mounted on a confocal imaging chamber (See Section 2.7.1).

2.7 Live Imaging

2.7.1 Confocal Live Imaging

Embryos of interest were collected and dechorionated, as previously mentioned. In order to prevent desiccation after dechorionation, all embryos were immediately mounted on a confocal imaging chamber in gas permeable halocarbon oil (Methods for live imaging embryos are described in detail in (Reed *et al.*, 2004; Reed *et al.*, 2009)). The Zeiss Axiovert 100 confocal microscope and LSM 510 software were used to capture all LysoTracker images. All other confocal images were captured using the Nikon Eclipse Confocal Microscope and EZ-C1 software. All images were processed using ImageJ software (<http://rsb.info.nih.gov/ij/>).

2.7.2 Stereomicroscopic Live Imaging:

2.7.2.1 Larval Preparation: First to third instar larvae were removed from *Drosophila* medium and placed on a steel filter. Larvae were then washed with a copious amount of water and placed in an embryo dish. 1x PBS was added to the embryo dish and larvae were chilled at 4°C for 1 hour. Halocarbon oil was chilled in ice for 30 minutes prior to imaging. After 1 hour, larvae were mounted on a slide with chilled Halocarbon oil and single surface images were taken.

2.7.2.2 Pharate Adult Preparation: Pharate Adults were gently removed from vial walls, washed with water, and dried on a kim-wipe to clean the pupal case. Pharate adults were placed, dorsal-side up, on a slide. Surface photographs were taken every 6 minutes for approximately three to four days. Movies were compiled using ImageJ software. A Leica MZ 16 FA stereomicroscope and Leica Application Suite software were used for all larval and pupal live imaging.

2.7.2.3 Pharate Adult Dissection and Imaging: Pharate adults were removed from vials and washed as mentioned above (See Section 2.7.2.2). Pharate adults were placed dorsal-side up on double-sided sticky tape. Using forceps, the operculum was removed exposing the head of the pharate adult. Afterwards, the rest of the pupal case is peeled away leaving an intact pharate adult. Pharate adults were then placed on a slide in halocarbon oil and single surface images were taken.

2.8 Scanning Electron Microscopy

Adult *Drosophila* were anesthetized with carbon dioxide and their wings were removed with forceps. These flies were placed in a glass vial containing 70% acetone for 1 hour (within this hour the 70% acetone was changed 1x after thirty minutes). After 1 hr, the 70% acetone was replaced with 95% acetone and left for another hour (within this hour, the 95% acetone was changed 2 times). Finally, the flies were immersed in 100% acetone for 30 minutes (within this 30 minutes the acetone was changed 2 times). The flies were then collected in a nylon mesh basket and allowed to air dry for 10-15 minutes. Once dry, flies were mounted on steel stubs and transferred into a high-vacuum sputtering device. The flies were coated for 2 minutes at 18mA giving them a 30nm gold coating. The Hitachi S-570 scanning electron microscope and QuartzPCI software were used to image the flies.

2.9 Screen for Chromosomal Regions that Dominantly Interact with *Atg1^{6B}*

pnrGAL4+UAS-Atg1^{6B}/TM6B,Tb[Gal80] virgin females were crossed to males bearing either a deficiency or duplication *in trans* to a dominantly marked balancer chromosome. Crosses were maintained at 25°C, the temperature at which *pnrGAL4+UAS-Atg1^{6B}/+* shows the intermediate thoracic cleft and reduced scutellum phenotype. A total of 399 deficiency lines (*Df*) and 25 duplication (*Dp*) lines for the second and third chromosome were tested. *pnrGAL4+UAS-Atg1^{6B}/Df or Dp* and *Df or Dp/+;pnrGAL4+UAS-Atg1^{6B}/+* progeny were compared to the *pnrGAL4+UAS-Atg1^{6B}/Balancer* or *Balancer/+;pnrGAL4+Atg1^{6B}/+* sibs (these sibs were identified by dominantly marked balancers). The severity of the thoracic cleft and the reduced scutellum phenotype were evaluated and compared between the two groups. Any consistent difference (enhancement or suppression of the *pnrGAL4+UAS-Atg1^{6B}* phenotype) were noted and interactors were further tested for confirmation.

2.10 Screen for loci that dominantly interact with *Atg1^{6B}*

Crosses similar to those described above were also used to identify individual loci that exhibit dominant interactions with *Atg1^{6B}*. Candidate genes, located within the interacting regions identified by the enhancer and suppressor screen, were identified. Various alleles, representing each candidate gene, were tested for modification of the thoracic cleft and reduced scutellum phenotype. Any consistent differences were noted. In addition, a number of stocks were tested that were not located within the interacting regions identified by the enhancer and suppressor screen but were associated with cell death.

2.11 Confirmation of Genetic Interactions *BsgRNAi*⁴³³⁰⁷ and *EP(3)3614*

*pnrGAL4+UAS-BsgRNAi*⁴³³⁰⁷/*TM6B,Tb* or *pnrGAL4+EP(3)3614/TM3,Sb* virgin females were crossed to males bearing an interacting deficiency *in trans* to a dominantly marked balancer chromosome. Crosses were performed in a similar manner to those mentioned above (Section 2.9). Many of the strong suppressors and strong enhancers were tested. *pnrGAL4+UAS-BsgRNAi*⁴³³⁰⁷/*Df* or *Df/+;pnrGAL4+UAS-BsgRNAi*⁴³³⁰⁷ /+ progeny were compared to *pnrGAL4+UAS-BsgRNAi*⁴³³⁰⁷/*Balancer* or *Balancer/+;pnrGAL4+UAS-BsgRNAi*⁴³³⁰⁷/+ sibs (sibs were identified by dominantly marked balancers). The severity of the resulting black stripe down the midline of the thorax was evaluated and compared between the two groups. Any consistent differences in the black stripe phenotype between the two groups were considered possible interactors with *pannier* expression in the screen for chromosomal regions that dominantly interact with *Atg1*^{6B}.

Similarly, *pnrGAL4+EP(3)3614/Df* or *Df/+; pnrGAL4+EP(3)3614/+* progeny were compared to *pnrGAL4+EP(3)3614/Balancer* or *Balancer/+; pnrGAL4+EP(3)3614/+* sibs. The severity of the resulting hairless stripe down the midline of the thorax and abdomen was evaluated and compared between the two groups. Any consistent differences in the hairless phenotype between the two groups were also considered possible interactors with *pannier* expression. Afterwards, any deficiency or duplication that resulted in an enhancement or suppression of both *UAS-BsgRNAi*⁴³³⁰⁷ and *EP(3)3614* were considered true interactors of *pannier* expression.

2.12 Wing Disc Dissection

Wing disc dissections of wandering late third instar larvae were performed as in (Purves and Brachmann, 2007). Wing discs were mounted in 0.7% NaCl on a coverslip using the hanging drop method described in (Reed *et al.*, 2009) and viewed using the Nikon Eclipse Confocal Microscope. All images were processed using Image J software (<http://rsb.info.nih.gov/ij/>).

Chapter 3. Development of Methodologies For Evaluating Autophagy and Caspase Activity In Various Tissues

Note: Portions of this chapter have been published in the following journal article: Mohseni, N., McMillan, S.C., Chaudhary, R., Mok, J., Reed, B.H., 2009. Autophagy Promotes Caspase-Dependent Cell Death during *Drosophila* Development. *Autophagy* 5, 329-338.
To view written permission from the editor of *Autophagy* please see Appendix E.

Chapter 3. Development of Methodologies For Evaluating Autophagy and Caspase Activity In Various Tissues

3.1 PCD in the AS: Using LysoTracker To Evaluate Autophagy

LysoTracker, a membrane permeable dye that labels acidic organelles, is a reliable indicator of increased autolysosomal and lysosomal activity. Although not specific for autophagy, lysoTracker staining has been used as an indicator of autophagy in studies of starvation-induced autophagy and autophagic cell death (Rusten *et al.* 2004).

The main advantage of using lysoTracker is the ability to evaluate autophagy in living embryos, removing the need for fixation and embedding. In addition, lysoTracker staining is a rapid method that allows the evaluation of autophagy and negates the time consuming process of introducing GAL4 and UAS constructs into mutant strains under investigation.

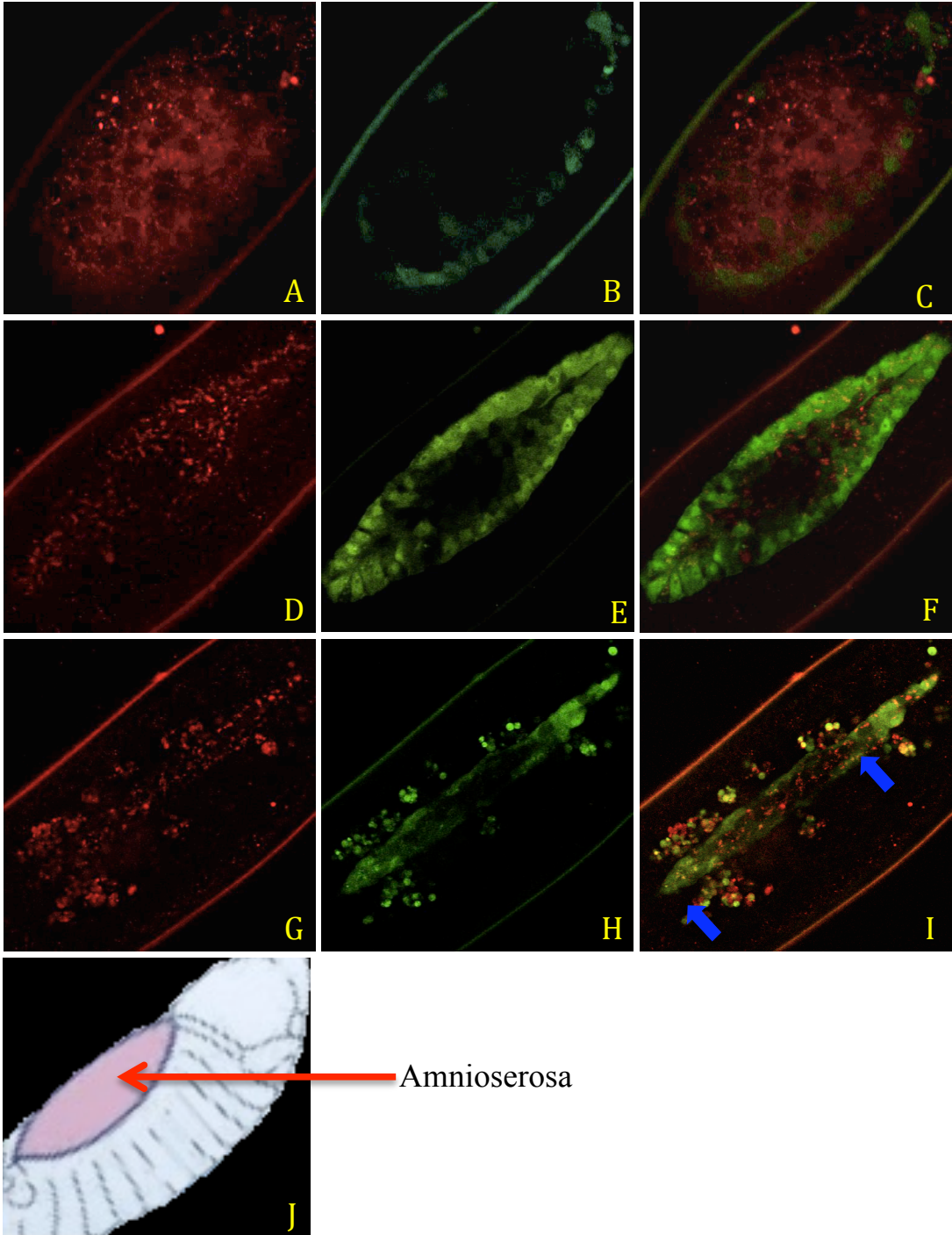
In the following four subsections, we have used lysoTracker as a vital stain for autophagy in the AS of wildtype and mutant backgrounds.

3.1.1 LysoTracker: Visualizing Autophagy In The AS Of Control Embryos

LysoTracker staining was initially performed on control embryos. Since future experiments were designed to use the GAL4-UAS system of inducible gene expression, the progeny of *Yet1*; *LPI-GAL4* outcrossed to a stock carrying the recessive visible markers *yellow* (*y* = yellow body color) and *white* (*w* = white eyes) were chosen as our control embryos. *Yet1* is a second chromosome vital enhancer trap that expresses GFP in the outer most cells (the perimeter cells) of the AS. Therefore, YET1 permits the easy identification of the AS in living embryos. *LPI-GAL4* is a third chromosome GAL4 driver with a high specificity for the AS throughout embryonic development (Reed *et al.*, 2004).

Confocal microscopy of lysotracker stained control embryos illustrates an increase in autophagy throughout dorsal closure in the AS (Figure 3.1). During early dorsal closure, the AS is largely lysotracker negative (lysotracker staining is weak, illustrating a few small punctate spots) (Figure 3.1A, C). Late dorsal closure stage embryos show the AS to be lysotracker positive (lysotracker staining is strong, illustrating many large punctate spots) (Figure 3.1D, F). Strong punctate lysotracker staining continues to be observed in the AS until it degenerates post dorsal closure (Figure 3.1G, I). It is interesting to note that macrophages, which are known to have large acidic compartments, stain prominently with lysotracker (Figure 3.1I). Furthermore, these results recapitulate observations made using LC3-GFP, and mCherry-DrAtg8a (fluorescent markers of autophagy). Expression of either fluorescent marker in the AS results in homogeneous localization during the early to mid dorsal closure stages of embryogenesis. However, expression from the late dorsal closure to the final stages of AS degeneration results in strong punctate localization of both fluorescent markers (data not shown; Reed Lab, Unpublished Data). These initial experiments served to demonstrate that lysotracker is a reliable indicator of autophagy in the AS.

Figure 3.1: Confocal micrographs of lysotracker stained control embryos expressing YET1 at three different stages of dorsal closure. (A-C) *Yet1/+; LPI-GAL4/+* embryo in the early stages of dorsal closure, illustrating lysotracker staining that is faint (small red punctate spots). (D-F) *Yet1/+; LPI-GAL4/+* embryo in the mid stages of dorsal closure, illustrating lysotracker staining that is strong with large red punctate spots. (G-I) *Yet1/+; LPI-GAL4/+* embryo post dorsal closure illustrating strong lysotracker staining (large red punctate spots) in the degenerating AS. (I) Macrophages have been stained red with lysotracker (blue arrows) (A,D,G) Lysotracker images (B,E,H) YET1 expression (C,F,I) Merged images of Lysotracker and YET1 expression. (J) Diagram illustrating the location of the amnioserosa (pink). All images were taken using the same confocal settings.



3.1.2 LysoTracker: Visualizing Autophagy In Apoptotic Defective Backgrounds

To determine whether autophagy is independent of caspase activation, autophagy was evaluated in embryos expressing the caspase inhibitor *p35* in the AS (Figure 3.2). Error was minimized in this experiment through the use of 3 controls. 1) *UAS-p35; UAS-p35 (X;2)* males were crossed to both *yw* and *Yet1; LPI-GAL4* virgin females in the same collection. Pooling our crosses in this way ensured that all embryos were treated in parallel throughout the experiment. During imaging, the genotypes of embryos from this pooled cross were identified by the presence or absence of *Yet1* expression in the perimeter cells. *Yet1* expression served to unambiguously identify embryos expressing the caspase inhibitor *p35* in the AS, whereas embryos not expressing *Yet1* represent an internal control. 2) All embryos collected from this pooled cross were stained in a single vial; therefore, all embryos were exposed to identical conditions throughout the lysotracker staining procedure. 3) All confocal laser settings were identical for each image captured.

Confocal microscopy of embryos expressing *p35* indicates there is no substantial difference between lysotracker staining of control and caspase-inhibited embryos (Figure 3.2D, F). It is interesting to note that caspase-inhibited embryos display a persistent AS phenotype (Figure 3.2D, E, F). The elongated “tube-like” appearance of the AS in this background has been observed in other apoptotic deficient genetic backgrounds (Figure 3.3A,C; Reed Lab Unpublished Data). Therefore, based on this phenotype, we are confident that this genetic background is associated with a high degree of caspase inhibition. This is further supported by the observation that macrophages are observed in the caspase-inhibited embryos by lysotracker staining but do not show any secondary acquisition of GFP that is normally associated with AS degeneration (Figure 3.2F). It is concluded that ectopic *p35*

expression and consequently the suppression of caspase activity did not alter lysotracker staining in the AS. Our interpretation of this result is that the induction of autophagy does not require caspase activity in the AS.

To further demonstrate that the induction of autophagy does not require caspase-activation, we sought to establish that autophagy continues unabated in mutants defective in the activation of apoptosis. Homozygous deficiencies of the pro-apoptotic gene cluster that includes *hid*, *grim*, and *rpr* (abbreviated as *HGR*) are well known to be completely deficient in apoptosis (White *et al.*, 1994) and display a persistent AS phenotype (Mohseni *et al.*, 2009). Therefore, the *HGR* deficient background was examined using lysotracker staining. In order to unambiguously identify embryos that lack both copies of the *HGR* genes we used two recombinant stocks, each carrying a single chromosomal deletion of the *HGR* genes. The first stock carried the *Df(3L)ED225* deletion and the *LPI-GAL4* driver and the second stock carried the *Df(3L)H99* deletion and a *UAS-mCD8-GFP* reporter. When using this elegant design, only embryonic progeny homozygous for deletions of the *HGR* genes express GFP.

Confocal micrographs of embryos from this cross demonstrate that *HGR* deficient embryos display unaltered levels of lysotracker staining, indicative of the normal progression of autophagy in this background (Figure 3.3A, C). Also, these embryos present a persistent AS phenotype, indicating that the embryos were defective for the activation of apoptosis (Figure 3.3A, B, C). In summation, the results of lysotracker staining in apoptotic defective backgrounds clearly demonstrate that the induction of autophagy does not require caspase activation or apoptosis.

Figure 3.2: Lysotracker staining of mid dorsal closure stage control embryos and late stage caspase-inhibited embryos. (A-C) Montage of a lysotracker stained *UAS-p35/+; UAS-p35/+* embryo, in the mid stage of dorsal closure. The total depth of the montage is 4.54 μ m, which has been divided into 3 slices. Depth increases from A to C. Image depicts strong punctate lysotracker staining throughout the AS (D) Single image of *UAS-p35/+; UAS-p35/Yet1; LPI-GAL4/+* embryo illustrating strong punctate lysotracker staining in a persistent AS. (E) Image of *UAS-p35/+; UAS-p35/Yet1; LPI-GAL4/+* embryo. YET1 expression (green) can be seen clearly in the perimeter cells of the AS, identifying embryos that are expressing *p35*. (F) Merged lysotracker and YET1 image of *UAS-p35/+; UAS-p35/Yet1; LPI-GAL4/+* embryo, illustrating punctate lysotracker staining in the persistent AS. Macrophages also observed (blue arrow) with no GFP acquisition in caspase-inhibited embryos. All crosses were performed at 25°C. All confocal micrographs were taken using identical settings.

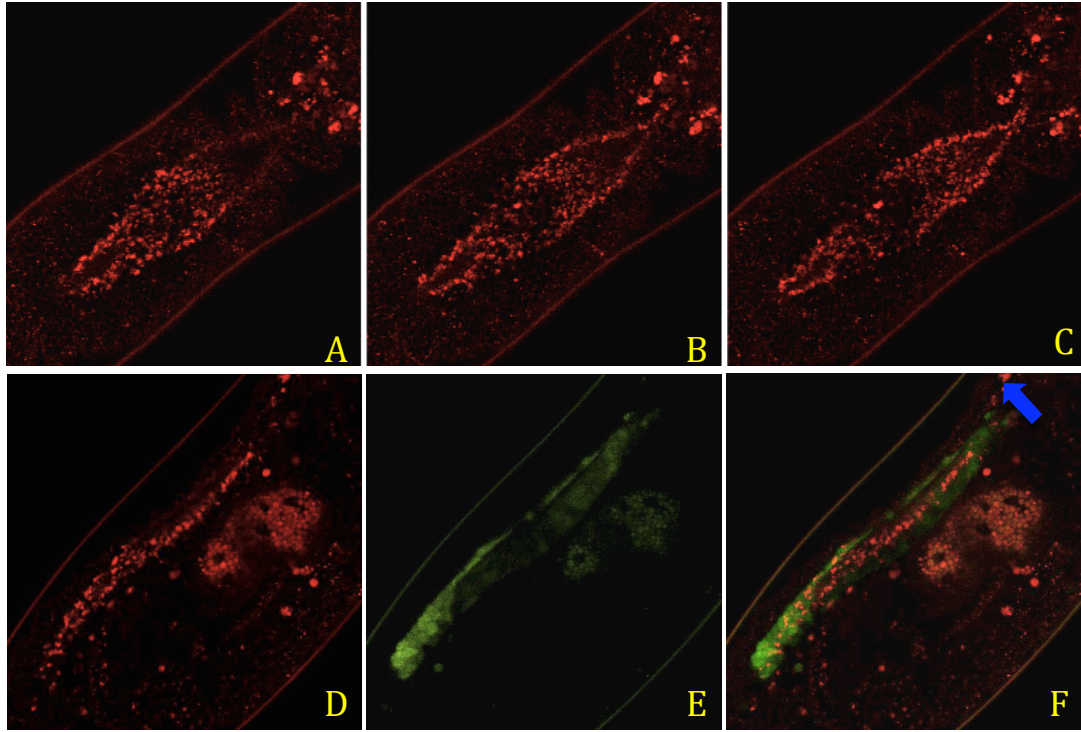
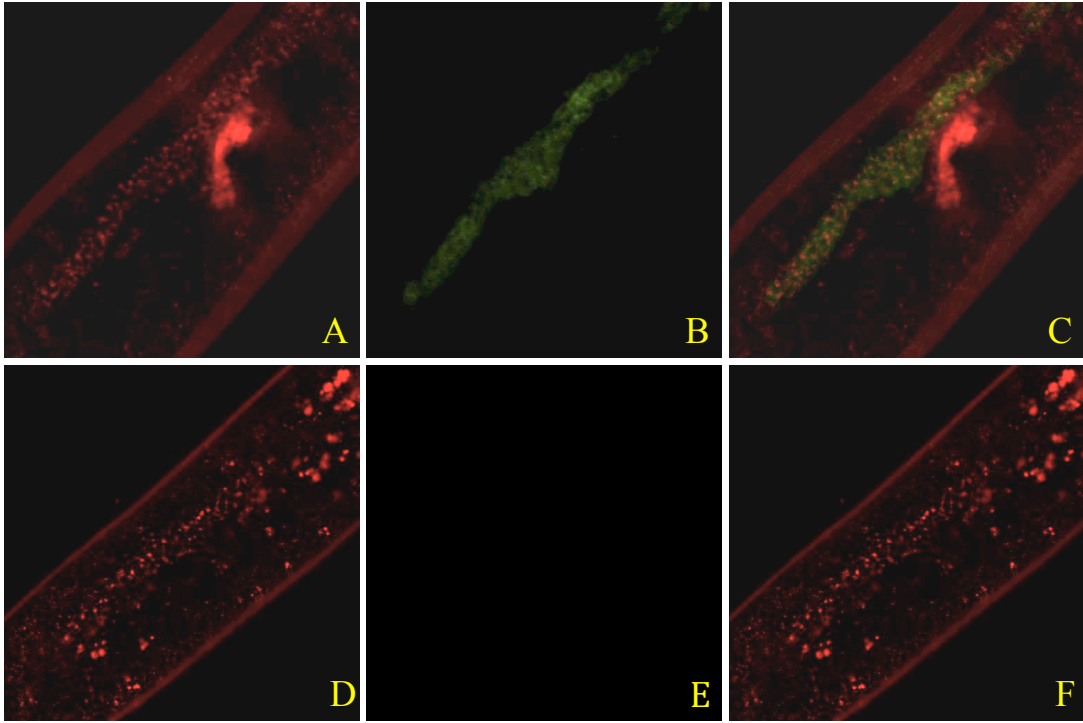


Figure 3.3: Lysotracker staining of *HRG* deficient embryo. (A-C) Lysotracker staining of an embryo with the genotype: *yw; LPI-GAL4, Df(3L)ED225/UAS-mCD8-GFP+Df(3L)H99*. (D, E, F) Control embryo that has been stained by lysotracker. (A, D) Lysotracker staining is punctate in *HRG* deficient (A) and control (D) embryos, illustrating autophagy proceeds unabated in *HRG* deficient embryos. (B, E) Illustrates the presence and absence of mCD8-GFP expression in *HRG* deficient (B) and control (E) embryos respectively. (C) Image illustrating both lysotracker staining and mCD8-GFP expression in an embryo that is *HRG* deficient. (F) Merged image illustrating lack of GFP and punctate lysotracker staining in the control embryo. All crosses were performed at 25°C and confocal settings were identical for the control and *HRG* deficient embryos.



3.1.3 Lysotracker: *Atg1* Overexpression Results In Increased Autophagy In The AS

The ectopic overexpression of *Atg1*, a key regulator of autophagy, is known to turn on or elevate autophagy during non-starvation conditions (Scott *et al.*, 2007). Therefore, we wished to evaluate the effect of *Atg1* overexpression in the AS. Lysotracker staining was performed on embryos overexpressing *Atg1* in the AS using *UAS-Atg1^{6A}* under the control of the *LPI-GAL4* driver (Figure 3.4B).

Confocal micrographs of *Atg1^{6A}* over-expressing embryos demonstrate that lysotracker staining in the AS of early DC stage embryos is greatly increased relative to the control (Figure 3.4). Similar results, using *UAS-mCherry-DrAtg8a* (*mCherry*), have been achieved, reinforcing this data (Reed Lab, Unpublished Data) (For details on mCherry See Section 3.3).

Interestingly, previous work has shown that high levels of Atg1 kinase expression results in early AS cell death. Such embryos fail in DC, and this defect is completely rescued through the ectopic expression of *p35*, a caspase inhibitor (Mohseni *et al.*, 2009). Together, these results suggest that high levels of autophagy induce caspase activation.

3.1.4 Lysotracker: Constitutive Activation of $\Delta\alpha InR$ Decreases Autophagy In The AS.

In contrast to the previous section, involving *Atg1^{6A}* overexpression, lysotracker staining was performed on embryos in which autophagy had been disrupted in the AS. Autophagy was inhibited in the AS through the expression of *UAS- $\Delta\alpha InR$* , an activated insulin receptor. Error was minimized in this experiment through the use of the same three 3 controls mentioned previously (See section 3.1.2). The downregulation of autophagy in these embryos resulted in a substantial decrease in lysotracker staining (Figure 3.5 A, C) relative to the control (Figure 3.5 D, F). Similar results, demonstrating a decrease in autophagy in the AS

of $\Delta\alpha InR$ expressing embryos, have been observed using LC3-GFP and transmission electron microscopy (TEM) (Mohseni *et al.*, 2009; Reed Lab Unpublished Data). Also, it has been shown that the expression of $UAS-\Delta\alpha InR$ results in a persistent AS phenotype (Mohseni *et al.*, 2009). Together, these results suggest that an increase in autophagy is required for the elimination of the AS.

Figure 3.4: Confocal micrographs of early dorsal closure stage embryos that have been stained by lysotracker. (A) Control, *yw*, embryo illustrating weak lysotracker staining with very few small punctae. (B) *UAS-Atg1^{6A}/LPI-GAL4* embryo, overexpressing *Atg1* in the AS. Image illustrates very strong lysotracker punctae in the AS. Crosses were performed at 29°C. Both images were taken with the same confocal settings.

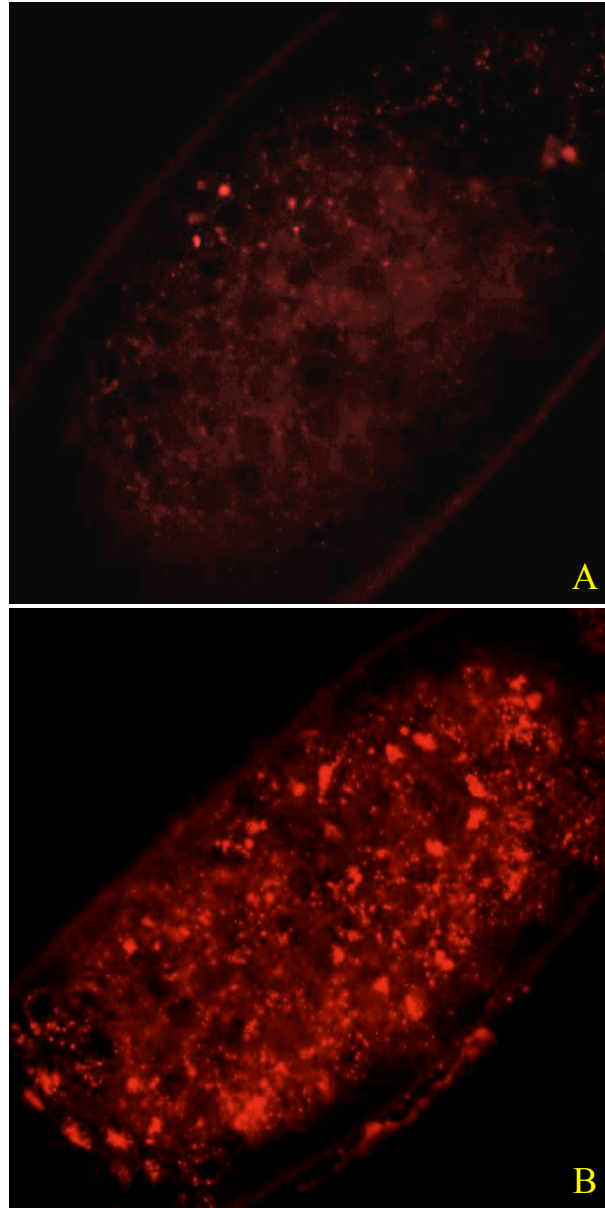
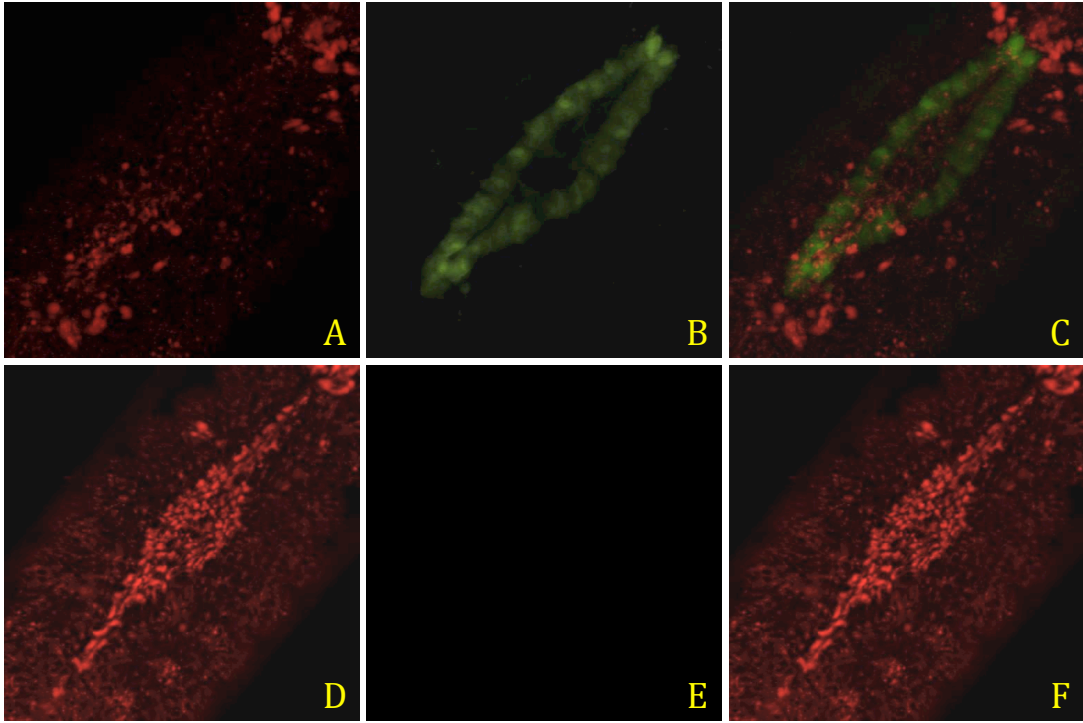


Figure 3.5: Confocal micrographs of mid to late dorsal closure stage embryos that have been stained by lysotracker. (A-C) Control embryo with the genotype *UAS-ΔαInR/+*. Image illustrates strong lysotracker staining with large punctae in the AS. (D-F) Autophagy inhibited, *Yet1/+;UAS-ΔαInR/LPI-GAL4*, embryo, illustrating weak lysotracker staining with very few small punctate spots in the AS. (A, D) Lysotracker images. (B) Image of YET1 expression in the perimeter cells of the AS. The presence of YET1 expression confirms the constitutive expression of $\Delta\alpha InR$. (E) The absence of YET1 expression in the perimeter cells of the AS confirms the absence $\Delta\alpha InR$ expression in the embryo. (C) Merged image illustrating lysotracker staining (red) and YET1 expression (green). (F) Merged image that illustrates only lysotracker staining, confirming $\Delta\alpha InR$ is not being expressed in the AS. All crosses were performed at 25°C. All images were taken with the same confocal settings.



3.2 Apoliner: Evaluating Caspase-Activity in Live Tissues Throughout Development

UAS-Apoliner, a caspase sensor, was employed to evaluate caspase activity in the AS, dorsal larval epidermis, and imaginal wing discs. Apoliner allows the detection of caspases in live tissues through the use of two fluorophores, RFP and GFP (Bardet *et al.*, 2008). Normally, when caspases are inactive, a caspase-sensitive site links the two fluorophores of Apoliner. However, upon activation of caspases the caspase-sensitive site between the two fluorophores is cleaved. Since each fluorophore is connected to a different subcellular localization signal, GFP to a nuclear targeting signal and RFP to a transmembrane domain, the cleavage of the caspase sensitive site allows GFP to accumulate in the nucleus, while the RFP persists at the membrane (Bardet *et al.*, 2008). Therefore, using this method, the activation of caspases in cells can be detected by the accumulation of GFP in the nucleus.

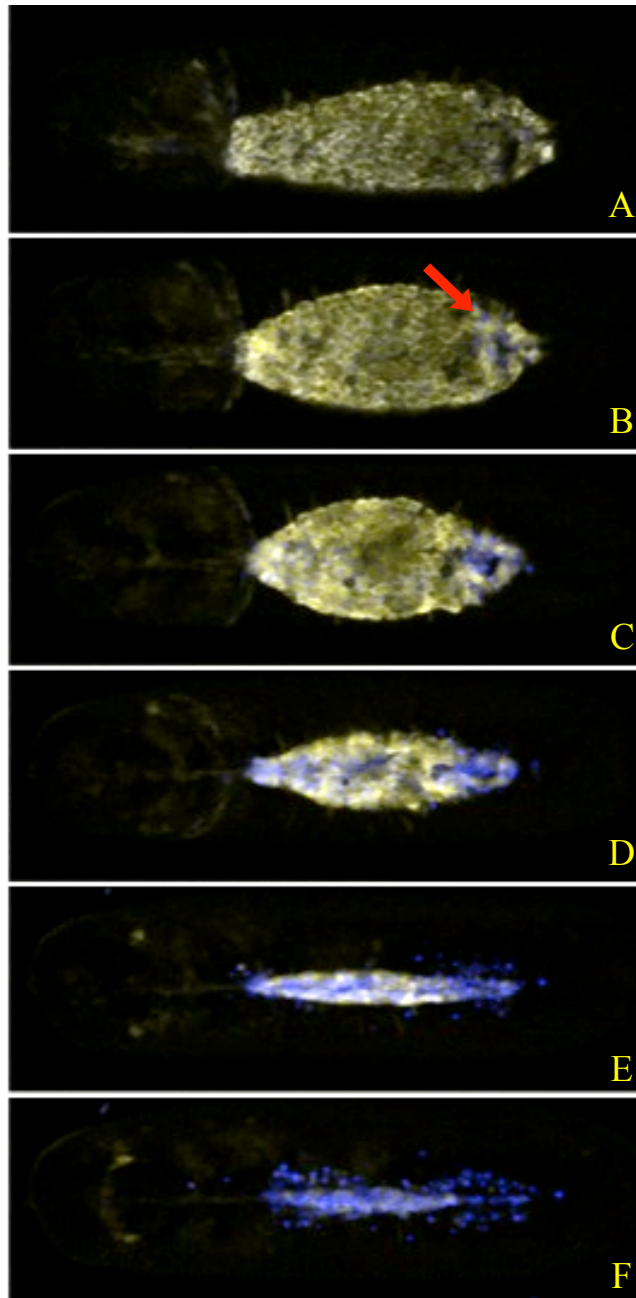
3.2.1 Apoliner: Evaluating Caspase Activity In The AS During Embryogenesis

Timelapse confocal microscopy of embryos expressing *UAS-Apoliner* was performed to assess the effectiveness of Apoliner as a caspase sensor during AS degeneration. Embryonic progeny carrying *UAS-Apoliner* and the AS-specific driver *LPI-GAL4* were imaged throughout dorsal closure. As a result, it was demonstrated that, prior to their elimination, GFP accumulates in the nucleus of AS cells expressing *UAS-Apoliner* (Figure 3.6). During the early DC stages of embryogenesis no caspase activity is detected in the AS with the exception of a few cells that were in the process of being extruded from the epithelium (Figure 3.6 A, B). Interestingly, the accumulation of nuclear GFP in AS cells prior to extrusion indicates that caspases are activated in cells before they are eliminated from the

epithelium (data not shown). During the mid-dorsal closure stage, a number of nuclear GFP positive AS cells are observed at the anterior and posterior ends of the AS, illustrating the induction of caspase activity (Figure 3.6C). By the late stages of dorsal closure, nuclear GFP is observed throughout the AS (Figure 3.6D). This accumulation of nuclear GFP continues in the AS well into the post-dorsal closure stages when the entire AS degenerates (Figure 3.6E, F). Together, these results indicate that Apoliner is a reliable indicator of caspase activation in the AS.

It has also been shown using Apoliner that the downregulation of autophagy, through the expression of *UAS-ΔαInR*, strongly reduces nuclear GFP localization (Reed Lab Unpublished Data). Therefore, an increase in autophagy is required for caspase activation in the AS. In summation, these results suggest that the relationship between autophagy and caspase activation is epistatic, whereby autophagy acts to induce caspase activation during the elimination of the AS (Figure 1.5).

Figure 3.6: Diagram illustrating the induction of caspase activity in the AS of an embryo with the genotype $+/+$; *UAS-Apoliner*/ $+$; *LPI-GAL4*/ $+$, throughout embryogenesis. (A) Early DC stage embryo illustrating no nuclear GFP. Both RFP and GFP co-localize at the membrane. (B) Early DC stage embryo illustrating an AS cell with nuclear GFP that is in the process of being extruded from the epithelium (red arrow). (C) Mid DC stage embryo illustrating a large number of AS cells with nuclear GFP at the posterior and anterior regions of the AS. (D) Late DC stage embryo illustrating nuclear GFP throughout the AS. (E) Post DC stage embryo illustrating cells with nuclear GFP throughout the AS. (F) Post DC stage embryo illustrating a degenerating AS. Nuclei at this stage are unobservable. In all images: GFP (yellow) RFP (blue). This cross was performed at 25°C.



3.2.2 Apoliner: Evaluating Caspase Activity In The Dorsal Third Instar Larval Epidermis

As outlined in the previous sections, it has been shown that high levels of autophagy in the AS result in caspase activation. Also, it has been shown that Apoliner is a reliable method to assess caspase activation. Expanding upon these findings, Apoliner was used to examine autophagy-induced cell death in the larval epidermis.

To visualize dorsal larval epithelial segments, a new recombinant stock, *pnrGAL4+UAS-Apoliner/TM6,Tb* was constructed on the third chromosome (For crossing Scheme See Appendix B – Figure B.3). This stock contains *pnrGAL4*, a GAL4 driver that enables ectopic gene expression in a medial-dorsal stripe throughout development, and *UAS-Apoliner* (See Section 3.2). This recombinant stock allows the assessment of caspase activity by outcrossing *pnrGAL4 + UAS-Apoliner* to any other available UAS-construct. In the progeny, the dorsal larval epidermis is readily examined by stereomicroscopy for the absence or presence of nuclear localized GFP (RFP was not examined in the larval epidermis due to the absence of a red filter on the stereomicroscope)(Figure 3.7).

To test the recombinant stock, preliminary live imaging was performed on control larvae that express *UAS-Apoliner* under the control of *pnrGAL4*. Throughout the live imaging sessions, larval epithelial cells of the 1st to 4th abdominal segments were clearly visible as distinct bands of non-nuclear localized GFP on the dorsal surface of the third larval instar (Figure 3.7A).

To evaluate the effect of *Atg1^{6B}* overexpression in the larval epidermis the same recombinant stock, *pnrGAL4+UAS-Apoliner/TM6,Tb*, was crossed to *UAS-Atg1^{6B}*. Stereomicroscopic live imaging of third instar larval progeny overexpressing *Atg1^{6B}* illustrates a severe decrease in the number of cells expressing *UAS-Apoliner* (Figure 3.7C).

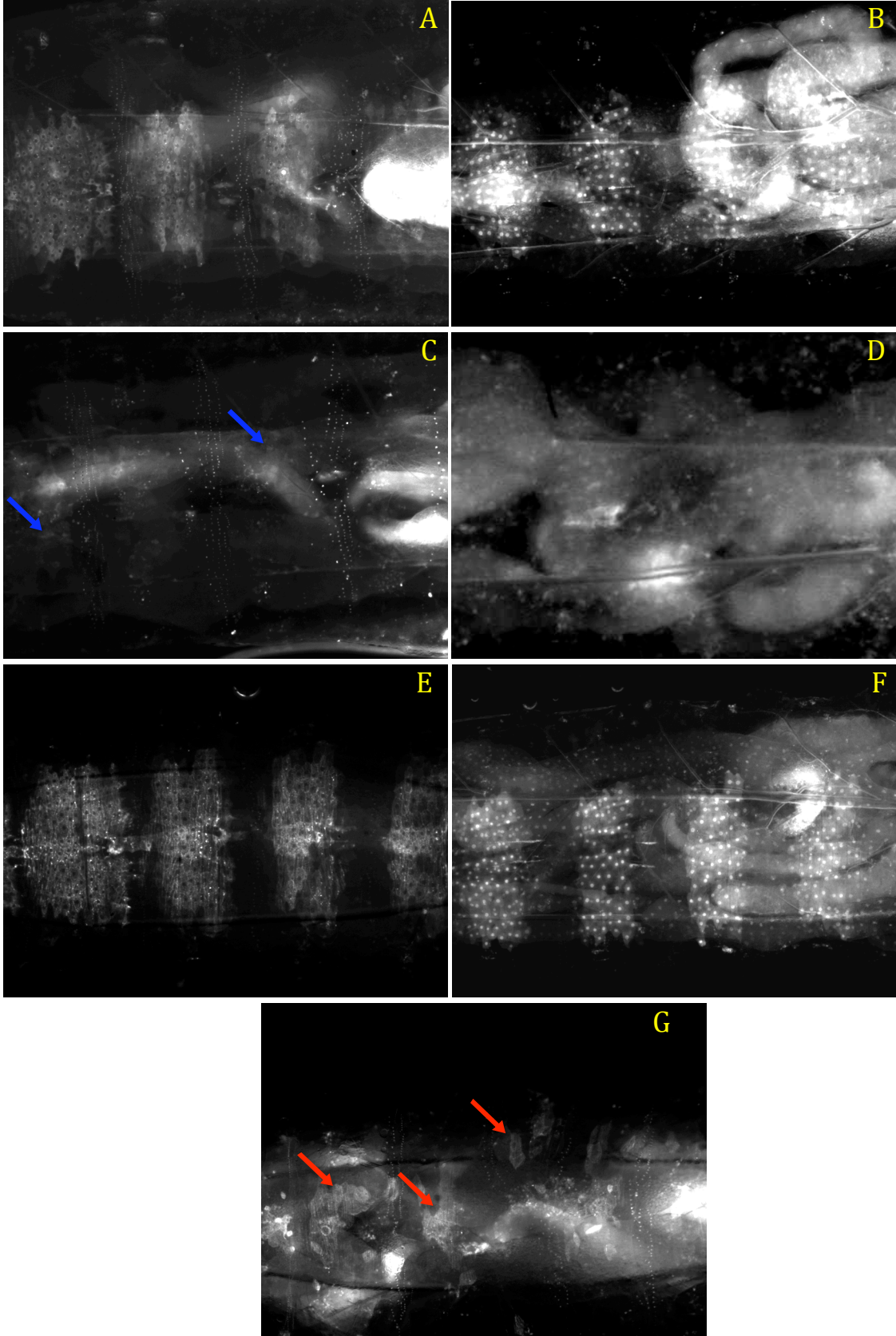
Also, the remaining larval epidermal cells contained nuclear localized GFP, suggesting that the *Atg1^{6B}* overexpressing cells are being eliminated through caspase-activation.

To determine whether the disappearance of the larval epidermal cells overexpressing *Atg1^{6B}* was a consequence of caspase activation, *UAS-p35; UAS-p35* virgin females were crossed to the newly constructed *pnrGAL4+UAS-Atg1^{6B}+UAS-Apoliner/TM6,Tb[GAL80]* stock (Crossing Scheme Available in Appendix B – Figure B.3). Non-nuclear localization of GFP, in small patches of larval epidermal cells, was observed in third instar progeny co-expressing *p35*, *Atg1^{6B}*, and *Apoliner* (Figure 3.7 G). Therefore, the co-expression of *p35* partially rescued the elimination of larval epidermal cells overexpressing *Atg1^{6B}*.

To ensure that the ectopic expression of *p35* in the larval epidermis resulted in a control phenotype, *UAS-p35; UAS-p35* virgin females were crossed to *pnrGAL4+UAS-Apoliner/TM3,Sb* males. As a result, non-nuclear GFP localization in the larval epidermis was observed in third instar progeny ectopically expressing *p35* (Figure 3.7 E). Therefore, ectopic *p35* expression does not alter the subcellular localization of GFP in larval epidermal cells.

In order to better visualize the larval epidermis, similar experiments were performed using a nuclear GFP reporter instead of *Apoliner* (Figure 3.7,B, D, F) (For details on the construction of the *pnrGal4+UAS-GFP^{nls}/TM3,Sb* Stock See Appendix B – Figure B.1). Comparable to previous results, the overexpression of *Atg1^{6B}* results in a severe decrease in cells expressing nuclear GFP (Figure 3.7D). Also, the ectopic expression of *p35* resulted in a phenotype identical to the control (Figure 3.7B), as nuclear GFP was expressed in distinct bands along the dorsal surface of the larval epidermis (Figure 3.7F).

Figure 3.7: Stereomicroscopic images of the 1st to 4th abdominal segments of the third instar dorsal epidermis using *UAS-Apoliner* and *UAS-GFP^{nls}*. (A) Control, *pnrGAL4+UAS-Apoliner/+*, larvae expressing non-nuclear GFP in the larval epidermis. (B) Control, *pnrGAL4+UAS-GFP^{nls}/+*, larvae expressing nuclear GFP in the larval epidermis. (C) *pnrGAL4+UAS-Atg1^{6B}+UAS-Apoliner/+* larvae overexpressing *Atg1^{6B}* in the dorsal larval epidermal cells. Image illustrates two small patches of cells with nuclear GFP expression (blue arrows). (D) *pnrGAL4+UAS-GFP^{nls}/UAS-Atg1^{6B}* larvae overexpressing *Atg1^{6B}* in the larval epidermal cells. Image illustrates an absence of cells containing nuclear GFP in the dorsal abdominal segments. (E) Control, *UAS-p35/+; UAS-p35/+; pnrGAL4+UAS-Apoliner/+*, larvae expressing non-nuclear GFP in the larval epidermis. (F) Control, *UAS-p35/+; UAS-p35/+; pnrGAL4+UAS-GFP^{nls}/+*, larvae expressing nuclear GFP in the larval epidermis. (G) *UAS-p35/+; UAS-p35/+; pnrGAL4+ UAS-Atg1^{6B} + UAS-Apoliner/+* larvae illustrating small patches of non-nuclear localized GFP in the larval epidermis (red arrows).



3.2.3 Apoliner: Evaluating Caspase Activity In The Third Instar Imaginal Wing Disc

In a recent study, Scott *et al.*, have demonstrated that the overexpression of *Atg1* in patches of the imaginal wing disc results in the induction of autophagy-dependent caspase activation (2007). Therefore, we sought to confirm and evaluate the activation of caspases by autophagy in the proximal area of the third instar imaginal wing disc.

First, confocal microscopy of control embryos expressing *UAS-Apoliner* was performed to evaluate Apoliner expression with respect to its utility in visualizing the proximal area of the wing disc. As a result, GFP and RFP were co-localized and clearly visible at the membrane of the imaginal disc cells (Figure 3.8A, B, C). Therefore, it was determined that Apoliner is a useful tool to observe caspase activation in the wing disc.

To determine whether the overexpression of *Atg1^{6B}* in the wing disc induces caspase activation, the *UAS-Apoliner+UAS-Atg1^{6B}+pnrGAL4/TM6,Tb[Gal80]* stock was outcrossed to a *yw* stock. As a result, nuclear localized GFP and membrane tethered RFP were clearly observed in cells overexpressing *Atg1^{6B}*, demonstrating that high levels of autophagy in the wing disc results in caspase activation (Figure 3.8 D, E, F).

Next, to establish whether the overexpression of *Atg1^{6B}* in the wing disc resulted in autophagy-dependent caspase activation, *UAS-p35; UAS-p35* virgin females were crossed to *UAS-Apoliner+UAS-Atg1^{6B}+pnrGAL4/TM6,Tb[Gal80]* males. As a result, non-nuclear localized GFP was observed in the wing discs of progeny co-expressing *p35*, *Atg1^{6B}*, and *Apoliner* (Figure 3.8 J, K, L).

To ensure that *p35* expression in the wing disc does not result in an observable phenotype, *UAS-p35; UAS-p35* virgin females were crossed to *pnrGAL4+Apoliner/TM6, Tb*

males. As a result, wing discs appeared similar to the controls as non-nuclear localized GFP was observed in progeny co-expressing *Apoliner* and *p35* (Figure 3.8 G, H, I).

Together, these observations indicate that the induction of autophagy, via the overexpression of *Atg1^{6B}*, results in autophagy-dependent caspase activation in the wing disc of third instar larvae.

3.3 mCherry: Evaluating Autophagy in Wing Discs Overexpressing *Atg1^{6B}*

To ensure that autophagy levels are increased in wing discs overexpressing *Atg1^{6B}*, autophagosomes and autolysosomes were detected using *UAS-mCherry-DrAtg8a*. mCherry is an acid-insensitive fluorescent protein that is fused to DrAtg8, an autophagy related protein that is essential for the formation of autophagosomes (Nezis *et al.*, 2009).

In the controls, the expression of *mCherry-DrAtg8a*, in the proximal area of the wing disc, results in homogeneous RFP localization in the cytoplasm, illustrating low levels of autophagosome and autolysosome formation. This result confirms the occurrence of low levels of autophagy in the wing discs of third instar larvae (Figure 3.9A, C).

However, larvae expressing *UAS-Atg1^{6B}* and *UAS-mCherry-DrAtg8a*, in the proximal area of the wing disc, had strong punctate RFP localization in the cytoplasm, illustrating a strong increase in autophagosome and autolysosome formation (Figure 3.9D, F). This result indicates that the level of autophagosome and autolysosome formation is increased in the wing disc when *Atg1^{6B}* is overexpressed. It is assumed from this data that autophagy levels are increased in wing discs overexpressing *Atg1^{6B}*, however, further research should be performed to verify that the flux through the autophagy pathway has increased as well as the number of autophagosomes and autolysosomes.

Figure 3.8: Confocal Micrographs of wing discs dissected from third instar larvae. (A-C) Control wing disc with the genotype: *pnrGAL4+UAS-Apoliner/+*. Images illustrate a wing disc in which GFP and RFP are co-localized (white) at the cell membrane. (D-F) Wing disc with the genotype: *pnrGAL4+UAS-Apoliner+UAS-Atg1^{6B}/+*. These images illustrate the nuclear localization of GFP (red arrows) due to caspase activity. (G-I) Control wing disc with the genotype *UAS-p35/+; UAS-p35/+; pnrGAL4+UAS-Apoliner/+*. These images illustrate the co-localization of GFP and RFP at the cell membrane due to an absence of caspase activity. (J-L) *UAS-p35/+; UAS-p35/+; pnrGAL4 + UAS-Apoliner + UAS-Atg1^{6B}/+*: wing disc, illustrating a rescue phenotype. GFP and RFP are co-localized and reside at the membrane. Scale bars indicate a distance of 50µm. All images illustrate GFP (yellow) and RFP (blue).

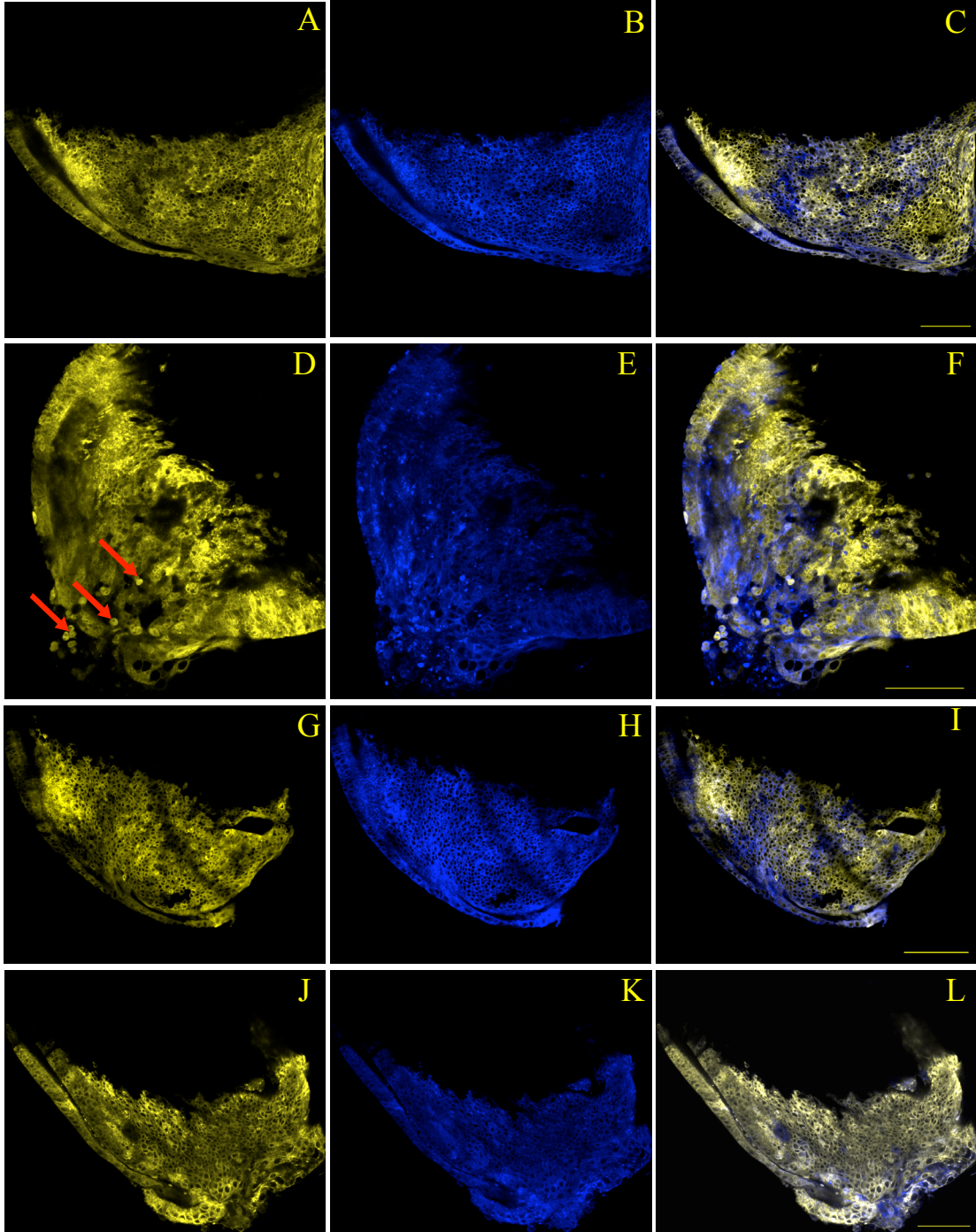
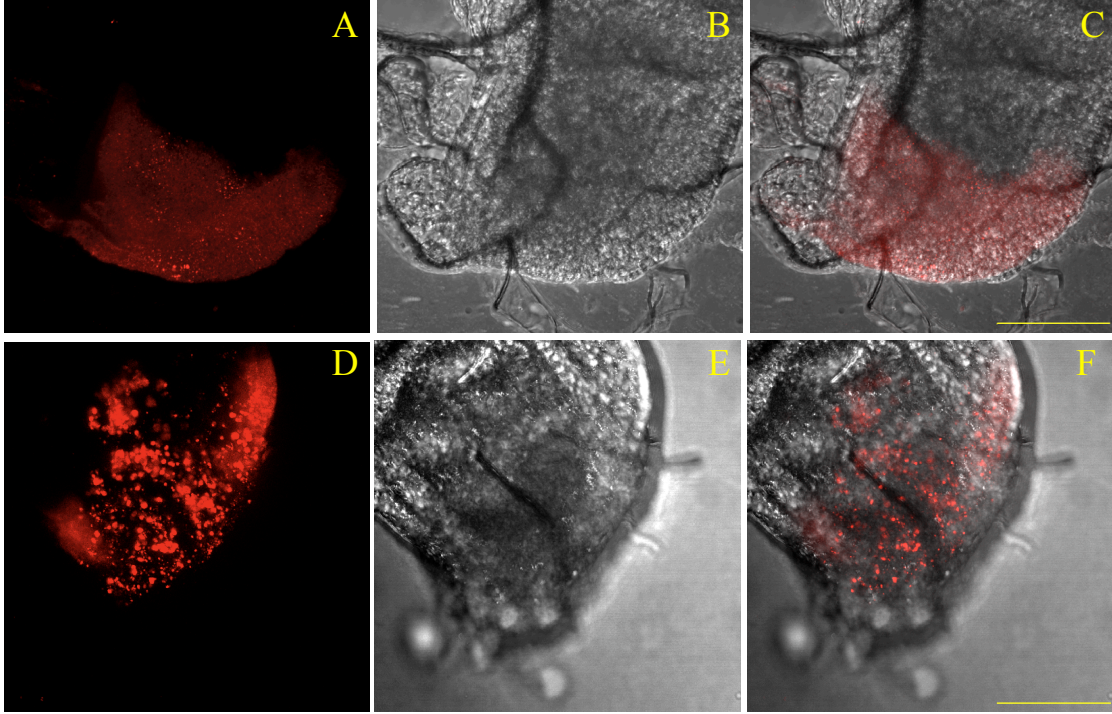


Figure 3.9: Confocal Micrographs of third instar wing discs expressing *UAS-mCherry-DrAtg8a*. (A-C) Control wing disc with the genotype: *pnrGAL4/UAS-mCherry-DrAtg8a*. (A) Image illustrating homogeneous RFP (red) localization in the control wing disc. (B) Transmitted light image of the proximal area of the control wing disc. (C) mCherry and transmitted light images merged together. (D-F) Wing disc with the genotype: *pnrGAL4+Atg1^{6B}/UAS-mCherry-DrAtg8a*. (D) Image illustrating strong punctate RFP due to *Atg1^{6B}* overexpression. (E) Transmitted light image of the proximal area of a wing disc overexpressing *Atg1^{6B}*. (F) mCherry and transmitted light images of the wing disc overexpressing *Atg1^{6B}*. Scale bars indicate a distance of 50 μ m.



3.4 Results: Studying Autophagy-Dependent Caspase Activation in Adult Cuticular Structures

In the previous sections it was determined that the overexpression of *AtgI^{6B}* in the larval wing disc results in a dramatic increase in autophagosome and autolysosome formation and is associated with caspase-activation. Similarly, the overexpression of *AtgI^{6B}* results in the inappropriate elimination of the larval epidermal cells. Together, the elimination of these tissues promotes an interesting adult cuticular phenotype. This phenotype was examined in detail using Scanning Electron Microscopy (SEM).

When compared to *yw*, *pnrGAL4* adults exhibit normal thorax and abdomen development, demonstrating a wildtype phenotype (Figure 3.10). Therefore, *pnrGAL4* was used as the control for all subsequent SEM images (Figure 3.11 A, B).

After establishing *pnrGAL4* as a control, SEM was performed on adult *Drosophila* overexpressing *AtgI^{6B}* along the dorsal midline throughout development. Scanning electron micrographs of adults overexpressing *AtgI^{6B}* illustrate strong thoracic and moderate abdominal clefts and a reduced scutellum (Figure 3.11 E, F). To establish whether this adult cuticular phenotype was the result of autophagy-induced caspase activation, *p35* was co-expressed in tissues overexpressing *AtgI^{6B}* throughout development. As a result, the co-expression of *p35* is pupal lethal and does not suppress the thoracic, abdominal or scutellar phenotype associated with *AtgI^{6B}* overexpression (data not shown). Additionally, adults ectopically expressing *p35* alone demonstrate a slight cleft down the dorsal midline of the notum and mild abdominal cleft (Figure 3.11 C, D).

Interestingly, since we are using an expression system that can be modulated by a shift in temperature, we know that these adult cuticular phenotypes can be enhanced or suppressed based on the levels of *AtgI^{6B}* expression. Adults raised at 29°C, increasing *AtgI^{6B}* expression

in tissues specified by *pnrGAL4*, completely lack a scutellum and display a more prominent thoracic and abdominal cleft (Figure 3.11 G, H). In contrast, adults that were allowed to develop at 18°C, decreasing *Atg1^{6B}* expression, have a less prominent thoracic and abdominal cleft, and the scutellum is only slightly reduced (data not shown).

Figure 3.10: Scanning Electron Micrograph of *Drosophila* adult cuticular structures. (A,B) Images illustrating the thorax and scutellum, collectively called the notum. (C, D) Images illustrating the dorsal surface of the abdomen. (A,C) Adult cuticular structures of a fly with the genotype: *yw*. (B, D) Adult cuticular structures of a fly with the genotype: *pnrGAL4/+*. Adults were 3-7 days old. These crosses were performed at 25°C.

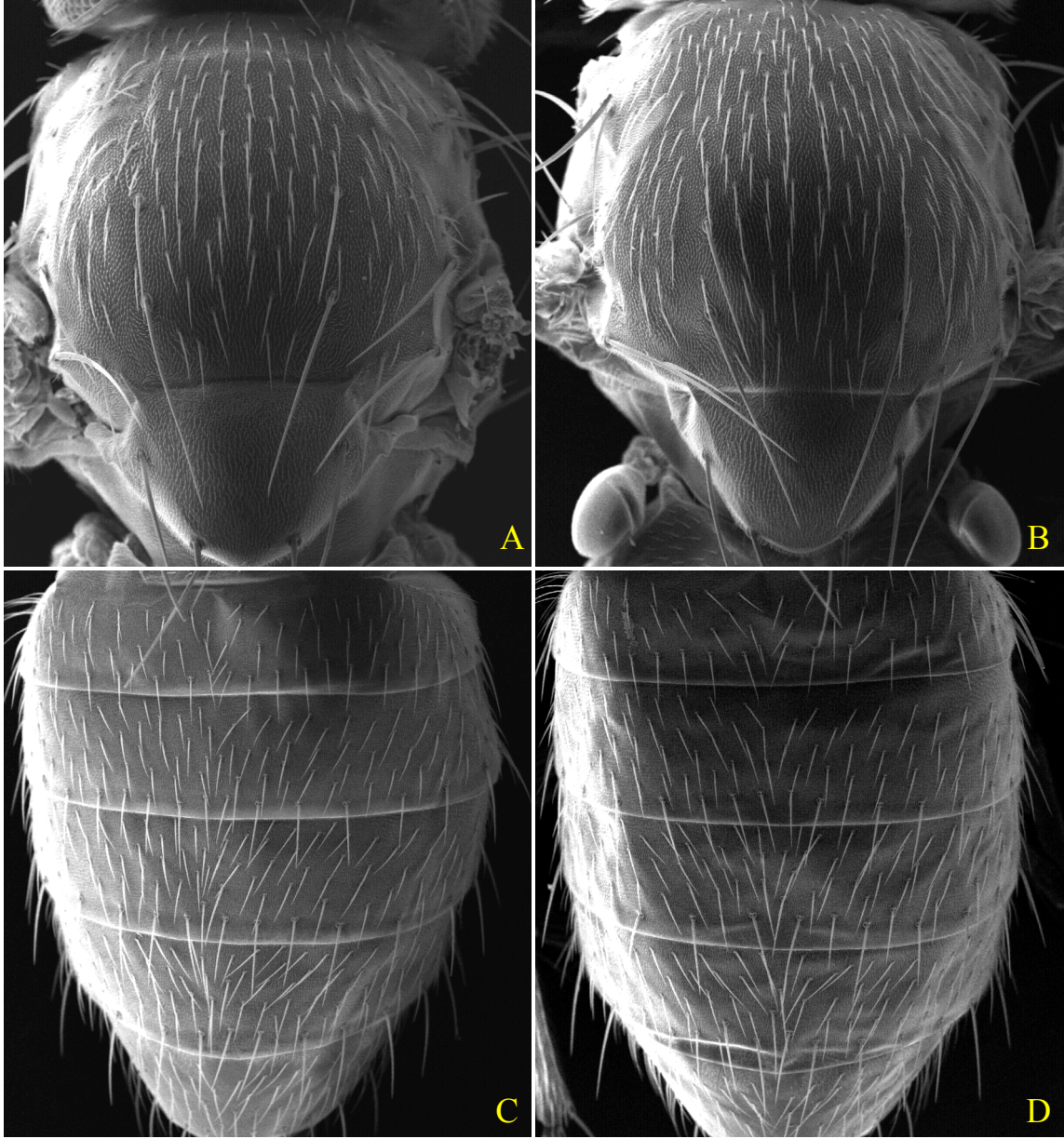
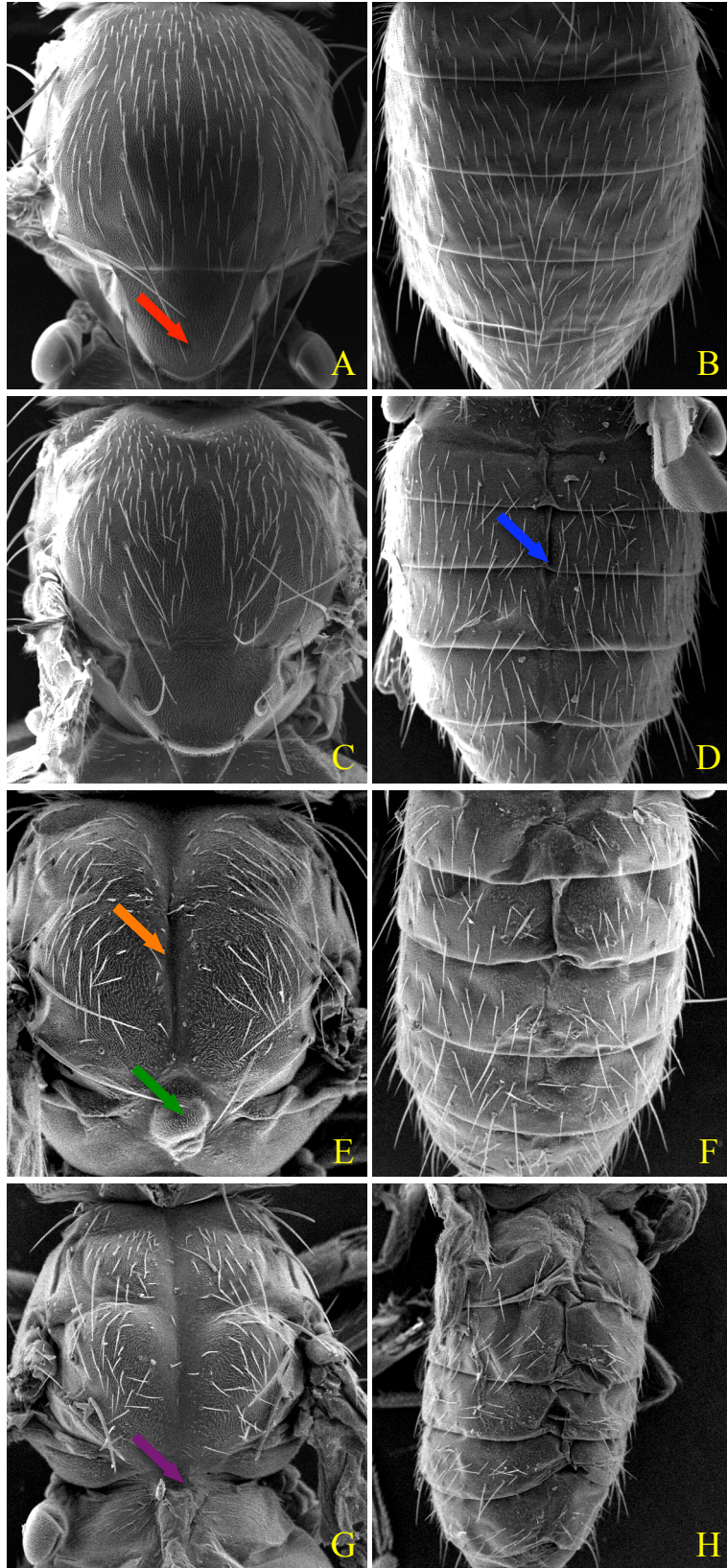


Figure 3.11: Scanning Electron Micrographs of adult cuticular structures. (A, B) *pnrGAL4/+* adult notum (A) (scutellum identified by the red arrow) and abdomen (B) demonstrating a wildtype phenotype. (C, D) *UAS-p35/+; pnrGAL4/+* adult developed at 25°C exhibiting a hairless line with a slight indent down the midline of the thorax (C) and a mild abdominal cleft (blue arrow)(D). (E, F) *pnrGAL4/UAS-Atg1^{6B}* adult that developed at 25°C exhibiting a reduced scutellum (green arrow) and a thoracic cleft (orange arrow) (E). A moderate cleft down the abdomen is also observed (F). (I, J) *pnrGAL4/UAS-Atg1^{6B}* adult that developed at 29°C illustrating a severe cleft down the dorsal midline of the thorax (I) and a strong cleft down the abdomen (J). Scutellum is absent (purple arrow)(I).



3.5 Results: Evaluating Autophagy Dependent Caspase-Activity during Metamorphosis.

In the previous section it was observed that the overexpression of *Atg1^{6B}*, in tissues specified by *pnrGAL4*, results in a striking adult cuticular phenotype (Figure 3.11E, F). Unfortunately, this adult cuticular phenotype could not be rescued through co-expression of *p35*. Also, the ectopic expression of *p35* alone results a mild abdominal cleft along with a slight cleft along the midline of the notum (Figure 3.11 C, D).

Since these results were unexpected, the larval epidermis and presumptive adults cells were observed in detail throughout metamorphosis. In particular, the effect of ectopic *p35* expression was observed in tissues overexpressing *Atg1^{6B}*. To visualize these dorsal epithelial segments, *pnrGAL4+UAS-GFP^{nls}/TM3,Sb* and *pnrGAL4+UAS-Atg1^{6B}+UAS-Apoliner/TM6, Tb[GAL80]* were crossed to the various UAS-constructs. When using this elegant design, only the GFP expressing progeny, resulting from these two parental stocks, are those expressing the UAS-constructs.

3.5.1 Autophagy-Activated Apoptosis During Pharate Adult Formation

Timelapse stereomicroscopic live imaging of control pupae expressing nuclear GFP under the control of the *pnrGAL4* driver reveals the dynamic behavior of tissues during metamorphosis. Through this form of live imaging it is demonstrated that the large polyploid larval epidermal cells undergo PCD and dissociate as the abdominal histoblast nests expand and fuse with neighboring nests (For more information on abdomen development, See Appendix A Section A.4). Interestingly, the formation of the adult abdomen occurs much later than the fusion of the wing imaginal discs to form the notum. Thoracic larval epidermal PCD and the fusion of the imaginal wing discs could not be properly evaluated as thorax

development occurs too quickly. However, the formation of the scutellum, from a protrusion at the dorsal-posterior end of the fused wing disc, can be observed clearly using this method (Figure 3.12 – Control) (For more information on thorax development, See Appendix A - Section A.3).

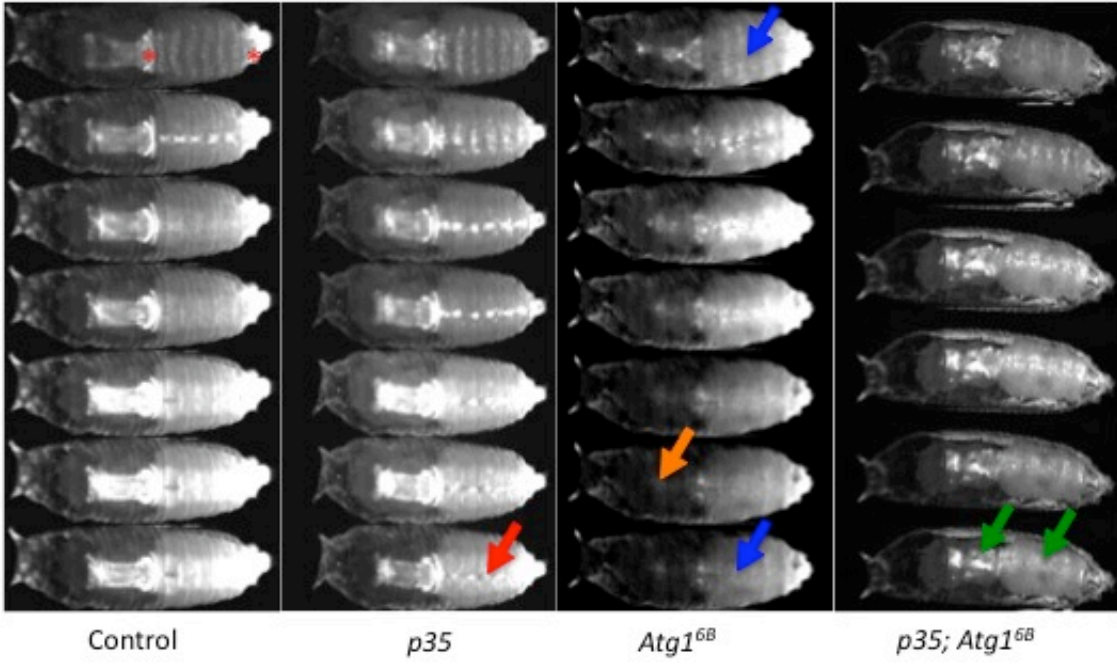
Afterwards, stereomicroscopic live imaging was performed on pupae ectopically expressing *p35*. The ectopic expression of *p35*, in tissues specified by *pnrGAL4*, results in a persistent larval epidermis. The continued presence of the abdominal larval epithelial cells inhibits the proper fusion of the histoblast nests, resulting in an abdominal cleft down the dorsal midline. Also, a slight thoracic cleft is observed in the later stages of development (Figure 3.12 – *p35*). The development of the scutellum appears to be unaffected by the ectopic expression of *p35*.

In contrast to previous results involving *p35* expression, the ectopic overexpression of *Atg1^{6B}* results in the premature elimination of larval epithelial cells (As observed previously in Figure 3.7 C, D). Furthermore, upon entering the domain of *pnrGAL4*, histoblast nests acquire ectopic overexpression of *Atg1^{6B}* and subsequently undergo cell death. This premature larval epithelial and inappropriate histoblast cell death appears to inhibit the proper fusion of histoblast nests, resulting in a strong abdominal cleft down the dorsal midline (Figure 3.12 - *Atg1^{6B}*). During the later stages of development, a thoracic defect could also be observed in pupae overexpressing *Atg1^{6B}* (Figure 3.12 - *Atg1^{6B}*). Although wing disc fusion could not be directly assessed, it is presumably the elimination of the larval epidermal cells and imaginal wing disc cells that inhibits thorax closure, resulting in an adult cuticular phenotype. This assumption was reinforced by previous work, revealing that the pre-pupal to the mid phanerocephalic stages, a developmental period in which wing discs grow, divide and fuse

with their counterparts (Fristrom and Fristrom, 1993), were the most sensitive developmental stages, with respect to *Atg1^{6B}* overexpression (See Appendix C).

Finally, as expected the co-expression of *p35* does not rescue the adult cuticular phenotype associated with the overexpression of *Atg1^{6B}* (Figure 3.12 – *p35; Atg1*). Upon initial observation, the larval epidermis is absent, indicating *p35* could not rescue the premature cell death of the larval epidermis during the pupal stages. Furthermore, upon entering the domain of *pnrGAL4*, histoblast nests are eventually eliminated after acquiring *p35* and *Atg1^{6B}* expression. The elimination of histoblast nests inhibits abdomen formation, resulting in a strong abdominal cleft. During the later stages of development, a strong defect in the notum (a strong cleft and absent scutellum) was observed in pupae co-expressing *Atg1^{6B}* and *p35* (Figure 3.12 – *p35; Atg1*). Eventually, the co-expression of *Atg1^{6B}* and *p35* results in lethality during the late pupal stages.

Figure 3.12: Timelapse stereomicroscopic live imaging of four *Drosophila* pupae. Each subsequent image is 7.5 hrs with the earliest developmental stage at the top and the latest developmental stage at the bottom. The captions along the bottom of the diagram indicate the control or the genotype of the four pupae. (Control) Pupae with the genotype: *pnrGAL4+UAS-GFP^{nl5}/+*, expressing nuclear GFP in the abdominal larval epidermis (between red stars) and notum. The abdominal larval epidermal cells undergo PCD while the histoblast nests expand and fuse with their counterparts. (*p35*) Pupae with the genotype: *UAS-p35/+; pnrGAL4+UAS-GFP^{nl5}/+*, ectopically expressing *p35* in the domain of *pnrGAL4*. Persistent larval epidermal cells inhibit the fusion of the histoblast nests (red arrow), resulting in an abdominal cleft. (*Atg1^{6B}*): Pupae with the genotype: *pnrGAL4+UAS-GFP^{nl5}/UAS-Atg1^{6B}*, overexpressing *Atg1^{6B}* in the domain of *pnrGAL4*. Larval epidermal cells are absent (top blue arrow). AS abdominal histoblasts acquire *Atg1^{6B}* overexpression as they enter the domain of *pnrGal4* and subsequently die, resulting in a large abdominal cleft (bottom blue arrow). Near the end of development a thoracic cleft is present (orange arrow). (*p35;Atg1^{6B}*) Pupae with the genotype: *UAS-p35/+;UAS-p35/+;UAS-Atg1^{6B}+pnrGAL4+UAS-Apoliner/+*, ectopically expressing *p35* in cells overexpressing *Atg1^{6B}*. There is no rescue of the larval epidermis, resulting in an abdominal and thoracic cleft (green arrows). All crosses were performed at 25°C.



Chapter 4. Genetic Screen

Chapter 4. Genetic Screen

In previous chapters, it was established that autophagy induces caspase-activity in the third instar wing disc and presumably the larval epidermis. Unfortunately, the striking adult cuticular phenotype associated with the overexpression of *Atg1^{6B}* could not be rescued through the co-expression of *p35*. The inability to rescue the adult cuticular phenotype indicates there is no direct correlation between the adult phenotype and autophagy-dependent caspase activation. However, through changes in temperature, it was demonstrated that the adult cuticular phenotype could be enhanced or suppressed based on the levels of *Atg1^{6B}* expression. Two possibilities might explain these observations. First, high levels of autophagy could result in the caspase-independent autophagic death of tissues during the late stages of metamorphosis. Second, it could be that the adult cuticular phenotype is independent of cell death and results from a failure of autophagic cells to secrete adult cuticle.

In either case, the adult cuticular phenotype is an attractive background to screen for dose-sensitive modifiers of *Atg1^{6B}* overexpression. Any chromosomal regions identified as harboring a dose-sensitive modifier might be associated with either the progression of autophagy or a disruption of the expression of the *pnrGAL4* driver. While the disruption of *pnrGAL4* might be considered a false positive in the genetic screen, the regulation of the *pannier* gene is itself of interest in terms of pattern formation during *Drosophila* development. Clearly, however, it is the goal of this study to identify genes that regulate autophagy and, in particular, promote caspase activation in response to the up-regulation of autophagy.

A dose-sensitive modifier screen of the adult cuticular phenotype will certainly “cast a broad net” and will potentially identify regions of the genome that house genes involved in

any aspect of the regulation of autophagy. Also, any regions that affect the regulation of the *pnrGAL4* driver, and the secretion of the adult cuticle could be identified. Therefore, a secondary screen will be required to separate these different categories of interactors (See Future Directions).

4.1 Genetic Screen for Chromosomal Regions that Dominantly Interact with *Atg1^{6B}*

A genetic screen, using *Atg1^{6B}* overexpression at 25°C in the domain of *pnrGAL4* expression as our sensitized genetic background, was performed to find dose-sensitive modifiers of the *Atg1^{6B}* overexpression phenotype. 399 deficiencies were tested,¹ 198 on the 2nd chromosome and 201 on the 3rd chromosome that collectively remove an estimated 92% of the 2nd and 3rd chromosomes (Table 4.2). In addition, 25 duplications, that cover an estimated 66% of the 2nd and 3rd chromosomes, were tested (See Appendix D for a complete list of duplications and deficiencies). During the genetic screen, progeny carrying one copy of the deficiency (or duplication) and overexpressing *Atg1^{6B}* were compared to sibling *Atg1^{6B}* overexpressing progeny carrying a balancer chromosome (For details see Materials and Methods). The severity of the thoracic and abdominal clefts and the reduced scutellum phenotype was evaluated and compared between the two groups. Dominant interacting deficiencies and duplications were identified based on the criteria given on Table 4.1. It should be noted that the “Undefined Modifier” phenotypes are so named because they exhibit characteristics of both enhancers and suppressors. These “Undefined Modifiers” have no thoracic cleft, indicating a suppressed phenotype; however, the notum is small with no scutellum and the abdomen possesses a strong to moderate cleft, indicating an enhanced

¹ Deficiency = Single Chromosomal Deletion

phenotype. In addition, some interacting deficiencies were identified as false positives. False positives are classified as any modifier that effects *pannier* expression, deletes the *pannier* region, deletes a region that contains a *haplo-insufficient* lethal loci, or a deletes a *Minute* region.² However, an interacting deficiency covering a *Minute* region is not classified as a false positive if another non-interacting deficiency covers the same area as the *Minute*. Deficiencies and duplications suspected to be false positives are indicated in Appendix D.

Based on the previously mentioned criteria (Table 4.1), seventy-nine out of the 399 deficiencies were identified that modify the *Atg1^{6B}* overexpression phenotype. Of the seventy-nine deficiencies, forty-two are dominant enhancers, twenty-four are dominant undefined modifiers, and thirteen deficiencies are dominant suppressors (Figures 4.2-4.5, Tables 4.2-4.7). These interacting deficiencies account for 19.80% of all tested deficiencies (Table 4.2). Of the seven interacting duplications, two are dominant suppressors, four are dominant enhancers, and one is an undefined modifier (Figures 4.2- 4.5; Tables 4.3-4.7). These interacting deficiencies and duplications represent a collective 44 “interacting regions” on the second and third chromosomes (Tables 4.3-4.7; Figures 4.2- 4.5). Interacting regions, in this thesis, are defined as cytological locations on the chromosome that contain overlapping interacting deficiencies and/or duplications. These interacting regions do not contain non-interacting deficiencies (Figure 4.1A). If an interacting deficiency does not overlap with another interacting deficiency the interacting region is identical to the cytology of that deficiency (Figure 4.1B).

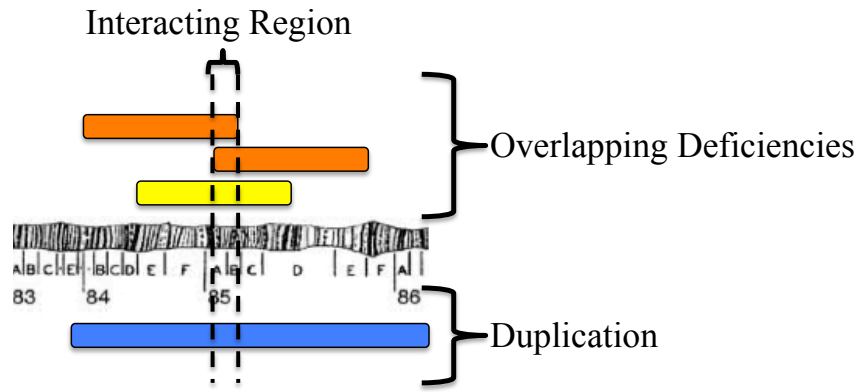
² *Minute* regions contain loci that code for ribosomal proteins. The deletion of a *Minute* region results in a developmental delay and short, usually thin, bristles (Ashburner, 1989).

Table 4.1: Criteria For The Classification Of Phenotypes During The Genetic Screen

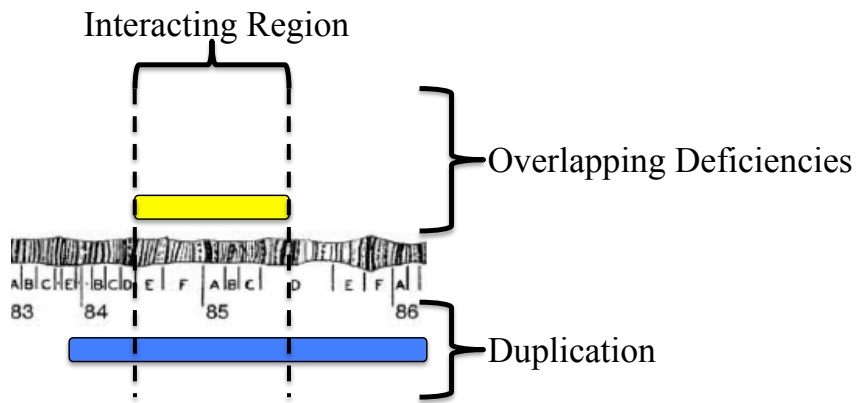
Class	Associated Phenotypes³
Undefined Modifier (UM)	<p>A “Coherent thorax phenotype”.</p> <ul style="list-style-type: none"> - No thoracic cleft but thorax is small. - No scutellum - Strong to moderate abdominal clefts
Enhancer (EN+)	<p>A Moderate Enhancer – Semi Lethal Phenotype</p> <ul style="list-style-type: none"> - 5+ escapers - Strong thoracic clefts - Strong abdominal clefts. - No scutellum.
Enhancer (EN++)	<p>A Strong Enhancer – Lethal Phenotype</p> <ul style="list-style-type: none"> - 1 - 4 escapers - Strong thoracic clefts - Strong abdominal clefts - No scutellum
Suppressor (SU-)	<p>A Moderate Suppression Phenotype</p> <ul style="list-style-type: none"> - Viable - Mild thoracic cleft - An indent along the midline of the thorax. Overall size similar to wildtype. - Moderate to mild abdominal clefts. - Mild reduction in scutellar size (no less than ½ the size of wildtype).
Suppressor (SU--)	<p>A Strong Suppression Phenotype</p> <ul style="list-style-type: none"> - Viable - No thoracic cleft - A hairless line and a very slight indent along the thoracic midline. Overall size close to that of wildtype. - Mild to no abdominal cleft - Scutellum only slightly reduced (no less than ¼ the size of wildtype).

³ All identified enhancements, suppressions and undefined modifiers were classified based on these criteria.

Figure 4.1: Diagram illustrating the definition of an “interacting region” and the criteria for identifying targeted interacting regions (A) Diagram illustrating the interacting region associated with three overlapping deficiencies (orange and yellow rectangles) and a complementing interacting single duplication (blue rectangle). (B) Diagram illustrating the interacting region associated with a single, non-overlapping deficiency (yellow rectangle) with a complementing single duplication (blue rectangle). The interacting regions are located between the two dashed lines. It should be noted that the deficiencies and duplications depicted on these diagrams do not reflect the results from the genetic screen.



(A)



(B)

Table 4.2: Summary Table Illustrating The Results Of The Genetic Screen.

	Total Number of Deficiencies	Percent Chromosome Coverage⁴	Total Interacting Deficiencies⁵	Percent Interacting Deficiencies⁶
Chromosome 2	198	≈ 91%	30	15.15%
Chromosome 3	201	≈ 94%	49	24.38%
Total⁷	399	≈92%	79	19.80%

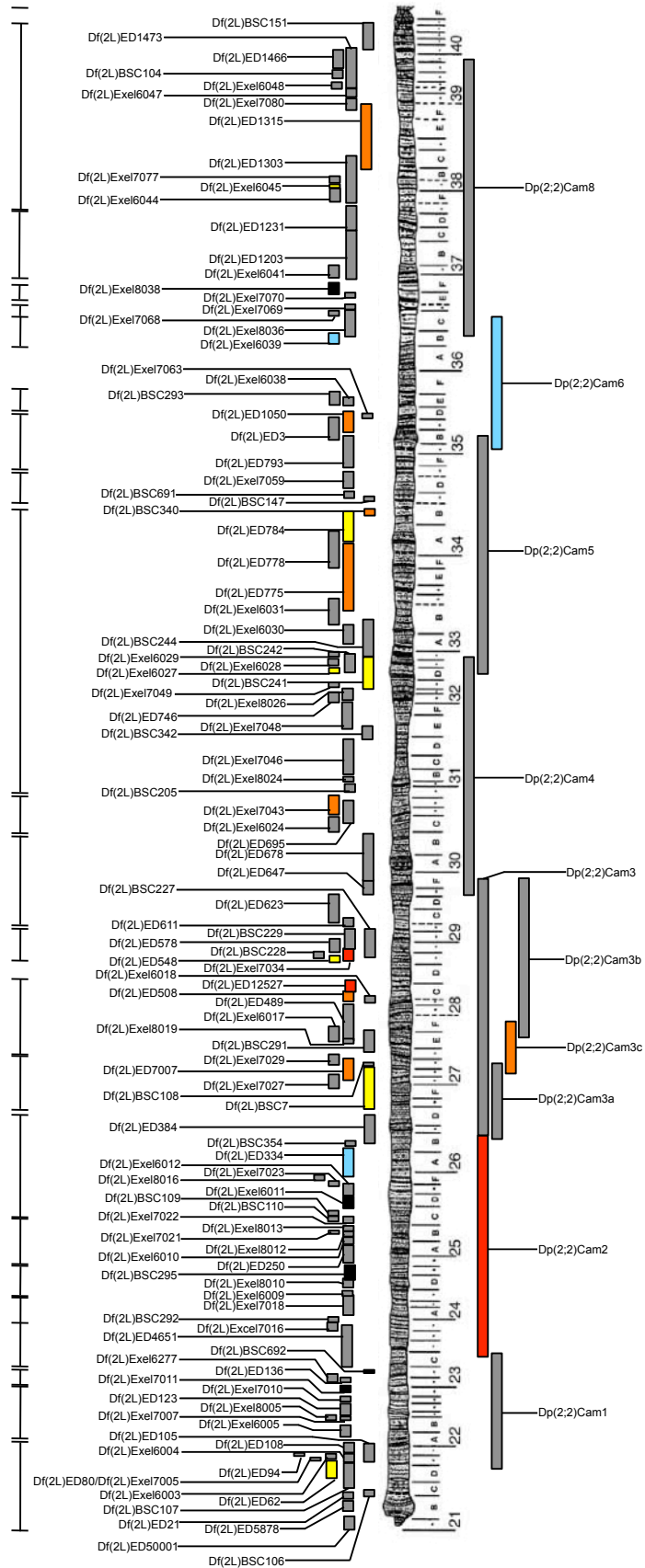
⁴ Percent chromosome coverage was calculated by dividing the total coverage given by black lines and by the total length of the chromosome arm (Figures 4.2-4.5).

⁵ Total Interacting Deficiencies = the total number of deficiencies that are identified suppressors, enhancers or are undefined modifiers of the *Atg1^{6B}* overexpression phenotype.

⁶ The Percent Interacting Deletions was calculated by dividing the total interacting deletions by the total number of deletions tested.

⁷ Total was calculated by adding the numbers from Chromosomes 2 and 3.

Figure 4.2: Diagram of the 2L deficiency and duplication map. Deficiencies are illustrated as the boxes above of the chromosome and duplications are shown as boxes below the chromosome. Black lines indicate the approximate coverage of the duplications and deficiencies. The black lines above the chromosome indicate the deficiency coverage was approximately 93%. The black line below the chromosome indicates the duplication coverage was approximately 92%. Black rectangles indicate the deficiency is a false positive. The class false positive is given to any modifier that contains a *haplo-insufficient* lethal gene, or a deletes a *Minute* region. Light Blue rectangles indicate a moderate suppression. Dark Blue indicates a strong suppression. Red rectangles indicate a strong enhancement and orange rectangles indicate a moderate enhancement. Yellow rectangles indicate an undefined modifier phenotype.



Legend

- Suppression
- Moderate Suppression
- Strong Enhancers - Lethal
- Moderate Enhancers - Semi-Lethal
- Unidentified Modifiers (Viable)
- No Effect
- False Positives

Figure 4.3: Diagram of the 2R deficiency and duplication map. Deficiencies are illustrated as boxes above the chromosome and duplications are shown as boxes below the chromosome. Black lines indicate the approximate coverage of the duplications and deficiencies. The black lines above the chromosome indicate deficiency coverage was approximately 89%. The black lines below the chromosome indicate approximate duplication coverage was 95%. Black rectangles indicate that the associated interaction is a false positive. The class false positive is given to any modifier that contains a *haplo-insufficient* lethal gene, or a deletes a *Minute* region. Light Blue rectangles indicate a moderate suppression. Dark Blue indicates a strong suppression. Red rectangles indicate a strong enhancement and orange rectangles indicate a moderate enhancement. Yellow rectangles indicate an undefined modifier phenotype.

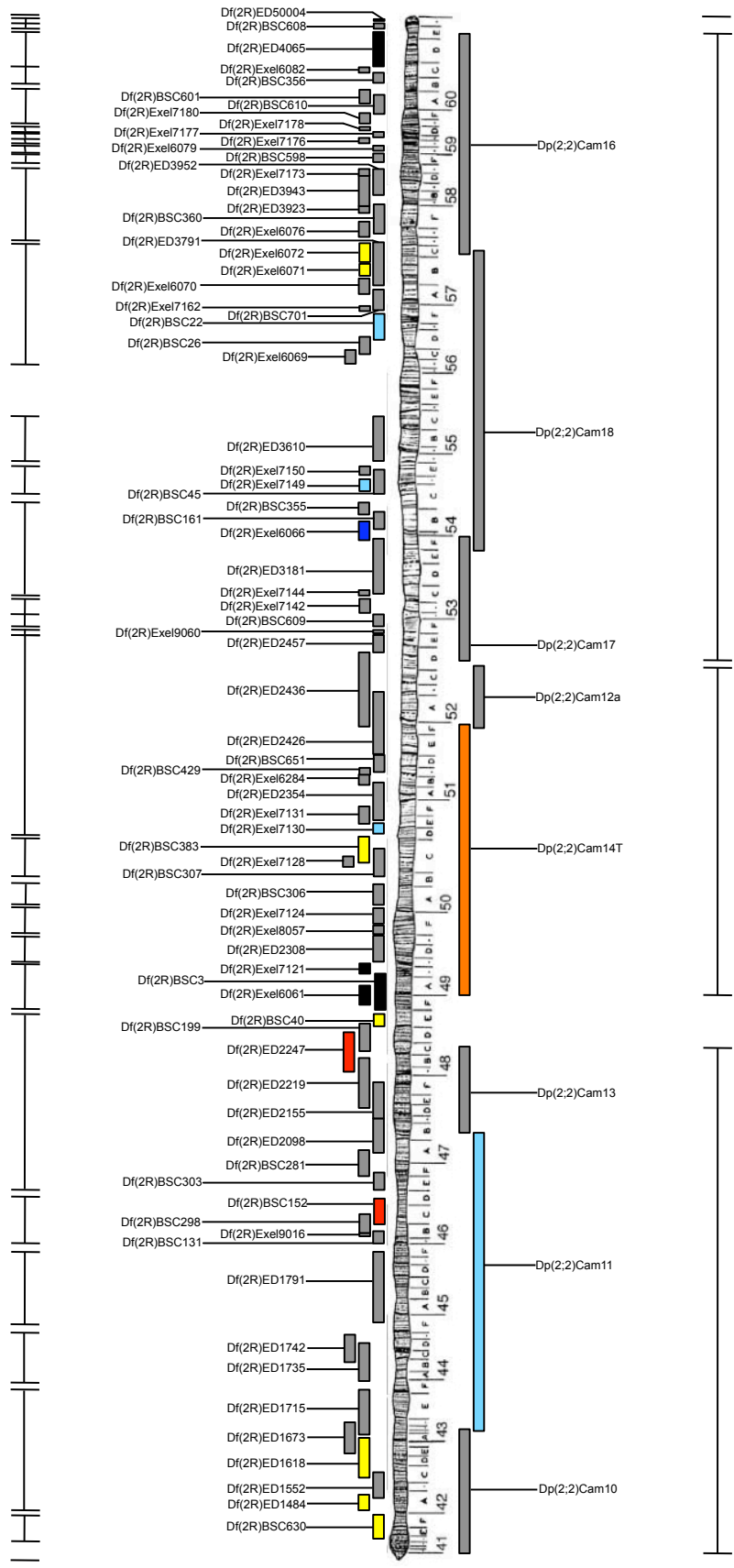
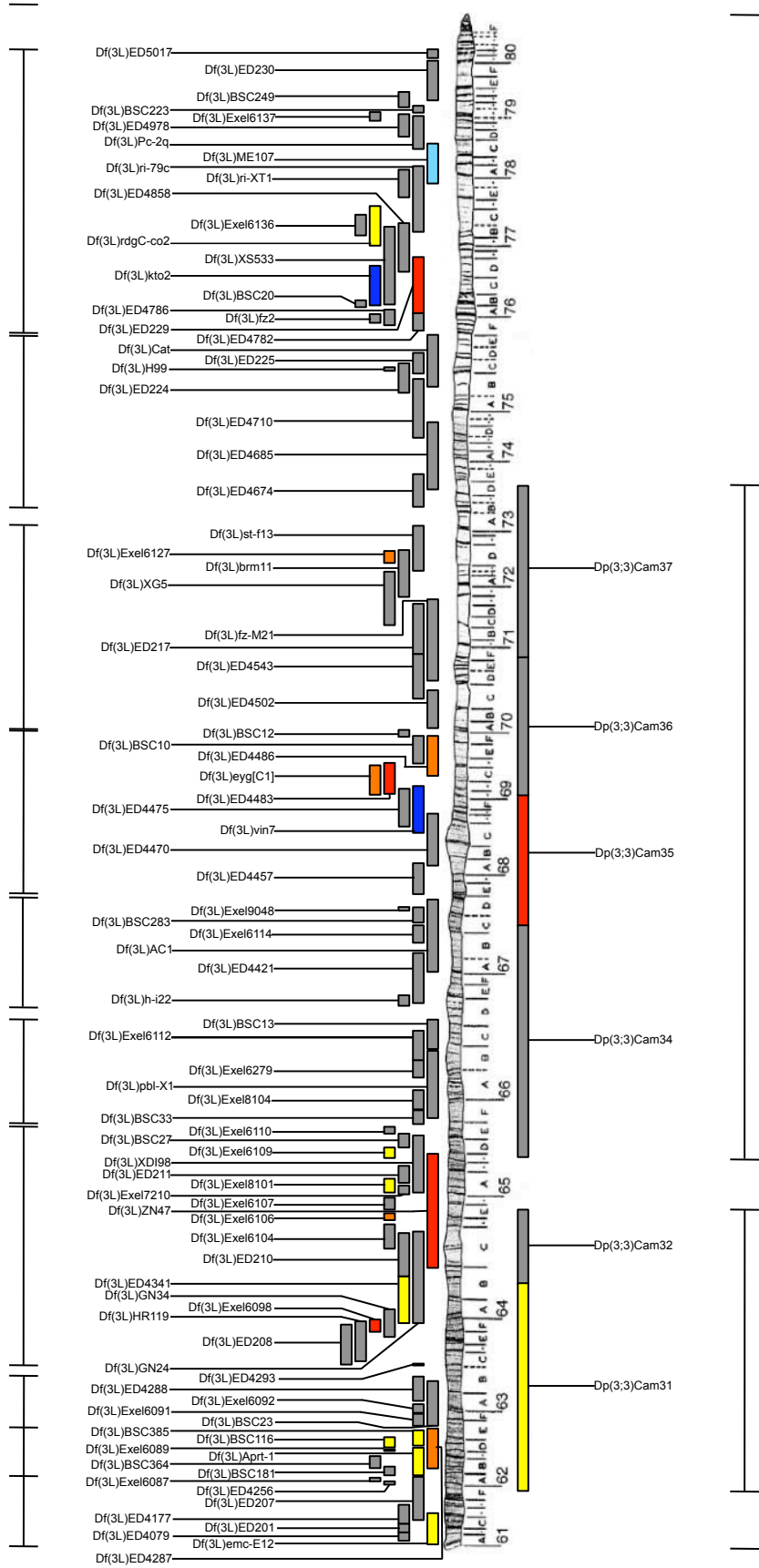


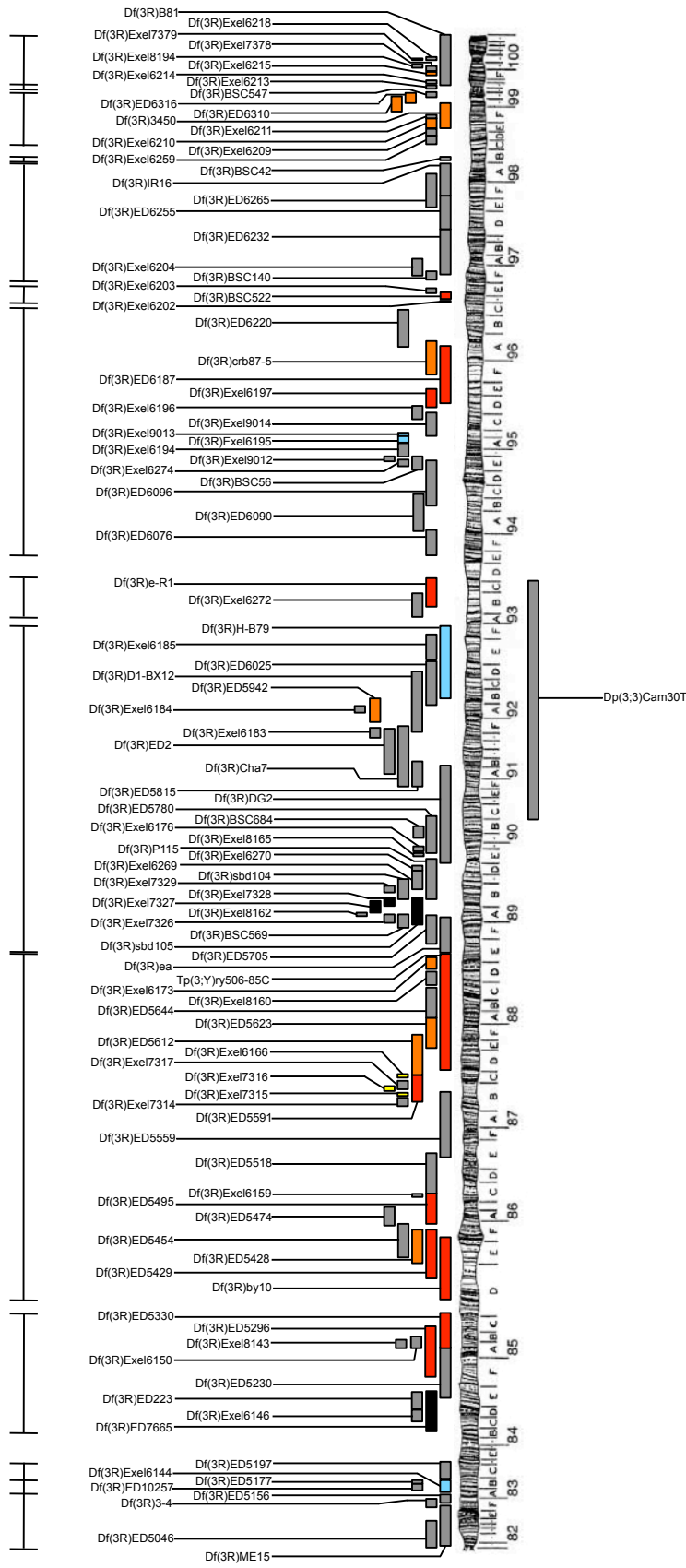
Figure 4.4: Diagram of the 3L deficiency and duplication map. Deficiencies are illustrated to above the chromosome and duplications are shown below the chromosome. Black lines indicate the coverage of the duplications and deficiencies. The black lines above the chromosome indicate the deficiency coverage was approximately 94%. The black lines below the chromosome indicate the duplication coverage was approximately 63%. Black rectangles indicate a false positive enhancement. The class false positive is given to any modifier that contains a gene that is *haplo-insufficient* lethal, or a deletes a *Minute* region. Light Blue rectangles indicate a moderate suppression. Dark Blue indicates a strong suppression. Red rectangles indicate a strong enhancement and orange rectangles indicate a moderate enhancement. Yellow rectangles indicate an undefined modifier phenotype.



Legend

- Suppression
- Moderate Suppression
- Strong Enhancers - Lethal
- Moderate Enhancers - Semi-Lethal
- Unidentified Modifiers (Viable)
- No Effect
- False Positives

Figure 4.5: Diagram of the 3R deficiency and duplication map. Deficiencies are illustrated as the boxes above the chromosome and duplications are shown as boxes below the chromosome. Black lines indicate the approximate coverage of the duplications and deficiencies. The black lines above the chromosome indicate the deficiency coverage was approximately 93%. The line below the chromosome indicates the duplication coverage was approximately 16%. Black rectangles indicate the interaction is a false positive. The Class false positive is given to any modifier that interacts with *pnrGAL4*, contains a gene that is *haplo-insufficient* lethal, or a deletes a *Minute* region. Light Blue rectangles indicate a moderate suppression. Dark Blue indicates a strong suppression. Red rectangles indicate a strong enhancement and orange rectangles indicate a moderate enhancement. Yellow rectangles indicate an undefined modifier phenotype.



Legend

- Suppression
- Moderate Suppression
- Strong Enhancers - Lethal
- Moderate Enhancers - Semi-Lethal
- Unidentified Modifiers (Viable)
- No Effect
- False Positives

Table 4.3: Strong Suppressors Identified In The Genetic Screen

Chromosome Aberration (Stock)	Cytology Of Dp or Df	Associated Interacting Regions*
<i>Df(2R)Exel6066</i> (7548)	53F9; 54B6	53F10; 54B2
<i>Df(3L)vin7</i> (2612)	68C8-11; 69B4-5	Conflicting Overlap
<i>Df(3L)kto2</i> (3617)	76B1-2; 76D5	Conflicting Overlap

* “Conflicting Overlap” indicates there exists another deficiency in the same region that did not exhibit an interaction with the *Atg1^{6B}* overexpression phenotype.

Table 4.4: Moderate Suppressors Identified In The Genetic Screen.

Chromosome Aberration (Stock)	Cytology Of Dp or Df	Associated Interacting Regions*
<i>Df(2L)ED334</i> (9343)	25F2; 26B2	25F2; 26B1
<i>Dp(2;2)Cam6</i> (4518)	35B; 36C	35D1; 35D2
<i>Df(2L)Exel6039</i> (7522)	36A10; 36B3	36A10; 36B1
<i>Dp(2;2)Cam11</i> (2626)	43B3-C1; 47B10-14	46C7; 46D6
<i>Df(2R)Exel7130</i> (7875)	50D4; 50E4	50C9; 50E4
<i>Df(2R)Exel7149</i> (7890)	54C10; 54D5	Conflicting Overlap
<i>Df(2R)BSC22</i> (6647)	56D7-E3; 56F9-12	56D10; 56F11
<i>Df(3L)ME107</i> (4429)	77F3; 78C8-9	78A2; 78C5
<i>Df(3R)Exel6144</i> (7623)	83A6; 83B6	83A6
<i>Df(3R)H-B79</i> (4962)	92B3; 92F13	Conflicting Overlap
<i>Df(3R)Exel6195</i> (7674)	95A4; 95B1	95A4; 95B5
<i>Df(3R)Exel9013</i> (7991)	95B1; 95B5	95A4; 95B5

*“Conflicting Overlap” indicates there exists another deficiency in the same region that did not exhibit an interaction with the *Atg1^{6B}* overexpression phenotype.

Table 4.5: Strong Enhancers Identified In The Genetic Screen

Chromosome Aberration (Stock)	Cytology Of Dp or Df	Associated Interacting Regions*
<i>Dp(2;2)Cam2</i> (3394)	23D1-2; 26C1-2	25F2; 26B1
<i>Df(2L)ED12527</i> (24129)	28C4; 28D3	28C1; 28E5
<i>Df(2L)Exel7034</i> (7807)	28E1; 28F1	28C1; 28E5
<i>Df(2L)ED784</i> (7421)	34A4; 34B6	34B4; 34B6
<i>Df(2R)BSC152</i> (9539)	46C1; 46D6	46C7; 46D6
<i>Df(2R)ED2247</i> (8912)	48A3; 48D5	48B6; 48C5
<i>Dp(2;3)Cam14T</i> (4519)	49A; 51E-F	50D4; 50E4
<i>Df(3L)Exel6098</i> (7577)	63F2; 63F7	Conflicting Overlap
<i>Df(3L)ZN47</i> (3096)	64C; 65C	64D6; 64E2
<i>Dp(3;3)Cam35</i> (5745)	67C5-11; 69A4-5	68C8-11; 69A4-5
<i>Df(3L)ED4483</i> (8070)	69A4; 69D3	69C4; 69D3
<i>Df(3L)ED229</i> (8087)	76A1; 76E1	76A5; 76A7
<i>Df(3R)ED5296</i> (9338)	84F6; 85C3	85B6; 85C3
<i>Df(3R)ED5330</i> (9077)	85A5; 85D1	85B6; 85C3
<i>Df(3R)by10</i> (1931)	85D8-12; 85E7-F1	85E1; 85E5
<i>Df(3R)ED5429</i> (8919)	85D19; 85F8	85E1; 85E5
<i>Df(3R)ED5495</i> (9215)	85F16; 86C7	86B1; 86C3
<i>Df(3R)ED5591</i> (9086)	87B7; 87C7	87C3; 88A4
<i>Df(3R)Tp(3;Y)ry506 85C</i> (1534)	87D1-2; 88E5-6	87E3; 88A4 88D7; 88E1
<i>Df(3R)e-R1</i> (3340)	93B6-7; 93D2	93B13; 93D2
<i>Df(3R)Exel6197</i> (7676)	95D8; 95E1	95D10; 95E1
<i>Df(3R)ED6187</i> (9347)	95D10; 96A7	95F7; 96A7
<i>Df(3R)Exel6202</i> (7681)	96D1; 96D1	96D1; 96D1
<i>Df(3R)BSC522</i> (25050)	96D1; 96E3	96D1; 96D1

*“Conflicting Overlap” indicates there exists another deficiency in the same region that did not exhibit an interaction with the *Atg1^{6B}* overexpression phenotype.

Table 4.6: Moderate Enhancers Identified In The Genetic Screen.

Chromosome Aberration (Stock)	Cytology	Associated Interacting Regions*
<i>Dp(2;2)Cam3c</i> (8541)	27C; 27F	Conflicting Overlap
<i>Df(2L)ED508</i> (8944)	28B1; 28C4	28C1; 28D3
<i>Df(2L)Exel7043</i> (7816)	30D1; 30F1	30E4; 30F1
<i>Df(2L)ED775</i> (8907)	33B8; 34A3	33C2; 33E9
<i>Df(2L)BSC340</i> (24364)	34B4; 34B8	34B6; 34B8
<i>Df(2L)ED1050</i> (8946)	35B8; 35D4	35D1; 35D2
<i>Df(2L)ED1315</i> (9269)	38B4; 38F5	38C6; 38F3
<i>Df(3L)ED4287</i> (8096)	62B4; 62E5	62D4; 62E1 62C4; 62D1
<i>Df(3L)Exel6106</i> (7585)	64D6; 64E2	64D6; 64E2
<i>Df(3L)eyg^{C1}</i> (5492)	69A4-5; 69D4-6	69C4; 69D4
<i>Df(3L)ED4486</i> (8072)	69C4; 69F6	69C4; 69D4
<i>Df(3L)Exel6127</i> (7606)	72D1; 72D9	Conflicting Overlap
<i>Df(3R)ED5428</i> (9227)	85E1; 85F8	Conflicting Overlap
<i>Df(3R)ED5612</i> (9088)	87C7; 87F6	87E3; 87F6
<i>Df(3R)ED5623</i> (8921)	87E3; 88A4	87E3; 87F6
<i>Df(3R)Exel6173</i> (7652)	88D7; 88E1	88D7; 88E1
<i>Df(3R)crb87-5</i> (2363)	95F7; 96A17-18	95F7; 96A7
<i>Df(3R)Exel6210</i> (7688)	98E1; 98F5	98E3; 98F5
<i>Df(3R)3450</i> (430)	98E3; 99A6-8	99A5; 99A8
<i>Df(3R)ED6310</i> (8961)	98F12; 99B2	99A5; 99A8
<i>Df(3R)ED6316</i> (8925)	99A5; 99C1	99A5; 99A8
<i>Df(3R)Exel6215</i> (7693)	99F6-7; 99F8	Conflicting Overlap

* “Conflicting Overlap” indicates there exists another deficiency in the same region that did not exhibit an interaction with the *Atg1^{6B}* overexpression phenotype.

Table 4.7: Undefined Modifiers Identified In The Genetic Screen

Chromosome Aberration (Stock)	Cytology	Associated Interacting Regions*
<i>Df(2L)ED62</i> (8937)	21D1; 21E2	Conflicting Overlap
<i>Df(2L)BSC7</i> (6374)	26D10-E1; 27C1	26D10-E1; 26F5 27B1; 27B4
<i>Df(2L)ED548</i> (24130)	28E1; 28E9	28E1; 28E5
<i>Df(2L)BSC241</i> (9716)	32C1; 32F2	32D2; 32D4
<i>Df(2L)Exel6027</i> (7510)	32D2; 32D5	32D2; 32D4
<i>Df(2L)Exel6045</i> (7527)	38A3; 38A7	Conflicting Overlap
<i>Df(2R)BSC630</i> (25705)	41D3; 41F11	41D3; 41F11
<i>Df(2R)ED1484</i> (9683)	42A2; 42A14	42A2; 42A11
<i>Df(2R)ED1618</i> (8939)	42C4; 43A1	42C7; 42E1
<i>Df(2R)BSC40</i> (7146)	48E1-2; 48E2-10	48E4; 48E10
<i>Df(2R)BSC383</i> (24407)	50C6; 50D2	50C18; 50D2
<i>Df(2R)Exel6071</i> (7553)	57B3; 57B16	Conflicting Overlap
<i>Df(2R)Exel6072</i> (7554)	57B16; 57D4	Conflicting Overlap
<i>Df(3L)emc-E12</i> (2577)	61A; 61D3	61A1; 61A5
<i>Dp(3;3)Cam31</i> (5743)	61F7-8; 64B10-12	Conflicting Overlap
<i>Df(3L)Aprt-1</i> (600)	62A10-B1; 62D2-5	62C4; 62D1
<i>Df(3L)ED4341</i> (8060)	63F6; 64B9	Conflicting Overlap
<i>Df(3L)BSC385</i> (24409)	62D4; 62E1	62D7; 62E1
<i>Df(3L)BSC116</i> (8973)	62D7; 62E5	62D7; 62E1
<i>Df(3L)Exel8101</i> (7928)	65A3; 65A9	Conflicting Overlap
<i>Df(3L)Exel6109</i> (7588)	65C3; 65D3	Conflicting Overlap
<i>Df(3L)rdgC-co2</i> (2052)	77A1; 77D1	Conflicting Overlap
<i>Df(3R)Exel7315</i> (7931)	87B8; 87B9	87B9
<i>Df(3R)Exel7316</i> (7970)	87B9; 87B11	87B9
<i>Df(3R)Exel6166</i> (7645)	87C5; 87C7-8	87C5; 87C7-8

* “Conflicting Overlap” indicates there exists another deficiency in the same region that did not exhibit an interaction with the *Atg1^{6B}* overexpression phenotype.

After the primary screen was performed, many of the strong interacting deficiencies and duplications were tested to ensure that the level of *pannier* expression was not affected. In this experiment, progeny carrying one copy of a strong interacting chromosomal aberration and *pnrGAL4+UAS-BsgRNAi⁴³³⁰⁷* were compared to siblings carrying *pnrGAL4+UAS-BsgRNAi⁴³³⁰⁷* and a balancer chromosome (for more details see Materials and Methods). The [*pnrGAL4+UAS-BsgRNAi⁴³³⁰⁷/Df or Dp*] or [*Df or Dp/+; pnrGAL4+UAS-BsgRNAi⁴³³⁰⁷/+*], progeny were evaluated based on the severity of the resulting black stripe down the midline of the thorax, a novel phenotype associated with RNAi knockdown of *Bsg* transcripts. The intensity and thickness of the black stripe serves here as an indicator of the levels of *pannier* expression. Normally, *pnrGAL4+UAS-BsgRNAi⁴³³⁰⁷/+* results in a solid black stripe down the thorax (Figure 4.6B). Accordingly, any interactions associated with a decrease in the intensity of the black stripe, could indicate a decrease in *pannier* expression (Figure 4.6A), while an increase in the intensity and an extension of the black stripe down the abdomen could indicate an increase in *pannier* expression (Figure 4.6C). Any consistent differences in the black stripe phenotype between the balancer and non-balancer groups were considered possible interactors with *pannier* in the screen for chromosomal regions that dominantly interact with *Atg1^{6B}*.

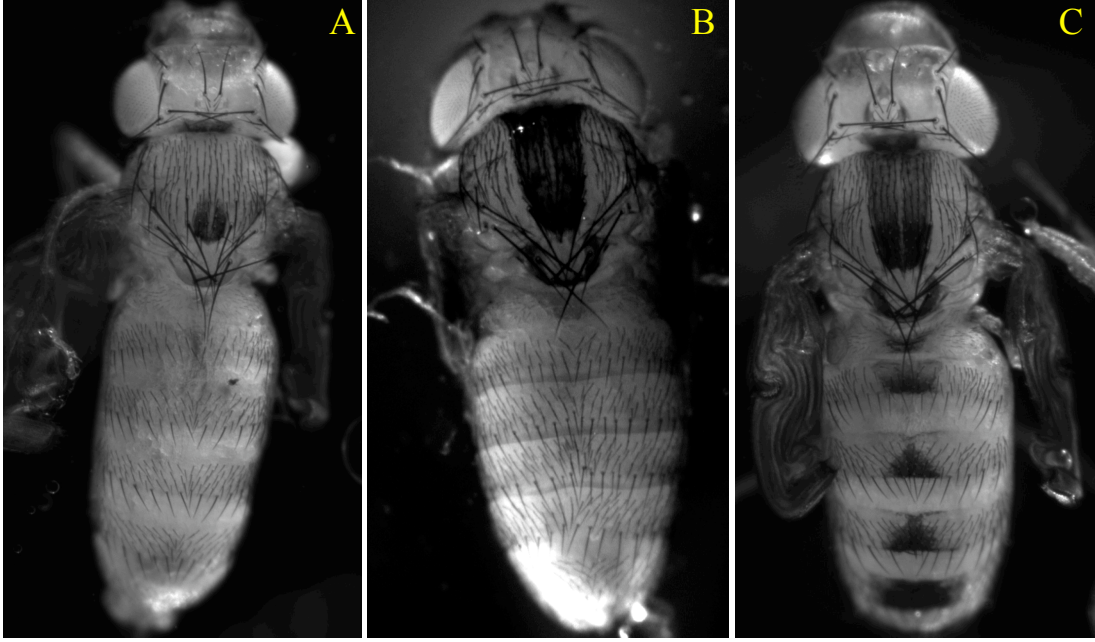
However, the chromosomal aberrations that result in a change in the intensity and thickness of the black stripe could be affecting *BsgRNAi⁴³³⁰⁷* and not *pannier* expression. For example, progeny carrying *Df(2L)Exel7034* and *pnrGAL4+BsgRNAi⁴³³⁰⁷* displayed a strong black stripe down the abdomen, indicating an increase *pannier* expression (Figure 4.6C). However, the *Df(2L)Exel7034* deficiency deletes the *Bsg* gene; therefore, it is presumably the further decrease in *Bsg* by the *Df* that is acting to enhance the knockdown phenotype.

Since it is expected that true false positives would disrupt *pannier* expression no matter what the UAS-construct, the same strong interactors were crossed to *pnrGAL4+EP(3)3614*. Normally, the expression of *EP(3)3614*, under the control of *pnrGAL4*, results in the complete loss of dorso-central and scutellar macrochaetae and microchaetae along dorsal midline including the abdomen (Peña-Rangel *et al.*, 2002). [*pnrGAL4+EP(3)3614/Df or Dp*] or [*Df or Dp/+; pnrGAL4+EP(3)3614/+*] progeny were compared to siblings carrying *pnrGAL4+EP(3)3614* and a balancer chromosome with respect to the severity of the resulting hairless stripe down the midline of the thorax and abdomen (for more details see Materials and Methods). Any interactions associated with an increase in the number of micro- and macrochaetae along the dorsal midline would indicate a decrease in *pannier* expression, while a lateral expansion of the hairless line phenotype down the dorsal midline would indicate an increase in *pannier* expression (data not shown). Any consistent differences in the hairless phenotype between the two groups were considered possible interactors with *pannier* expression (Tables 4.3, 4.5). Afterwards, any deficiency or duplication that resulted in an interaction with both *UAS-BsgRNAi⁴³³⁰⁷* and *EP(3)3614* were considered true interactors of *pannier* expression.

To date, no interacting deficiency or duplication has interacted with both constructs. However, progeny carrying *UAS-BsgRNAi⁴³³⁰⁷* and *Df(3L)ZN47* displayed a strong black stripe down the abdomen. Similarly, progeny carrying *Df(3R)Exel6202* and *EP(3)3614* displayed a lateral expansion of the hairless line phenotype down the dorsal midline and were semi-lethal. Since these deficiencies resulted in the enhancement of only one of the two constructs, their effects are likely due to the interaction with *UAS-BsgRNAi⁴³³⁰⁷* or *EP(3)3614* respectively. Therefore these deficiencies are still considered modifiers of the *Atg1^{6B}*

overexpression phenotype. In the future it is hoped that all interacting deficiencies will be crossed to the *pnrGAL4+UAS-BsgRNAi*⁴³³⁰⁷ and *pnrGAL4+EP(3)3614* stocks to determine whether the levels of *pannier* expression are affected.

Figure 4.6: Stereomicroscopic Imaging of *Drosophila* expressing *UAS-BsgRNAi*⁴³³⁰⁷ in tissues specified by *pnrGAL4*. (A) *UAS-BsgRNAi*^{43308/+}; *pnrGAL4/+* *Drosophila* carrying *UAS-BsgRNAi*⁴³³⁰⁸ on the second chromosome. Image illustrates a decrease in the intensity of the black stripe phenotype. Only a small black circle, just above the scutellum, is observed. (B) *pnrGAL4/UAS-BsgRNAi*⁴³³⁰⁷ *Drosophila* carrying *UAS-BsgRNAi*⁴³³⁰⁷ on the third chromosome. Image illustrates an intermediate black stripe. (C) *UAS-BsgRNAi*^{43307/+} *pnrGAL4/ Df(2L)Exel7034* *Drosophila* carrying *UAS-BsgRNAi*⁴³³⁰⁷ and a *Deficiency* on the third chromosome. Image illustrates an increase in the severity of the black stripe phenotype. The black stripe can be observed down the midline of the abdomen.



4.2 Target Interacting Regions that dominantly interact with *Atg1^{6B}*

Of the 44 interacting regions previously identified in the genetic screen, 9 interacting regions have been targeted as the best candidates to find dose-sensitive modifiers of *Atg1^{6B}* expression (Table 4.8). The following rationale was used to choose these regions. First, a region was chosen if it had consistent overlap of three or more interacting deficiencies of a similar class (See Table 4.1 for Class descriptions). Second, a region was chosen if it encompassed an interacting deficiency with a complementing interacting duplication (Figure 4.1). Each of these target regions contains a relatively small number of genes (Table 4.8). Therefore, in the future, all genes within these 9 promising interacting regions will be tested to determine whether they modify the adult cuticular phenotype and whether they promote or inhibit autophagy-dependent caspase activation (See Future Directions). It is hoped that some of these promising interacting regions will possess genes that are involved with autophagy-dependent caspase activation. Recently, candidate genes that may be involved in the regulation of autophagy-dependent caspase activation have been chosen from the targeted interacting regions (Table 4.8). For example, *miR-308* was identified in the target region 50D4; 50E4. Since miRNAs are involved in cell growth and apoptosis (Su *et al.*, 2009), *miR-308* is a strong candidate for the regulation of autophagy-dependent apoptosis. Already, many of the candidate genes located within these targeted interacting regions, such as *Atg6* and *Tsc1*, and other non-targeted interacting regions have been tested (Table 4.9).

Table 4.8: List of 9 Target Interacting Regions and Associated Information

Interacting Regions ⁸	Associated Deficiencies and Duplications (Class)	Reason for Being Chosen ⁹	Estimated # of Genes In Region	Genes of Note
25F2; 26B1	<i>Df(2L)ED334</i> (SU-) <i>Dp(2;2)Cam2</i> (EN++)	Complimenting Df and Dp	26	<i>bchs</i> (lysosomal transport)
46C7; 46D6	<i>Df(2R)BSC152</i> (EN++) <i>Dp(2;2)Cam11</i> (SU--)	Complimenting Df and Dp	10	<i>CG1418</i> (Rab GTPase binding) <i>CG12133</i> (Serine endopeptidase activity)
50D4; 50E4	<i>Df(2R)Exel7130</i> (SU-) <i>Dp(2;2)Cam14T</i> (EN++)	Complimenting Df and Dp	27	<i>miR-308</i> (autophagy) <i>O-fut1</i> (protein catabolic process)
62D7; 62E1	<i>Df(3L)BSC385</i> (UM) <i>Df(3L)BSC116</i> (UM) <i>Df(3L)ED4287</i> (EN+)	Df Overlap Similar Class	9	
69C4; 69D3	<i>Df(3L)ED4483</i> (EN++) <i>Df(3L)eyg^{C1}</i> (EN+) <i>Df(3L)ED4486</i> (EN+)	Df Overlap Similar Class	20	<i>vih</i> (cell cycle)
85E1; 85E5	<i>Df(3R)by10</i> (EN++) <i>Df(3R)ED5429</i> (EN++) <i>Df(3R)ED5428</i> (EN+)	Df Overlap Similar Class	24	<i>hyd</i> (developmental growth)
87E3; 87F6	<i>Df(3R)Exel6166</i> (UM) <i>Df(3R)ED5612</i> (EN+) <i>Df(3R)Tp(3;Y)ry506-85C</i> (EN++) <i>Df(3R)ED5623</i> (EN+)	Df Overlap Similar Class	48	<i>CG8795</i> (developmental growth)
95D10; 95E1	<i>Df(3R)Exel6197</i> (EN++) <i>Df(3R)ED6187</i> (EN++) <i>Df(3R)crb87-5</i> (EN+)	Df Overlap Similar Class	21	<i>Atg6</i> (autophagic cell death) <i>Tsc1</i> (autophagy)
99A5; 99A8	<i>Df(3R)3450</i> (EN+) <i>Df(3R)ED6310</i> (EN+) <i>Df(3R)ED6316</i> (EN+)	Df Overlap Similar Class	4	<i>stg</i> (cell cycle)

⁸ “Interacting Regions” column indicates the cytological locations of all deficiencies and duplications combined into one interacting region.

⁹ “Complimenting Df and Dp” indicates that the class of the deficiency is opposite to that of the duplication. “Df Overlap, Similar Class” indicates that all the mentioned deficiencies in that region were overlapping and displayed a similar class as given in Table 4.1.

4.3 Screen For Loci That Dominantly Interact With *Atg1^{6B}*

Crosses similar to those described in the initial genetic screen were used to identify individual loci that exhibit dominant interactions with *Atg1^{6B}*. Candidate genes were chosen based on previously identified relationships (Drysdale and Crosby, 2005). For example some candidate genes were chosen based on their association with autophagy, autophagic cell death or apoptosis. Other genes were chosen because of their involvement in cell adhesion, cell cycle, or vesicular transport. Also, some candidate genes were chosen because of their involvement in cell signaling pathways such as the JNK or Dpp pathways, which have many different functions but are also associated with cell death (Drysdale and Crosby, 2005).

Mutant alleles of each candidate gene were tested for modification of the thoracic cleft and reduced scutellum phenotype (Table 4.8). Any consistent differences based on the previously mentioned criteria (Table 4.1) were noted. Out of the 60 mutants, three alleles *Apc^{N175K}*, *Apc2^{Q8}* (these two alleles were tested as two separate mutations on the same chromosome), and *dpp^{hr92}* were identified as dominant modifiers of *Atg1^{6B}* expression (Table 4.8). It is hypothesized that *dpp^{hr92}* is a good candidate for the modification of *Atg1^{6B}* expression, as it does not affect *pannier* expression when crossed to *pnrGal4+BsgRNAi⁴³³⁰⁷* (data not shown). Also, the undefined modifier phenotype associated with the *Apc^{N175K}* and *Apc2^{Q8}* mutant alleles is similar to the corresponding interacting (*Df(3R)ED6187*, *Df(3R)Exel6210* and *Df(3R)3450*) (Tables 4.5, 4.6) deficiencies, indicating that *Apc^{N175K}* and *Apc2^{Q8}* may be bona fide dose-sensitive undefined modifiers of the *Atg1^{6B}* overexpression phenotype. However, further research must be performed to confirm these results. During this screen another allele of *dpp*, *dpp^{H46}*, resulted in a dominant interaction but was ruled out as it is a *haplo-insufficient* lethal (Table 4.9). Also, the *TM6B* balancer, in some cases, gave a

strong suppression phenotype (data not shown). Since *Tubby* (*Tb*) exists as a dominant mutation in these *TM6B* balancer stocks, the *Tb* mutation, separated from the *TM6B* balancer chromosome, was tested for the modification of the adult cuticular phenotype. As a result, *Tb* did not suppress the *Atg1^{6B}* overexpression adult cuticular phenotype (data not shown). Therefore, it is likely that the *Tb* mutation is not the source of the interaction associated with the *TM6B* balancer chromosome. In the future, further research should be performed to determine the mechanism by which this balancer suppressed the *Atg1^{6B}* overexpression phenotype.

Table 4.9: Alleles Of Candidate Genes Tested In The Genetic Screen

Locus (abbrev.) (cytology)	Associated with Interacting Regions ¹⁰ ?	Allele	Genetic Interaction ¹¹
<i>decapentaplegic (dpp)</i> (22F1-22F3)	No	<i>H46</i>	HI ¹¹
		<i>hr92</i>	SU (-) NR ¹²
		<i>H48</i>	NC
<i>thickveins (tkv)</i> (25D1-25D2)	No	7	NC
		<i>K16713</i>	
		<i>04535a</i>	NC
<i>Macroglobulin complement-related (Mcr)</i> (28E1-28E3)	28E1; 28E5	<i>EY07421</i>	NC
<i>Mkk4</i> (85A5)	No	<i>e01485</i>	NC
<i>polychaetoid (pyd)</i> (85B2-85B7)	85B6; 85C3	<i>KG02008</i>	NC
<i>Vacuolar H⁺-ATPase 55kD B subunit (Vha⁵⁵)</i> (87C2-87C3)	87C3; 88A4	16	NC
		12	NC
		<i>j2E9</i>	NC
<i>Daughters against dpp (Dad)</i> (89E11)	No	<i>j1E4</i>	NC
<i>Autophagy-specific gene 6 (Atg6)</i> (95D10)	95D10; 95E1	<i>00096</i>	NC
<i>tuberous sclerosis complex 1 (Tsc1)</i> (95E1)	95D10; 95E1	<i>f01910</i>	NC
<i>u-shaped (ush)</i> (21E1-21E2)	No	2	NC
<i>dachsous (ds)</i> (21E2)	No	<i>05142</i>	NC
<i>Excitatory amino acid transporter 2 (Eaat2)</i> (21E2)	No	<i>e03003</i>	NC
<i>Autophagy-specific gene 4 (Atg4)</i> (21E4)	No	<i>MB03551</i>	NC
<i>PNUTS</i> (21E2)	No	<i>KG00572</i>	NC

¹⁰ If a candidate gene is located within an interacting region the cytology of the interacting region is given in the Associated Interacting Regions Column.

¹¹ All alleles were classified based on the criteria from Table 4.1. E (+) = Moderate enhancer that is semi-lethal; E (++) = Strong enhancer that is Lethal; Su (-) = Moderate suppressor; Su (--) = Strong suppressor; UM = Undefined Modifier; NC = No Change.

¹² NR is defined as not relevant as it indicates that the gene does not map to a bona fide interacting region. HI indicates the allele was *haplo-insufficient* lethal.

Hepatocyte growth factor regulated tyrosine kinase substrate (Hrs) (23A3)	No	D28	NC
<i>cyclope (cype)</i> (25D6)	No	e03803	NC
		03771	NC
<i>vri</i> (vri) (25D4-25D5)	No	KG10174	NC
		k05901	NC
		KG01220	NC
<i>midline (mid)</i> (25E2)	No	2	NC
		1	NC
Regulator of cyclin A1 (<i>Rca1</i>) (27C1)	No	2	NC
		IX	NC
<i>lethal (2) k09022 (l(2)k09022)</i> (27C1-27C2)	No	k09022	NC
<i>wee</i> (27C4)	No	ES1	NC
cAMP-dependent protein kinase 1 (<i>Pka-C1</i>) (30C5)	No	H2	
		DN	NC
		BG02142	NC
<i>Ced-12 (elmo)</i> (33C4)	33C2; 33E9	C06760	NC
<i>Rab-protein 6 (Rab6)</i> (33C4)	33C2; 33E9	D23D	NC
		08323	NC
		k13606	NC
<i>Son of sevenless (Sos)</i> (34D1)	No	34Ea-6	NC
		k05224	NC
<i>spitz (spi)</i> (37F2)	No	1	NC
<i>screw (scw)</i> (38A1)	No	l1	NC
		5	NC
<i>skittles (sktl)</i> (57B3)	No	05475	NC
		K12405	NC
		DG24311	NC
<i>lethal(3)63Eb (Sc2)</i> (63F5; 63F6)	No	05634	NC
<i>Ubiquitin-63E (Ubi-p63E)</i> (63F5)	No	EY07341	NC
<i>Ubiquinol-cytochrome c reductase Cytochrome c1 (CG4769)</i> (64C13)	No	KG05986	NC

<i>Uev1a</i> (64C13)	No	DG14805	NC
<i>Kinesin-like protein at 64D (Klp64D)</i> (64C13)	No	k1	NC
		n123	NC
<i>lethal with a checkpoint kinase (lack)</i> (54C12-54D1)	No	KG07014	NC
<i>belphegor (bor)</i> (89B9)	No	c05496	NC
<i>Delta (Dl)</i> (92A1-92A2)	No	7	NC
		9P	NC
<i>Adenomatous polyposis coli tumor suppressor homolog 2 (Apc2)</i> 95E6-95E6	No	N175K*	UM(✓) ¹³
<i>Enhancer of split (E(spl))</i> (96F10)	No	rv1	NC
<i>APC-like (Apc)</i> (98E5-98E6)	98E3; 98F5	Q8*	UM (✓)
<i>Darkener of apricot (Doa)</i> (98F2)	98E3; 98F5	3	NC

¹³A checkmark indicates that the allele showed the same or similar result as its corresponding interacting region or deficiency.

* Both alleles (*Apc*^{Q8} and *Apc2*^{N175K}) were tested together as they exist as two mutations in one stock.

Chapter 5. Discussion

Chapter 5. Discussion

This study has investigated the process of autophagy and its relationship with cell death. Through the use of scanning electron microscopy, stereomicroscopic live imaging, and confocal microscopy it was demonstrated that ectopic expression of Atg1 kinase activates a full autophagic response. This autophagic response results in a marked induction of cell death in various tissues throughout development and is associated with an adult cuticular phenotype. Using this striking adult cuticular phenotype, a genetic screen was performed with the goal of identifying dose-sensitive modifiers of *Atg1^{6B}* expression. The identification of these interacting regions is significant, as it will enable the discovery of novel regulators of autophagy-dependent caspase activation in *Drosophila melanogaster*.

5.1 Evaluating Autophagy Dependent Caspase Activation in the AS

The primary objective of this study was to analyze autophagy in AS cells that were defective in autophagy or the activation of apoptosis. Upon completion of this objective, the following conclusions were made. First, it was demonstrated that autophagy increases prior to AS degeneration, and that autophagy is independent of caspase activity. In addition, *Atg1^{6B}* overexpression in the AS results in a dramatic increase in autophagy. In a study by Mohseni *et al.*, it was shown that this upregulation of autophagy results in the premature elimination of the AS, which can be completely suppressed by the co-expression of the caspase inhibitor *p35* (2009). Another conclusion of this thesis was that the activation of the InR/PI3K pathway results in a severe decrease in autophagy. Interestingly, it has been shown that the downregulation of autophagy, strongly reduces caspase activation, and results in a persistent AS phenotype (Reed Lab Unpublished Data; Mohseni *et al.*, 2009). Together, the results of this study, along with the results from Mohseni *et al.*, demonstrate that the relationship

between autophagy and caspase activation, in the amnioserosa (AS) is epistatic, whereby autophagy operates upstream of caspase activation. It was from these experiments that the term “autophagy-dependent caspase activation” was created (Mohseni *et al.*, 2009) (Figure 1.5).

Similar to studies involving AS degeneration, an epistatic relationship between autophagy and caspase activation has been recently demonstrated during *Drosophila* oogenesis (Nezis *et al.*, 2009). Nezis *et al.* have shown that the increase in autophagy observed during development in the germarium and during the mid-stages of oogenesis, is followed by caspase activation. Also, in *Atg* germline mutants, it was shown that there was a decrease in the number of cells showing caspase activation and morphological characteristics associated with apoptosis. These results suggest that autophagy functions to activate apoptosis during oogenesis (2009). In contrast to the previous results, Hou *et al.* have suggested that several genes involved in the activation of apoptosis also function to regulate autophagy induced cell death during oogenesis. However, in this case Hou *et al.* have not confirmed the presumed hierarchical relationship between autophagy and caspase activation through epistasis experiments (2008). Also, similar to the AS, the study performed by Hou *et al.*, supports a model whereby caspases and autophagy function cooperatively during cell death.

Together, studies of AS degeneration and oogenesis give credence to the argument that an epistatic relationship exists between autophagy and apoptosis, however further research must be performed to elucidate the mechanisms regulating the activation of both PCD pathways.

5.2 Autophagy Dependent Caspase Activation In the Third Instar Wing Disc and Larval Epidermis

Expanding upon previous findings, autophagy-dependent caspase activation was explored in the dorsal larval epidermis. Using Apoliner and a nuclear GFP reporter, it was established that the upregulation of autophagy is associated with caspase activity and the elimination of cells from the third instar larval epidermis. Also, it was determined that the co-expression of *p35* partially rescues the elimination of *Atg1^{6B}* overexpressing third instar larval epidermal cells. These results confirm that autophagy and caspases act cooperatively during larval epidermal cell death.

To further demonstrate that the induction of autophagy induces caspase activation, Apoliner was observed in wing discs overexpressing *Atg1^{6B}*. Similar to the AS, the overexpression of *Atg1^{6B}* in the proximal area of the third instar wing disc results in an increase in autophagosome and autolysosome formation and subsequently caspase-activation.

Similar to these results, Scott *et al.*, have demonstrated in patches of the imaginal wing disc and fat body that the overexpression of *Atg1* results in caspase activation and subsequently apoptosis (2007).¹⁴ Furthermore, this induction of cell death can be rescued by *Atg* mutant backgrounds, demonstrating the requirement of an intact autophagy pathway for the induction of caspases. This study also reported that the co-expression *p35* was able to delay and reduce the death of *Atg1*-overexpressing patches in the wing-disc and fat body respectively (Scott *et al.*, 2007). Similarly, *Atg1* overexpression in the imaginal eye disc reduces the overall size of the adult eye in *Drosophila* (Scott *et al.*, 2007). The ability to suppress the reduced eye size phenotype, through the use of caspase inhibitors, indicates that

¹⁴ The fat body is a collective name for the sheets of adipose tissue that are distributed throughout the fly. This organ is analogous to the vertebrate liver (Jiang *et al.*, 2005).

the induction of autophagy, above a certain threshold, in the imaginal eye disc results in caspase activation and subsequently apoptosis (Scott *et al.*, 2007).

Together, these results re-enforce that high levels of autophagy induce caspase activation. However, before any conclusions are made, the effectiveness of Apoliner as a caspase sensor in the third instar wing disc and larval epidermis should be further assessed. In the event that Apoliner is a useful tool to detect caspases in the wing disc, the interacting deficiencies and duplications that were identified in the genetic screen can be further assessed with regards to autophagy-dependent caspase activation (See Future Directions).

5.3 Stereomicroscopic Live Imaging and Scanning Electron Microscopy: Analyzing Cell Death During Metamorphosis

Originally, it was hypothesized that the striking adult cuticular phenotype was attributable to a process involving autophagy-induced caspase activation. Unfortunately, this adult cuticular phenotype could not be rescued through co-expression of the caspase inhibitor *p35*. Therefore, there is no direct correlation between the adult phenotype and autophagy-dependent caspase activation. However, it was demonstrated, through changes in temperature, that the adult cuticular phenotype could be modulated based on *Atg1^{6B}* expression. There are several possible explanations for these observations.

The most promising explanation is that, even though the co-expression of *p35* did not rescue the adult cuticular phenotype, autophagy above a certain threshold induces the execution of apoptosis in these tissues (Section 1.1.2.5 – Figure 1.5). The inhibition of executioner caspases, through the ectopic expression of *p35*, may have been sufficient to prevent cell death in the presumptive adult tissues, but resulted in an overgrowth phenotype that resembles the adult cuticular phenotype. Previously, Pérez-Garijo *et al.*, have shown that

cells undergoing apoptosis in the wing disc emit growth signals. These growth signals induce compensatory proliferation in the surrounding surviving cells to restore the normal size of the affected tissue. However, “undead cells”, or cells that have initiated but not completed PCD due to the inhibition of executioner caspases, continuously emit these growth signals. The continuous emission of these growth signals results in large overgrowths and subsequently abnormal development (2004).

Another possibility is that the adult cuticular phenotype is the result of an autophagic cell death that is independent of caspase activity (See Section 1.1.2.4 – Figure 1.4). Although the following result could be due to incomplete caspase inhibition, it was observed that the co-expression of *p35* does not rescue the premature cell death of *Atg1^{6B}* overexpressing larval epidermal cells during the pre-pupal stages (Figure 3.12 – *p35*; *Atg1^{6B}*). In a recent study, Berry and Baehrecke have demonstrated that the co-expression of *p35* in the *Drosophila* salivary gland does not suppress the premature cell death phenotype associated with *Atg1* overexpression (2007). It was concluded in this study that the inability to rescue the *Atg1* overexpression phenotype was due to the cooperative, but parallel, relationship between autophagy and apoptosis during salivary gland degeneration (Berry and Baehrecke, 2007; Lee and Baehrecke, 2001). However, Berry and Baehrecke may not have achieved complete caspase inhibition in the salivary glands. Increasing caspase inhibition, through the co-expression of two copies of *p35* in the salivary glands, may suppress this premature cell death. Since Berry and Baehrecke have not established complete caspase inhibition in the salivary glands, the only known tissue demonstrating the existence of a caspase-independent autophagic cell death, it is questionable whether a bona fide caspase-independent autophagic

cell death exists. In summation, it is unlikely that autophagic cell death is the cause of the adult cuticular phenotype.

Another explanation is that the adult cuticular phenotype could be the result of a combination of reduced cell growth and increased cell death. It is possible that autophagic cells are degrading factors that promote cell growth, preventing the proliferation in the wing disc and histoblast nests. Scott *et al.*, have shown that the overexpression of *Atg1* results in a marked induction of autophagy and a severe decrease in cell growth in the imaginal eye and wing discs and the fat body (2007). Since cells cannot proliferate until they reach a certain critical size (Vellai *et al.*, 2008), the eversion and subsequent dorsal movement of the proximal area of the wing discs and the dorsal movement of the histoblast nests could be prevented when these tissues are autophagic. At the same time, the prolonged induction of autophagy, via the overexpression of *Atg1^{6B}*, throughout development could also result in the degradation of factors that are required for survival. The degradation of these factors could result in the activation of caspases and subsequently apoptosis (Neufeld and Baehrecke, 2008; Debnath *et al.*, 2005; Berry and Baehrecke, 2007; McPhee and Baehrecke, 2009). Therefore, the ectopic expression of *p35* would inhibit the execution of cell death in tissues overexpressing *Atg1^{6B}*, but not the resulting growth defects, which could account for the inability to rescue the adult cuticular phenotype.

Lastly, the adult cuticular phenotype may be the result of an inability of autophagic cells to secrete adult cuticle along the dorsal midline. Since, a rise in ecdysone is necessary for the secretion of adult cuticle in the imaginal discs and abdominal histoblasts (Fristrom and Fristrom 1993; Johnson and Milner 1990), it is hypothesized that the induction of autophagy either down-regulates protein synthesis or the selectively degrades components involved in

ecdysone biosynthesis in these tissues. Such a reduction in ecdysone signaling could inhibit the secretion of adult cuticle along the midline of the adult notum and abdomen, resulting in the observed prominent clefts and reduced scutellum. Interestingly, it has been shown that the overexpression of *Atg1* throughout the embryo results in a thin embryonic cuticle (Nilufar Mohseni MSc. Thesis, 2007), a phenotype that is frequently observed in embryos that are defective in ecdysone biosynthesis (Kozlova and Thummel 2003).

5.4 Genetic Screen

Since altering the level of *Atg1^{6B}* expression, in a temperature dependent fashion, can modulate the adult cuticular phenotype, a broad based genetic screen to identify dose-sensitive modifiers of autophagy, was performed. 79 interacting deficiencies were identified that exhibit dose-sensitive interactions with *Atg1^{6B}*. Of the 79 interacting deficiencies, 42 were dominant enhancers, 24 deficiencies were dominant undefined modifiers, and 13 deficiencies were dominant suppressors (Figures 4.2-4.5, Tables 4.3-4.7). These interacting deficiencies represent 19.80% of the total deficiencies tested (Table 4.2), indicating that the screen was effective in identifying deficiencies that are associated with the regulation of autophagy.

Furthermore, 44 interacting regions were identified based on the 79 interacting deficiencies. From these 44 interacting regions, 9 were targeted as good candidates to find genes that are dose-sensitive modifiers of *Atg1^{6B}* expression (Table 4.8). These targeted regions contain a relatively small number of genes; therefore, all genes within these regions will be tested with respect to modulating the adult cuticular phenotype.

Already 60 alleles representing 39 candidate genes were tested for modification of the adult cuticular phenotype (Table 4.9). These candidate genes were chosen because they map

to the targeted interacting regions identified by the primary genetic screen or because of previously established relationships with autophagy and cell death. Of the 60 alleles, three loss-of-function mutants, *Apc*^{N175K}, *Apc2*^{O8} and *dpp*^{hr92}, resulted in a dominant interaction with *Atg1*^{6B}.

The *Apc* loss-of-function mutants were identified as undefined modifiers of the *Atg1*^{6B} overexpression phenotype. The APC proteins are tumor suppressors that function in the negative regulation of Armadillo,¹⁵ an integral part of the Wnt/Wingless signaling pathway (Ahmed *et al.*, 1993). Therefore, it is speculated in this thesis that autophagic cells in the wing disc degrade cytoplasmic Armadillo, reducing the cell's ability to mediate *wingless* signaling. Under these circumstances, the *Apc/Apc2* loss-of-function mutants should result in an increase in cytoplasmic Armadillo, restoring the cell's ability to mediate *wingless* signaling. If this hypothesis is correct, it will be possible to test for suppression of the adult cuticular phenotype through the co-expression of *UAS-Armadillo*.

The *dpp*^{hr92} loss-of-function mutant was identified as a dominant moderate suppressor of the *Atg1*^{6B} overexpression adult cuticular phenotype. *decapentaplegic* (*dpp*) is a secreted morphogen that is involved in a variety of processes such as the determination of the dorsal-ventral axis in the blastoderm embryo, dorsal closure in the embryo, and the patterning of the imaginal wing discs (Affolter *et al.*, 2001). It is speculated in this thesis that autophagic cells, through some unknown mechanism, upregulate *dpp* expression in the presumptive adult tissues. Under these circumstances, the *dpp*^{hr92} loss-of-function mutant decreases *dpp* expression, suppressing the adult cuticular phenotype. In the future, *in situ* hybridization

¹⁵ Armadillo is the *Drosophila* homologue of β -catenin (Ahmed *et al.*, 1993).

experiments can be performed in the wing disc to assess *dpp* expression in cells overexpressing *Atg1^{6B}*.

In summation, although the mechanisms by which these two genes interact with *Atg1^{6B}* are not clear, it is suggested that these two genes function in the regulation of autophagy, which is a novel and interesting finding.

Conclusion

There is growing evidence in the field that, in certain contexts, high levels of autophagy can induce caspase activation. The precise molecular mechanism by which this might occur, however, remains unknown. This thesis has provided evidence towards autophagy-dependent caspase activation in the AS, and the third instar larval epidermis and wing discs. Also, it is presented in this thesis that the overexpression of *Atg1^{6B}* results in an adult cuticular phenotype that cannot be directly attributed to caspase activity. Nonetheless, altering the level of *Atg1^{6B}* expression can modulate this adult cuticular phenotype. Therefore, the adult cuticular phenotype was used in a genetic screen for dose-sensitive modifiers of the regulation of autophagy. In evaluating 92% of the major autosomal chromosomes via deficiency and duplication mapping, nine promising regions have been identified as having loci that behave as dose-dependent modifiers of *Atg1^{6B}* overexpression. However, further screening must be performed to determine which of the interactors are specific to autophagy-dependent caspase activity.

Chapter 6. Future Directions

Chapter 6. Future Directions

The following studies regarding the selective nature of autophagy and its relationship with caspase activation will be performed in the near future.

6.1 Caspase-Activation and Autophagosome Formation In The Wing Disc

In this study, it was demonstrated that the overexpression of *Atg1^{6B}* in the wing disc results in a dramatic increase in autophagy. Also it has been shown that this upregulation of autophagy results in the inappropriate cell death of the wing disc, which can be completely suppressed by the co-expression of *p35*. However, further control experiments should be performed to ensure that the overexpression of *Atg1^{6B}*, in this context, results in caspase activation. First, *pnrGal4+UAS-Atg1^{6B}/TM6,Tb[GAL80]* should be crossed to *UAS-Apomut*. Apomut is a caspase sensor that is identical to Apoliner except that its “caspase sensitive” site carries a mutation that inhibits cleavage by caspases (Bardet *et al.*, 2008). Since Apomut cannot be cleaved by caspases, the GFP and RFP should remain co-localized and clearly visible at the membrane of *Atg1^{6B}* overexpressing imaginal wing disc cells. If GFP accumulates in the nucleus, the cleavage observed in previous experiments, due to *Atg1^{6B}* overexpression, is not caspase-specific. Second, caspase activation should be induced in wing discs expressing *UAS-Apoliner* to ensure that the activation of caspases results in the nuclear localization of GFP. If Apoliner is a true indicator of caspase-activation in the wing disc, this methodology will be used, along with *UAS-mCherry-DrAtg8a* in a secondary screen for dose-sensitive modifiers of autophagy-dependent caspase activation (See Section 6.2).

6.2 Investigate Candidate Deficiencies and Loci Contained within Targeted Interacting Regions

The primary genetic screen identified 9 interacting regions as the regions most likely to contain loci that are dose-sensitive modifiers of *Atg1^{6B}* expression (Table 4.8). Therefore, in the future, all genes contained within these targeted interacting regions will be tested to determine whether they modify the adult cuticular phenotype. Afterwards, any interacting genes or deficiencies will be tested in a secondary screen to assess their involvement in autophagy-dependent caspase activation.

In the secondary screen, previously identified interacting deficiencies and genes will be crossed separately to *UAS-mCherry-DrAtg8a* and *UAS-Apoliner*. The wing discs of the resulting progeny that overexpress *Atg1^{6B}* and carry the deficiency or mutation will be compared to control wing discs. Any consistent differences between the two groups with respect to autophagosome and autolysosome formation (if crossed to *UAS-mCherry-DrAtg8a*) or nuclear localization of GFP (if crossed to *UAS-Apoliner*), will be used to test the effect of the interacting deficiency or mutation on autophagy-dependent caspase activation.

Afterwards, these interacting genes and deficiencies can be tested in the AS to elucidate regulators of developmentally induced autophagy-dependent caspase activation.

Appendix A. General Background

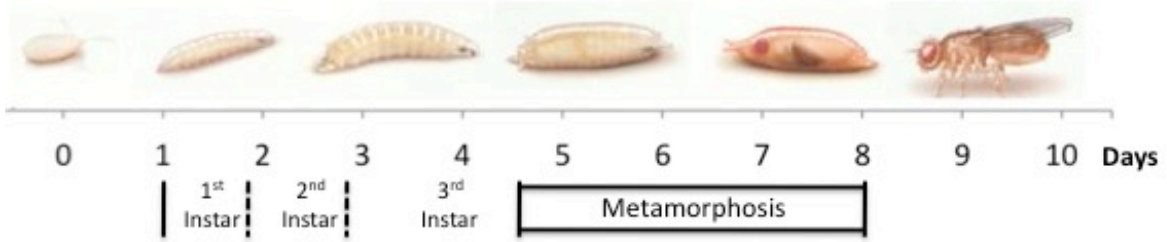
Appendix A. General Background

A.1 The *Drosophila* Life Cycle

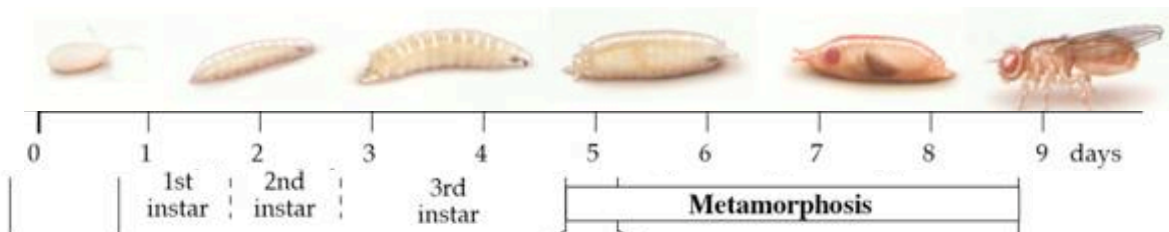
Under ideal conditions at 25°C, an embryo will develop into an adult fly in approximately 9 days (Figure A.1). Normally, 22-24hrs after embryos have been laid (AEL), the majority of larvae will hatch from the embryo. Subsequently, larvae will pass through three instars in 4 days (Demerec, 1985). The first and second instars last for 24hrs, while the third instar lasts for 48 hours. In the late third instar, larvae enter a wandering stage, in which larvae leave food and begin searching for a pupariation site. Pupariation, or the formation of the puparium, starts approximately 5 days AEL (Figure A.1). During pupariation, the larval body shortens, anterior spiracles evert, and the larval cuticle sclerotinizes to form the pupal case (Ashburner, 1989). After pupariation, pupation occurs. Pupation, the formation of the pupae, is the result of apolysis, which is the retraction of the epidermis from the hardened cuticle (Ashburner, 1989). Following apolysis, pupae are referred to as pharate adults. The duration from pupariation to eclosion is approximately 4 to 4.5 days (Figure A.1B) (Ashburner, 1989).

The time it takes for a fly to develop changes with temperature (Ashburner, 1989). Under ideal conditions, at 18°C, an embryo will develop into a fly in approximately 17 to 19 days (Figure A.1C). Under ideal conditions, at 29°C an embryo will develop into a fly in approximately 8 days (Figure A.1A) (Ashburner, 1989).

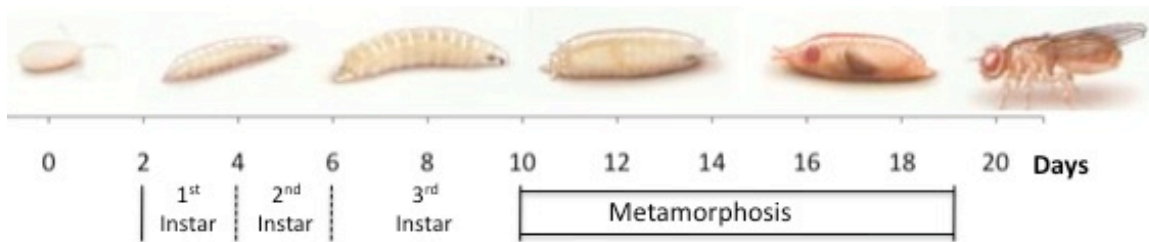
Figure A.1: A diagram demonstrating the life cycle of *Drosophila melanogaster*. (A) Developmental life cycle of *Drosophila* at 29°C takes about eight days (B) Developmental life cycle of *Drosophila* based on optimal growth conditions at 25°C takes about 9 days. (C) Developmental life cycle of *Drosophila* at 18°C takes about 17-19 days. In all diagrams the x-axis indicates the number of days associated with each stage in development during the *Drosophila* life cycle. The pictures above and below the diagrams indicate the developmental stage associated with the amount of days after egg lay (AEL).



(A)



(B)



(C)

A.2 The Amnioserosa - Embryogenesis

The amnioserosa (AS), an extraembryonic tissue, is eliminated during embryogenesis in *Drosophila* (Reed *et al.*, 2004). The AS plays a pivotal role in guiding major morphogenetic movements, including germband retraction and DC (Jacinto and Martin, 2001; Reed *et al.*, 2004). During DC 10% of the AS cells are basally extruded from the epithelium and undergo apoptosis while the lateral epidermal sheets lengthen along the dorsal-ventral axis (Mohseni *et al.*, 2009). Ultimately the lateral epidermal sheets meet and fuse along the dorsal midline, internalizing the remaining 90% of AS cells (Figure A.2). Once internalized, the AS tissue dissociates *en masse* and undergoes autophagy-dependent caspase activation (Mohseni *et al.*, 2009). It should be noted that the duration of embryogenesis changes with respect to temperature. Normally, embryogenesis takes approximately twenty-four hours at 25°C; however at 18°C embryogenesis takes approximately forty-one hours and fifteen minutes, almost doubling the development time. In contrast, development time is almost cut in half at 29°C with embryogenesis taking about fifteen hours (Ashburner, 1989).

Figure A.2: Process of dorsal closure during embryogenesis. The AS (pink) undergoes autophagy-dependent caspase activation and dissociates following a process called dorsal closure. This process occurs from 10.5-13 hours AEL at 25°C (Picture adapted from: Agnes *et al.*, 1999).



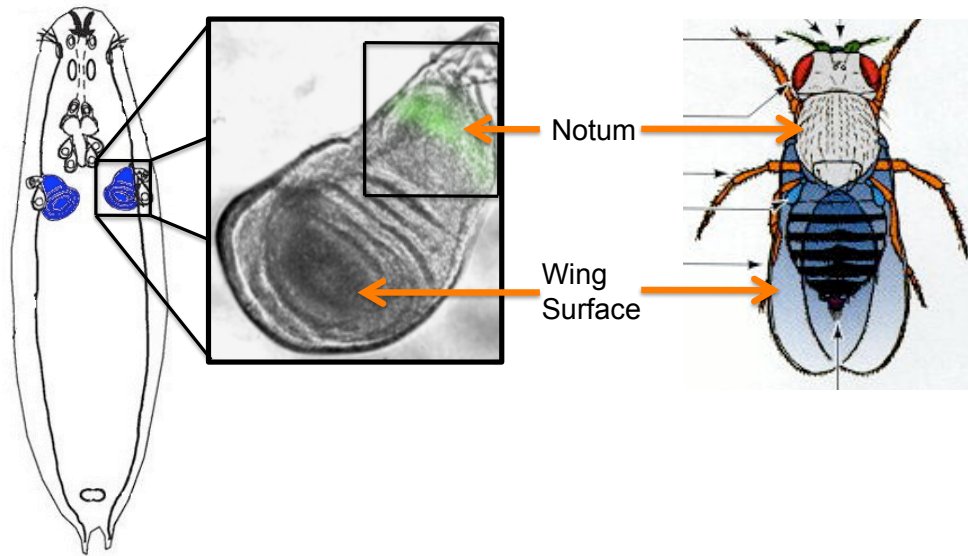
A.3 Thorax Closure

During *Drosophila melanogaster* pupation, wing imaginal discs, specialized epithelial sacs consisting of undifferentiated adult cells, proliferate and undergo regulated cell shape changes. This process of proliferation and cell shape changes results in the eversion and subsequent dorsal movement of the proximal area of the opposing wing discs (Figure A.3). Ultimately, these two wing discs meet and fuse along the dorsal midline, forming the adult notum in a process called thorax closure (Figure A.3). A confocal image illustrating nuclear GFP in the proximal area of the third instar wing disc is shown in Figure A.3A. The overexpression of *Atg1^{6B}* in the proximal area of the wing disc results in autophagy-dependent caspase activation and subsequently a thoracic cleft and reduced scutellum. It is noted that the distal areas of the two wing discs evert and proliferate to form the adult wings (Figure A.3).

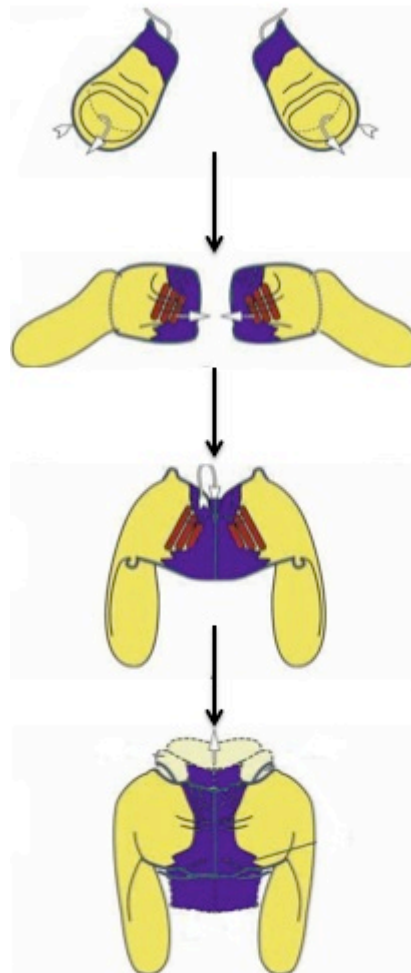
In addition, the spreading and fusing of the imaginal discs also results in the systematic replacement of larval epidermal tissues (Zeitlinger and Bohmann, 1999). These larval tissues are eliminated by PCD (Agnes *et al.*, 1999). At the end of thorax closure, the scutellum forms from a protrusion at the dorsal-posterior end of the fused wing disc, completing the development of the notum (Figure A.3) (Zeitlinger and Bohmann, 1999).

Figure A.3: The formation of the adult notum. (A) Image illustrating the location of the imaginal wing disc (blue) in larvae. Next to the larvae is a confocal image of a third instar wing disc at 20x magnification. The proximal area of the wing disc (green) will proliferate and evert to form the adult notum. The distal area of the wing disc (grey) will proliferate and evert to form the adult wing. (The Adult *Drosophila* cartoon was adapted from Gilbert, 2003). (B) Diagram illustrating the process of thorax closure. The domain of *pnrGAL4* expression is illustrated in purple. Arrows indicate the direction of tissue movement (Picture Adapted from: Zeitlinger and Bohmann, 1999).

(A)



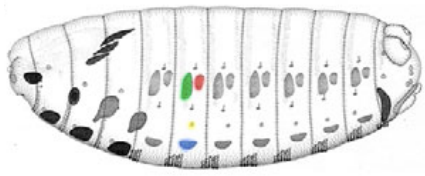
(B)



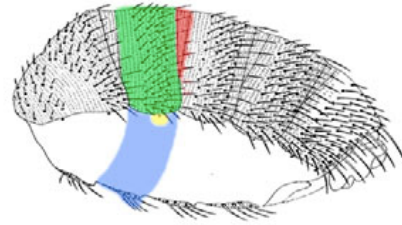
A.4 Abdomen Development

Another morphogenetic event that occurs during metamorphosis is abdomen development. During abdomen development, histoblasts, adult epidermal precursor cells grouped together into multiple nests, increase in volume and subsequently proliferate (Figure A.4). As a result, histoblast nests expand and fuse with neighboring nests. Ultimately, histoblast nests from the left and right sides of the pharate adult meet and fuse along the dorsal and ventral midlines (Figure A.4) (Ninov *et al.*, 2007). Throughout the expansion and fusion of histoblast nests, larval epithelial cells are systematically replaced by the imaginal histoblasts. These larval epithelial cells are eliminated by PCD (Ninov *et al.*, 2007). Finally, histoblasts differentiate, forming the various structures of the adult abdomen, including tendons for muscle attachment and the adult abdominal cuticle (Figure A.4) (Madhavan and Madhavan, 1980).

Figure A.4: Diagram illustrating the process of abdomen development during metamorphosis. The dorsal abdominal histoblasts (green and red) that originate in the embryo proliferate and expand during metamorphosis to form the dorsal adult tergites. Ventral imaginal discs (blue and yellow) proliferate, forming the sternites and pleurites (Picture Adapted From: Ninov *et al.*, 2007).



Embryo



Adult

Appendix B. Crossing Schemes

A variety of stocks were constructed to perform the experiments in this thesis. In particular, extensive genetic crosses were required to build the backgrounds used for the manipulation of *Atg1^{6B}*. The crossing schemes used to build the stocks used in this study are illustrated in this appendix.

Figure B.1: Crosses performed to make the *pnrGAL4 + UAS-GFP^{nls}* recombinant stock. To make the new recombinant stock, virgin females from the *w; pnrGAL4/TM6C,Sb,Tb (twi-lacZ)* stock were crossed to males from the *w; [UAS-GFP^{nls}]8* stock. In the F₁ progeny, *Tb⁺* (*Tubby⁺*) larvae, expressing GFP in a dorsal stripe down the midline, were selected. Freshly eclosed *w; pnrGAL4/[UAS-GFP^{nls}]8* virgin females were crossed to *yw/w; dronc⁵¹/TM6UW23-1(Tb, Sb)*. In the F₁ progeny, *Tb* larvae, expressing GFP in a dorsal stripe, were selected. The resulting *pnrGAL4+[UAS-GFP^{nls}]8/TM6UW23-1(Sb,Tb)* males from this selection were inspected for *Stubble (Sb)* expression and crossed to *Ly/TM3,Sb* virgin females. In the F₁ progeny, *Tb⁺*, GFP expressing larvae were selected and allowed to develop. From this selection, males and virgin females that were *Ly⁺* and exhibited *Sb* were selected and crossed with each other, resulting in the newly made *pnrGAL4+UAS-GFP^{nls}/TM3,Sb* recombinant stock. This stock is isogenic for the 3rd chromosome.

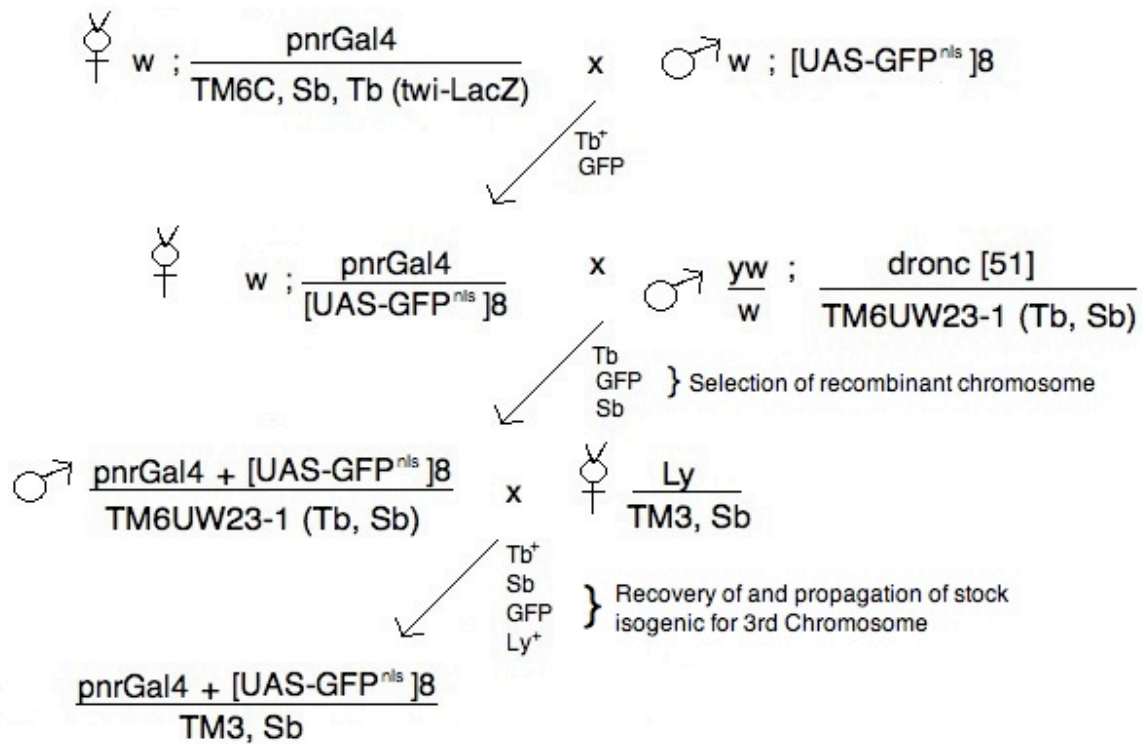


Figure B.2: Crossing scheme used to make the recombinant *pnrGAL4+UAS-Atg1^{6B}/TM6,Tb,[GAL80]* stock that was used in the genetic screen. To make the new recombinant stock, virgin females from the *pnrGAL4/TM6C,Sb,Tb* stock were crossed to males from the *UAS-Atg1^{6B}* stock. In the F₁ progeny, *Sb⁺* or *pnrGAL4/UAS-Atg1^{6B}* virgin females were selected and crossed to *Ly/TM3,Sb* males. In the F₁ progeny, a freshly eclosed male that exhibited *Sb* (*Stubble*), *Tb⁺* (*Tubby⁺*), and *Ly⁺*, and displayed an *Atg1^{6B}* overexpression phenotype was selected and crossed to *TM6B[GAL80]OV3,Tb/TM3,Sb*. In the F₁ progeny, males and virgin females were selected that exhibited the *Sb⁺*, *Tb* phenotypes and were propagated as a stock. These males and virgin females did not exhibit an *Atg1^{6B}* overexpression phenotype due to GAL80 expression.

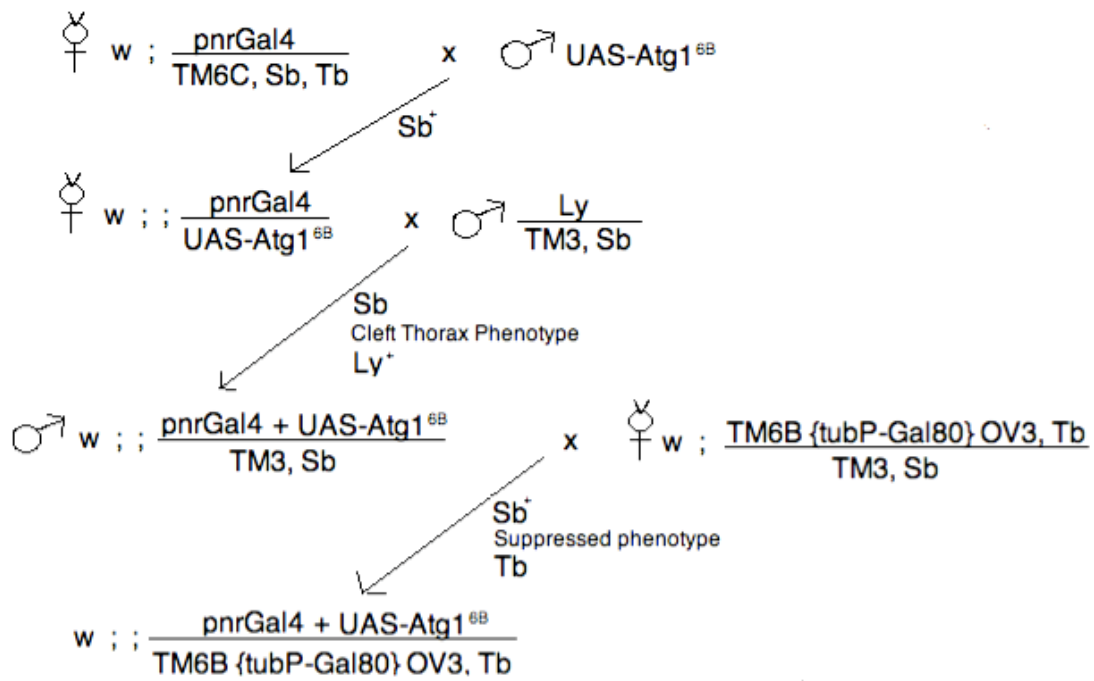
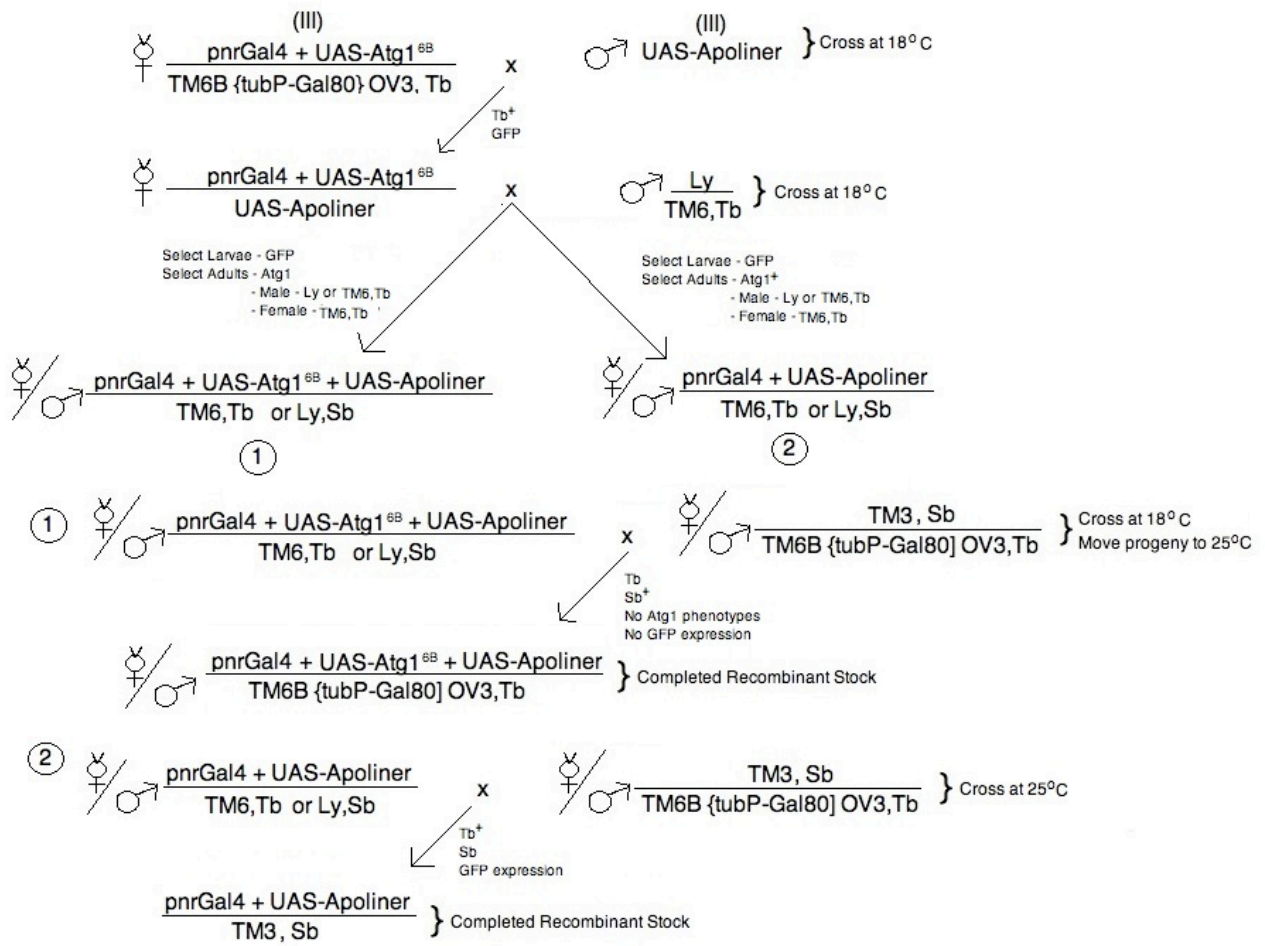


Figure B.3: Crossing scheme used to make the *pnrGAL4+UAS-Atg1^{6B}+UAS-Apoliner/TM6[GAL80],Tb* and the *pnrGal4+UAS-Apoliner/TM3,Sb* stocks. These stocks were used to evaluate caspase activation in the wing disc, larval epidermis and abdominal histoblast nests. Also, in the future this stock will be crossed to interacting deficiencies and genes to evaluate caspase activation.

(1) To make the *pnrGAL4+UAS-Atg1^{6B}+UAS-Apoliner/TM6[GAL80],Tb* stock virgin females from the *pnrGAL4+UAS-Atg1^{6B}/TM6,Tb[GAL80]* stock was crossed to males from the *UAS-Apoliner* stock at 18°C. This cross was performed at 18°C to increase the viability of the progeny overexpressing *Atg1^{6B}*. F₁, *pnrGAL4+Atg1^{6B}/UAS-Apoliner*, progeny that were *Tb*⁺ and expressed GFP, were selected and crossed to the *Ly/TM6,Tb* stock. In the F₁ progeny *Tb* larvae expressing GFP were selected and allowed to develop. Once eclosed, virgin females or males exhibiting the *Atg1^{6B}* overexpression phenotype were selected for. (Note: In the adult males, *Ly* was selected for in some cases instead of *Tb* in adult progeny). As a result only *pnrGAL4+UAS-Atg1^{6B}+UAS-Apoliner/[TM6,Tb or Ly,Sb]* flies were selected from this cross (Stock #1). These virgin females or males were then crossed to *TM3,Sb/TM6,Tb[GAL80]* at 18°C. The F₁ embryonic progeny resulting from this cross were moved to 25°C and allowed to develop into adults. *Tb* and *Sb*⁺ virgin females and males, that did not express GFP and had no recognizable *Atg1^{6B}* overexpression phenotype were selected and propagated as a stock.

(2) To make the *pnrGAL4+UAS-Apoliner/TM3,Sb* stock, virgin females from the *pnrGAL4+UAS-Atg1^{6B}/TM6,Tb[GAL80]* stock was crossed to males from the *UAS-Apoliner* stock at 18°C. F₁, *pnrGAL4+Atg1^{6B}/UAS-Apoliner*, progeny that were *Tb*⁺ and expressed GFP and *Atg1^{6B}*, were selected and crossed to the *Ly/TM6,Tb* stock. In the F₁ progeny *Tb* virgin females or (*Tb* or *Ly*) males that expressed GFP but did not have the *Atg1^{6B}* overexpression phenotype were selected (Stock #2). *pnrGAL4+UAS-Apoliner/TM6,Tb or Ly*, were then crossed to *TM3,Sb/TM6,Tb[GAL80]*. In the F₁ progeny, *Tb*⁺ virgin females and males that expressed GFP and exhibited *Sb* were selected and the stock was propagated.



Appendix C. GAL80^{ts} Experiment

Appendix C. GAL80^{ts} Experiment

C.1 Gal80^{ts}: Evaluation of *Atg1^{6B}* Overexpression During Development

Stereomicroscopic Live imaging and Scanning Electron Microscopy have shown that cell death, due to *Atg1^{6B}* overexpression in various tissues specified by *pnrGAL4*, contributes to an autophagy-induced adult cuticular phenotype. However, it is unknown which developmental stages or tissues are the most sensitive to *Atg1^{6B}* overexpression. Therefore, GAL80^{ts}, a temperature-sensitive protein, was employed to temporally regulate *UAS-Atg1^{6B}* during development (Figure C.1A) (Further details can be found in Materials and Methods Section). In progeny carrying both *GAL80^{ts}* and *UAS-Atg1^{6B}*, the viability and adult cuticular phenotypes associated with *Atg1^{6B}* overexpression, during various stages of development, were assessed (Figure C.1B).

As a result, it was determined that turning on *Atg1^{6B}* expression at any point between embryogenesis and the early phanerocephalic stages results in a strong thoracic and abdominal cleft and an absent scutellum. Also, *Atg1^{6B}* expression, during these stages, was largely lethal; therefore, the phenotypes were collected from escaper progeny or dissected pharate adults (Figure C.1B). Turning on *Atg1^{6B}* expression during the mid phanerocephalic stage onwards results in viable progeny that have a mild thoracic and abdominal cleft and a mildly reduced scutellum (Figure C.1B). By the Late phanerocephalic stages, turning on *Atg1^{6B}* expression shows no effect as the progeny exhibit a wildtype phenotype (Figure C.1B). These results indicate that progeny are most sensitive to *Atg1^{6B}* overexpression from embryogenesis to the mid phanerocephalic stages.

However, progeny in which *Atg1^{6B}* expression has been turned off by the third instar stages exhibit a wildtype phenotype (Figure C.1B). It is not until the pre-pupal stages before

Atg1^{6B} overexpression results in a mild thoracic and abdominal cleft and a slightly reduced scutellum. This result demonstrates that these progeny are not sensitive to *Atg1^{6B}* overexpression until the pre-pupal stages (Figure C.1B). Interestingly, progeny in which *Atg1^{6B}* expression has been turned off between the phanerocephalic and exarate adult stages are semi-lethal and exhibit a phenotype in which the notum is very small and lacks a scutellum, but has no identifiable thoracic cleft. Also, these progeny possess a strong to moderate abdominal cleft. It is likely that the absence of a thoracic cleft is due to a developmental delay, allowing wing discs to regenerate after *Atg1^{6B}* expression has been turned off.

Together, these results suggest that the developmental stages most sensitive to *Atg1^{6B}* overexpression are the pre-pupal to the mid phanerocephalic stages. Considering that it is between the pre-pupal to the mid phanerocephalic stage when both the wing discs and histoblast nests grow, divide and fuse with their counterparts (Fristrom and Fristrom, 1993), it is likely that *Atg1^{6B}* overexpression has the most severe effect on these morphogenetic processes.

Figure C.1: Summary Tables: GAL80^{ts} Experiment (A) Summary Table illustrating the developmental periods in which *Atg1^{6B}* was expressed. The red boxes indicate the developmental periods when *Atg1^{6B}* is being expressed. The white boxes indicate when *Atg1^{6B}* expression is turned off. The bottom row of the table indicates the developmental period in which *Atg1^{6B}* expression was either turned on or off. The far right column indicates the vial number associated with each shift in temperature. This vial number can be compared with the vial numbers in Figure B. (B) Summary Table illustrating the resulting adult phenotypes associated with *Atg1^{6B}* expression at various developmental periods. The top row illustrates all the possible phenotypes associated with the GAL80^{ts} experiment. With reference to the thoracic cleft phenotype: (None: Small) refers to a small thorax that does not possess a thoracic cleft. (None: Wildtype) refers to a thorax that appears similar to wildtype and does not possess a thoracic cleft. The left column indicates the vial number associated with the vial numbers in (A). An X was placed in any column where the progeny exhibited the associated phenotype. The far right column indicates the viability of the progeny within each vial.

C.2 Evaluation of *Atg1* Overexpression During Development using *GAL80^{ts}*

In the previous section *GAL80^{ts}* was used to determine the developmental stages or tissues that are the most sensitive to *Atg1^{6B}* overexpression. As a result, the developmental stages that appear to be the most sensitive to *Atg1^{6B}* overexpression are the pre-pupal to the mid phanerocephalic stages, a period in development when both the wing discs and histoblast nests are growing, dividing and fusing with their counterparts (Fristrom and Fristrom, 1993).

However, it should be noted that turning off *Atg1^{6B}* expression between the early phanerocephalic and exarate stages of development (Figure C.1 - Vials 18-22), resulted in progeny with a phenotype identical to the “undefined modifier” phenotype described in the genetic screen (Figure C.1B). These progeny exhibited a notum that had no identifiable cleft and an absent scutellum, and possessed a strong to moderate abdominal cleft. This result was unexpected since turning on *Atg1^{6B}* expression anywhere between the 1st instar and early phanerocephalic stages of development (Figure C.1 - Vials 1 to 6) resulted in flies with strong thoracic, abdominal, and scutellar defects. A possible explanation for the absence of a thoracic cleft in these progeny is that *Atg1^{6B}* is being turned off earlier than what was expected, allowing for compensatory proliferation in the wing disc. During this study it was observed that the overexpression of *Atg1^{6B}* results in a marked delay in development (data not shown). Therefore, the calculated developmental period in which *GAL80^{ts}* was turned on may have been overestimated, extending the period of time in which *Atg1^{6B}* was turned off before eclosion. During this time, surviving cells in the wing disc may have proliferated to compensate for the autophagy-induced cell death. In a study by Pérez-Garijo *et al.*, it has been demonstrated that after losing 50% of its cells due to apoptosis, wing discs use compensatory proliferation to regenerate and form normal adult cuticular structures (2004). However, the

compensatory proliferation in the wing disc after autophagy-induced cell death does not result in a wildtype phenotype. An obvious explanation for the different final adult cuticular phenotypes is that Pérez-Garijo *et al.*, induced apoptosis in the wing disc of third instar larvae (2004), whereas this thesis demonstrates the induction of cell death in the larval epidermis and wing discs. Also, *Atg1^{6B}* overexpression was not turned off until the pupal stages, giving the wing discs in this study less time to regenerate than those observed in the study by Pérez-Garijo *et al.* (2004). Together, these results indicate that wing discs are able to undergo compensatory proliferation when *Atg1^{6B}* expression has been turned off in the earlier stages of pupal development. However, further research should be performed to increase the resolution of this experiment before any firm conclusions are drawn.



C.3 Increasing the Resolution of the GAL80^{ts} Experiment

In the future, another GAL80^{ts} experiment will be performed to determine the specific stages during development that are the most sensitive to *Atg1^{6B}* overexpression. During this experiment crosses will be performed in an identical manner to the previous GAL80^{ts} experiment (See Materials and Methods). However, at various time-points during development, each vial will be shifted twice, once upwards, from 18°C to 29°C, and once downwards, from 29°C to 18°C (Figure C.2). This will result in *Atg1^{6B}* being turned on or off during a single stage of development (Figure C.2). Once eclosed, the severity of the thoracic cleft and the reduced scutellum phenotype of [*GAL80ts*]/+; *pnrGAL4+UAS-Atg1^{6B}/TM2* or *TM6B* progeny will be evaluated. Any consistent difference in the severity of the adult cuticular phenotype will indicate, with increased resolution, the developmental stages most sensitive to *Atg1^{6B}* overexpression.

Figure C.2: Summary diagram illustrating the future GAL80^{ts} experiment. During this experiment *Atg1^{6B}* expression will be turned on (red boxes) or off (white boxes) for a single developmental stage. The bottom row of the table indicates the developmental period in which *Atg1^{6B}* expression was either turned on or off. The far right column indicates the vial number associated with each shift in temperature.

A

Embryo	1 st Instar	2 nd Instar	Early 3 rd Instar	Late 3 rd Instar	Pre-Pupae	Phanerocephalic Metamorphosis				Exarate Adult	
						Early	Mid	Late	Exarate Adult		
Vial 1											
Vial 2											
Vial 3											
Vial 4											
Vial 5											
Vial 6											
Vial 7											
Vial 8											
Vial 9											
Vial 10											
Vial 13											
Vial 14											
Vial 15											
Vial 16											
Vial 17											
Vial 18											
Vial 19											
Vial 20											
Vial 21											
Vial 22											

 *Atg1^{6B}* expression ON
 *Atg1^{6B}* expression OFF

Appendix D. Stocks Used in Genetic Screen

Note: Rows that are shaded in gray are false positives because the deficiencies they encompass contain either *Haplo-insufficient* or *Minute* loci or they delete the *pannier* region. Also, 2 deficiencies are shaded in yellow and 1 deficiency is shaded in blue because they interact with *BsgRNAi*⁴³³⁰⁷ and *EP(3)3614* respectively.

Table D.1: Deficiency (2L) Stocks

Deficiency Name (Stock)	Cytology	Interaction (Su, En, NC)* Severity (+/-)
<i>Df(2L)ED50001</i> (24626)	21A1; 21B1	NC
<i>Df(2L)ED5878</i> (9353)	21B1; 21B3	NC
<i>Df(2L)ED21</i> (9177)	21B3; 21B7	NC
<i>Df(2L)BSC106</i> (8672)	21B7; 21C2	NC
<i>Df(2L)BSC107</i> (8673)	21C2; 21E2	NC
<i>Df(2L)ED62</i> (8937)	21D1; 21E2	UM
<i>Df(2L)ED80</i> (9191)	21E2; 21E2	NC
<i>Df(2L)Exel7005</i> (7775)	21E2; 21E2	NC
<i>Df(2L)ED6003</i> (7490)	21E2; 21E4	NC
<i>Df(2L)ED94</i> (8908)	21E2; 21E3	NC
<i>Df(2L)ED105</i> (24118)	21E2; 22A1	NC
<i>Df(2L)Exel6004</i> (7491)	21E4; 21F1	NC
<i>Df(2L)ED108</i> (24629)	21F1; 22A1	NC
<i>Df(2L)Exel6005</i> (7492)	22A3; 22B1	NC
<i>Df(2L)Exel7007</i> (7778)	22B1; 22B5	NC
<i>Df(2L)Exel8005</i> (7779)	22B2; 22B8	NC
<i>Df(2L)ED123</i> (8943)	22B8; 22D4	NC
<i>Df(2L)Exel7010</i> (7782)	22D4; 22E1	NC
<i>Df(2L)Exel7011</i> (7783)	22E1; 22F3	EN (++)

* All deficiencies were classified based on the criteria from Table 4.1. E (+) = Moderate Enhancer that is semi-lethal; E (++) = Strong Enhancer that is lethal; Su (-) = Moderate Suppressor; Su (--) = Strong Suppressor; UM = Undefined Modifier; NC = No Change

<i>Df(2L)ED136</i> (9176)	22F4; 23A3	NC
<i>Df(2L)Exel6277</i> (7744)	23A2; 23B1	NC
<i>Df(2L)BSC692</i> (26544)	23B3; 23B7	UM
<i>Df(2L)ED4651</i> (8904)	23B8; 23F3	NC
<i>Df(2L)Exel7016</i> (7787)	23E5; 23F3	NC
<i>Df(2L)BSC292</i> (23677)	23F6; 24A2	NC
<i>Df(2L)Exel7018</i> (7789)	24A1; 24C2	NC
<i>Df(2L)Exel6009</i> (7495)	24C3; 24C8	NC
<i>Df(2L)Exel8010</i> (7790)	24C8; 24D4	NC
<i>Df(2L)BSC295</i> (23680)	24D4; 24F3	UM
<i>Df(2L)ED250</i> (9270)	24F4; 25A7	NC
<i>Df(2L)Exel6010</i> (7496)	25A7; 25B1	NC
<i>Df(2L)Exel8012</i> (7793)	25B1; 25B5	NC
<i>Df(2L)Exel7021</i> (7795)	25B3; 25B5	NC
<i>Df(2L)Exel8013</i> (7796)	25B5; 25B10	NC
<i>Df(2L)Exel7022</i> (7794)	25B10; 25C3	NC
<i>Df(2L)BSC110</i> (8835)	25C1; 25C4	NC
<i>Df(2L)BSC109</i> (8674)	25C4; 25C8	NC
<i>Df(2L)Exel6011</i> (7497)	25C8; 25D5	EN (++)
<i>Df(2L)Exel6012</i> (7498)	25D5; 25E6	NC
<i>Df(2L)Exel7023</i> (7797)	25E5; 25F1	NC
<i>Df(2L)Exel8016</i> (7798)	25E6; 25F2	NC
<i>Df(2L)ED334</i> (9343)	25F2; 26B2	SU (-)

<i>Df(2L)BSC354</i> (24378)	26B1; 26B5	NC
<i>Df(2L)ED384</i> (9297)	26B2; 26D7	NC
<i>Df(2L)BSC7</i> (6374)	26D10-E1; 27C1	UM
<i>Df(2L)Exel7027</i> (7801)	26F6; 27B1	NC
<i>Df(2L)BSC108</i> (8847)	27C1; 27C6	NC
<i>Df(2L)Exel7029</i> (7802)	27C4; 27D4	NC
<i>Df(2L)BSC291</i> (23676)	27D6; 27F2	NC
<i>Df(2L)Exel8019</i> (7803)	27E2; 27E4	NC
<i>Df(2L)Exel6017</i> (7503)	27E4; 27F3	NC
<i>Df(2L)ED489</i> (9060)	27E4; 28B1	NC
<i>Df(2L)Exel6018</i> (7504)	28B1; 28C1	NC
<i>Df(2L)ED508</i> (8944)	28B1; 28C4	EN (+)
<i>Df(2L)ED12527</i> (24129)	28C4; 28D3	EN (++)
<i>Df(2L)Exel7034</i> (7807)	28E1; 28F1	EN (++)
<i>Df(2L)ED548</i> (24130)	28E1; 28E9	UM
<i>Df(2L)BSC228</i> (9705)	28E5; 28F4	NC
<i>Df(2L)BSC227</i> (9704)	28E8; 29B1	NC
<i>Df(2L)ED578</i> (24131)	28F1; 29A3	NC
<i>Df(2L)BSC229</i> (9706)	28F1; 29B1	NC
<i>Df(2L)ED611</i> (9298)	29B4; 29C3	NC
<i>Df(2L)ED623</i> (8930)	29C1; 29E4	NC
<i>Df(2L)ED647</i> (8678)	29E1; 29F5	NC
<i>Df(2L)ED678</i> (8906)	29F5; 30B12	NC

<i>Df(2L)Exel6024</i> (7507)	30C1; 30C9	NC
<i>Df(2L)ED695</i> (8041)	30C5; 30E4	NC
<i>Df(2L)Exel7043</i> (7816)	30D1; 30F1	EN (+)
<i>Df(2L)BSC205</i> (9632)	30F5; 31A2	NC
<i>Df(2L)Exel8024</i> (7817)	31A2; 31B1	NC
<i>Df(2L)Exel7046</i> (7819)	31B1; 31D9	NC
<i>Df(2L)BSC342</i> (24366)	31D9; 31E5	NC
<i>Df(2L)Exel7048</i> (7999)	31E3; 31F5	NC
<i>Df(2L)ED746</i> (8043)	31F4; 32A5	NC
<i>Df(2L)Exel8026</i> (7820)	31F5; 32B3	NC
<i>Df(2L)Exel7049</i> (7821)	32B1; 32C1	NC
<i>Df(2L)BSC241</i> (9716)	32C1; 32F2	UM
<i>Df(2L)Exel6027</i> (7510)	32D2; 32D5	UM
<i>Df(2L)BSC242</i> (24905)	32D4; 32F4	NC
<i>Df(2L)Exel6028</i> (7511)	32D5; 32E4	NC
<i>Df(2L)Exel6029</i> (7512)	32E4; 32F2	NC
<i>Df(2L)BSC244</i> (9718)	32F2; 33B6	NC
<i>Df(2L)Exel6030</i> (7513)	33A2; 33B3	NC
<i>Df(2L)Exel6031</i> (7514)	33B3; 33C2	NC
<i>Df(2L)ED775</i> (8907)	33B8; 34A3	EN (+)
<i>Df(2L)ED778</i> (7420)	33E9; 34A7	NC
<i>Df(2L)ED784</i> (7421)	34A4; 34B6	EN (++)
<i>Df(2L)BSC340</i> (24364)	34B4; 34B8	EN (+)

<i>Df(2L)BSC147</i> (9506)	34C1; 34C6	NC
<i>Df(2L)BSC691</i> (26543)	34C3; 34D1	NC
<i>Df(2L)Exel7059</i> (7826)	34D1; 34E1	NC
<i>Df(2L)ED793</i> (9061)	34E4; 35B4	NC
<i>Df(2L)ED3</i> (6963)	35B2; 35D1	NC
<i>Df(2L)ED1050</i> (8946)	35B8; 35D4	EN (+)
<i>Df(2L)Exel7063</i> (7831)	35D2; 35D4	NC
<i>Df(2L)Exel6038</i> (7521)	35D6; 35E2	NC
<i>Df(2L)BSC293</i> (23678)	35E1; 35F1	NC
<i>Df(2L)Exel6039</i> (7522)	36A10; 36B3	SU (-)
<i>Df(2L)Exel8036</i> (7835)	36B1; 36C9	NC
<i>Df(2L)Exel7068</i> (7838)	36C7; 36C10	NC
<i>Df(2L)Exel7069</i> (7837)	36C10; 36D3	NC
<i>Df(2L)Exel7070</i> (7839)	36E2; 36E6	NC
<i>Df(2L)Exel8038</i> (7840)	36E5; 36F5	SU (-)
<i>Df(2L)Exel6041</i> (7523)	36F6; 37A2	NC
<i>Df(2L)ED1203</i> (8935)	36F7; 37C5	NC
<i>Df(2L)ED1231</i> (9174)	37C5; 37E3	NC
<i>Df(2L)ED1303</i> (8679)	37E5; 38C6	NC
<i>Df(2L)Exel6044</i> (7526)	37F2; 38A3	NC
<i>Df(2L)Exel6045</i> (7527)	38A3; 38A7	UM
<i>Df(2L)Exel7077</i> (7850)	38A7; 38B2	NC
<i>Df(2L)ED1315</i> (9269)	38B4; 38F5	EN (+)

<i>Df(2L)Exel7080</i> (7853)	38F3; 39A2	NC
<i>Df(2L)Exel6047</i> (7529)	39A2; 39B4	NC
<i>Df(2L)Exel6048</i> (7530)	39B4; 39C2	NC
<i>Df(2L)ED1473</i> (9266)	39B4; 40A5	NC
<i>Df(2L)ED1466</i> (9340)	39E3; 40A5	NC
<i>Df(2L)BSC104</i> (8670)	39D5; 39E2	NC
<i>Df(2L)BSC151</i> (9510)	40A5; 40E5	NC

Table D.2: Deficiency (2R) Stocks

Deficiency Name (Stock)	Cytology	Interaction (Su, EN, NR)*
<i>Df(2R)BSC630</i> (25705)	41D3; 41F11	UM
<i>Df(2R)ED1484</i> (9683)	42A2; 42A14	UM
<i>Df(2R)ED1552</i> (8044)	42A11; 42C7	NC
<i>Df(2R)ED1618</i> (8939)	42C4; 43A1	UM
<i>Df(2R)ED1673</i> (9062)	42E1; 43D3	NC
<i>Df(2R)ED1715</i> (8931)	43A4; 43F1	NC
<i>Df(2R)ED1735</i> (9275)	43F8; 44D4	NC
<i>Df(2R)ED1742</i> (9276)	44B8; 44E3	NC
<i>Df(2R)ED1791</i> (9063)	44F7; 45F1	NC
<i>Df(2R)BSC131</i> (9296)	46A1; 46B4	NC
<i>Df(2R)Exel9016</i> (7867)	46B1; 46B2	NC
<i>Df(2R)BSC298</i> (23682)	46B2; 46C7	NC
<i>Df(2R)BSC152</i> (9539)	46C1; 46D6	E (++)
<i>Df(2R)BSC303</i> (23686)	46E1; 46F3	NC
<i>Df(2R)BSC281</i> (23666)	46F1; 47A9	NC
<i>Df(2R)ED2098</i> (9277)	47A7; 47C6	NC
<i>Df(2R)ED2155</i> (9344)	47C6; 47F8	NC
<i>Df(2R)ED2219</i> (8910)	47D6; 48B6	NC

* All deficiencies were classified based on the criteria from Table 4.1. E (+) = Moderate Enhancer that is semi-lethal; E (++) = Strong Enhancer that is lethal; Su (-) = Moderate Suppressor; Su (--) = Strong Suppressor; UM = Undefined Modifier; NC = No Change

<i>Df(2R)ED2247</i> (8912)	48A3; 48D5	EN (++)
<i>Df(2R)BSC199</i> (9626)	48C5; 48E4	NC
<i>Df(2R)BSC40</i> (7146)	48E1-2; 48E2-10	UM
<i>Df(2R)BSC3</i> (5879)	48E12-F4; 49A11-B6	UM
<i>Df(2R)Exel6061</i> (7543)	48F1; 49A6	UM
<i>Df(2R)Exel7121</i> (7869)	49B5; 49B12	SU (-)
<i>Df(2R)ED2308</i> (9268)	49C3; 49E7	NC
<i>Df(2R)Exel8057</i> (7871)	49F1; 49F10	NC
<i>Df(2R)Exel7124</i> (7872)	49F10; 50A1	NC
<i>Df(2R)BSC306</i> (23689)	50A3; 50B1	NC
<i>Df(2R)BSC307</i> (23690)	50B6; 50C18	NC
<i>Df(2R)Exel7128</i> (7873)	50C5; 50C9	NC
<i>Df(2R)BSC383</i> (24407)	50C6; 50D2	UM
<i>Df(2R)Exel7130</i> (7875)	50D4; 50E4	SU (-)
<i>Df(2R)Exel7131</i> (7876)	50E4; 50F6	NC
<i>Df(2R)ED2354</i> (8913)	50E6; 51B1	NC
<i>Df(2R)Exel6284</i> (7749)	51B1; 51C2	NC
<i>Df(2R)BSC429</i> (24933)	51C2; 51D1	NC
<i>Df(2R)BSC651</i> (25741)	51C5; 51E2	NC
<i>Df(2R)ED2426</i> (9064)	51E2; 52B1	NC
<i>Df(2R)ED2436</i> (8914)	51F11; 52D11	NC
<i>Df(2R)ED2457</i> (8915)	52D11; 52E7	NC
<i>Df(2R)Exel9060</i> (7885)	52E11; 52F1	NC

<i>Df(2R)BSC609</i> (25442)	52F6; 53A5	NC
<i>Df(2R)Exel7142</i> (7886)	53B1; 53C4	NC
<i>Df(2R)Exel7144</i> (7888)	53C8; 53D2	NC
<i>Df(2R)ED3181</i> (9213)	53C9; 53F10	NC
<i>Df(2R)Exel6066</i> (7548)	53F8; 54B6	SU (--)
<i>Df(2R)BSC161</i> (9596)	54B2; 54B17	NC
<i>Df(2R)BSC355</i> (24379)	54B16; 54C3	NC
<i>Df(2R)BSC45</i> (7441)	54C8-D1; 54E2-7	NC
<i>Df(2R)Exel7149</i> (7890)	54C10; 54D5	SU (-)
<i>Df(2R)Exel7150</i> (7891)	54E1; 54E9	NC
<i>Df(2R)ED3610</i> (9066)	54F1; 55C8	NC
<i>Df(2R)Exel6069</i> (7551)	56B5; 56C11	NC
<i>Df(2R)BSC26</i> (6866)	56C4; 56D6-10	NC
<i>Df(2R)BSC22</i> (6647)	56D7-E3; 56F9-12	SU (-)
<i>Df(2R)Exel7162</i> (7896)	56F11; 56F16	NC
<i>Df(2R)BSC701</i> (26553)	56F15; 57A9	NC
<i>Df(2R)Exel6070</i> (7552)	57A6; 57B3	NC
<i>Df(2R)ED3791</i> (9267)	57B1; 57D4	NC
<i>Df(2R)Exel6071</i> (7553)	57B3; 57B16	UM
<i>Df(2R)Exel6072</i> (7554)	57B16; 57D4	UM
<i>Df(2R)Exel6076</i> (7556)	57E1; 57F3	NC
<i>Df(2R)BSC360</i> (24384)	57E6; 58A4	NC
<i>Df(2R)ED3923</i> (8942)	57F6; 57F10	NC

<i>Df(2R)ED3943</i> (9158)	57F10; 58D4	NC
<i>Df(2R)ED3952</i> (9223)	58B10; 58E5	NC
<i>Df(2R)Exel7173</i> (7903)	58D4; 58E5	NC
<i>Df(2R)BSC598</i> (25431)	58F3; 59A1	NC
<i>Df(2R)Exel6079</i> (7559)	59A3; 59B1	NC
<i>Df(2R)Exel7176</i> (7905)	59B4; 59C2	NC
<i>Df(2R)Exel7177</i> (7906)	59C3; 59D2	NC
<i>Df(2R)Exel7178</i> (7908)	59D5; 59D10	NC
<i>Df(2R)Exel7180</i> (7909)	59E3; 59F6	NC
<i>Df(2R)BSC610</i> (25443)	59F6; 60A14	NC
<i>Df(2R)BSC601</i> (25434)	60A9; 60B1	NC
<i>Df(2R)BSC356</i> (24380)	60B8; 60C4	NC
<i>Df(2R)Exel6082</i> (7561)	60C4; 60C7	NC
<i>Df(2R)ED4065</i> (9069)	60C8; 60E8	EN (+)
<i>Df(2R)BSC608</i> (25441)	60E11; 60F2	NC
<i>Df(2R)ED50004</i> (24758)	60F5; 60F5	NC

Table D.3: Deficiency (3L) Stocks

Deficiency Name (Stock)	Cytology	Interaction (SU, EN, NR)*
<i>Df(3L)emc-E12</i> (2577)	61A; 61D3	UM
<i>Df(3L)ED4079</i> (8046)	61A5; 61B1	NC
<i>Df(3L)ED201</i> (8047)	61B1; 61C1	NC
<i>Df(3L)ED4177</i> (8048)	61C1; 61E2	NC
<i>Df(3L)ED207</i> (8053)	61C9; 62A6	NC
<i>Df(3L)Exel6087</i> (7566)	62A2; 62A6	NC
<i>Df(3L)ED4256</i> (8054)	62A3; 62A6	NC
<i>Df(3L)BSC181</i> (9693)	62A11; 62B7	NC
<i>Df(3L)Aprt-1</i> (600)	62A10-B1; 62D2-5	UM
<i>Df(3L)BSC364</i> (24388)	62B4; 62C4	NC
<i>Df(3L)ED4287</i> (8096)	62B4; 62E5	EN (+)
<i>Df(3L)Exel6089</i> (7568)	62D1; 62D4	NC
<i>Df(3L)BSC385</i> (24409)	62D4; 62E1	UM
<i>Df(3L)BSC116</i> (8973)	62D7; 62E5	UM
<i>Df(3L)BSC23</i> (6755)	62E8; 63B5-6	NC
<i>Df(3L)Exel6091</i> (7570)	62E8; 62F5	NC
<i>Df(3L)Exel6092</i> (7571)	62F5; 63A3	NC
<i>Df(3L)ED4288</i> (8057)	63A6; 63B7	NC
<i>Df(3L)ED4293</i> (8058)	63C1; 63C1	NC

* All deficiencies were classified based on the criteria from Table 4.1. E (+) = Moderate Enhancer that is semi-lethal; E (++) = Strong Enhancer that is lethal; Su (-) = Moderate Suppressor; Su (--) = Strong Suppressor; UM = Undefined Modifier; NC = No Change.

<i>Df(3L)ED208</i> (8059)	63C1; 63F5	NC
<i>Df(3L)HR119</i> (3649)	63C2; 63F7	NC
<i>Df(3L)GN34</i> (463)	63E6-9; 64A8-9	NC
<i>Df(3L)Exel6098</i> (7577)	63F2; 63F7	EN (++)
<i>Df(3L)ED4341</i> (8060)	63F6; 64B9	UM
<i>Df(3L)GN24</i> (3686)	63F6-7; 64C13-15	NC
<i>Df(3L)ED210</i> (8061)	64B9; 64C13	NC
<i>Df(3L)ZN47</i> (3096)	64C; 65C	EN (++)
<i>Df(3L)Exel6104</i> (7583)	64C8; 64C13	NC
<i>Df(3L)Exel6106</i> (7585)	64D6; 64E2	EN (+)
<i>Df(3L)Exel6107</i> (7586)	64E5; 64F5	NC
<i>Df(3L)Exel7210</i> (7927)	65A1; 65A5	NC
<i>Df(3L)XDI98</i> (4393)	65A2; 65E1	NC
<i>Df(3L)Exel8101</i> (7928)	65A3; 65A9	UM
<i>Df(3L)ED211</i> (8063)	65A9; 65B4	NC
<i>Df(3L)Exel6109</i> (7588)	65C3; 65D3	UM
<i>Df(3L)BSC27</i> (6867)	65D4-5; 65E4-6	NC
<i>Df(3L)Exel6110</i> (7589)	65E3; 65E5	NC
<i>Df(3L)BSC33</i> (6964)	65E10-F1; 65F2-6	NC
<i>Df(3L)pbl-X1</i> (1420)	65F3; 66B10	NC
<i>Df(3L)Exel8104</i> (7929)	65F7; 66A4	NC
<i>Df(3L)Exel6279</i> (7745)	66A17; 66B5	NC
<i>Df(3L)Exel6112</i> (7591)	66B5; 66C8	NC

<i>Df(3L)BSC13</i> (6460)	66B12-C1; 66D2-4	NC
<i>Df(3L)h-i22</i> (3024)	66D10-11; 66E1-2	NC
<i>Df(3L)ED4421</i> (8066)	66D12; 67B3	NC
<i>Df(3L)AC1</i> (997)	67A2; 67D11-13	NC
<i>Df(3L)Exel6114</i> (7593)	67B11; 67C5	NC
<i>Df(3L)BSC283</i> (23668)	67C7; 67D5	NC
<i>Df(3L)Exel9048</i> (7933)	67D1; 67D2	NC
<i>Df(3L)ED4457</i> (9355)	67E2; 68A7	NC
<i>Df(3L)ED4470</i> (8068)	68A6; 68E1	NC
<i>Df(3L)vin7</i> (2612)	68C8-11; 69B4-5	SU (--)
<i>Df(3L)ED4475</i> (8069)	68C13; 69B4	NC
<i>Df(3L)ED4483</i> (8070)	69A5; 69D3	EN (++)
<i>Df(3L)eyg^{Cl}</i> (5492)	69A4-5; 69D4-6	EN (+)
<i>Df(3L)ED4486</i> (8072)	69C4; 69F6	EN (+)
<i>Df(3L)BSC10</i> (6456)	69D4-5; 69F5-7	NC
<i>Df(3L)BSC12</i> (6457)	69F6-70A1; 70A1-2	NC
<i>Df(3L)ED4502</i> (8097)	70A3; 70C10	NC
<i>Df(3L)ED4543</i> (8073)	70C6; 70F4	NC
<i>Df(3L) fz-M21</i> (3126)	70D2-3; 71E4-5	NC
<i>Df(3L)ED217</i> (8074)	70F4; 71E1	NC
<i>Df(3L)XG5</i> (6551)	71C2-3; 72B1-C1	NC
<i>Df(3L)brm11</i> (3640)	71F1-4; 72D1-10	NC
<i>Df(3L)st-fl3</i> (2993)	72C1-D1; 73A3-4	NC

<i>Df(3L)Exel6127</i> (7606)	72D1; 72D9	EN (+)
<i>Df(3L)ED4674</i> (8098)	73B5; 73E5	NC
<i>Df(3L)ED4685</i> (8099)	73D5; 74E2	NC
<i>Df(3L)ED4710</i> (8100)	74D1; 75B11	NC
<i>Df(3L)ED224</i> (8080)	75B1; 75C6	NC
<i>Df(3L)Cat</i> (2990)	75B8; 75F1	NC
<i>Df(3L)H99</i> (1576)	75C1; 75C2	NC
<i>Df(3L)ED225</i> (8081)	75C1; 75D4	NC
<i>Df(3L)ED4782</i> (8082)	75F2; 76A1	NC
<i>Df(3L)ED4786</i> (8083)	75F7; 76A5	NC
<i>Df(3L)fz2</i> (6754)	75F10-11; 76A1-5	NC
<i>Df(3L)ED229</i> (8087)	76A1; 76E1	E (++)
<i>Df(3L)BSC20</i> (6646)	76A7-B1; 76B4-5	NC
<i>Df(3L)kto2</i> (3617)	76B2; 76D5	SU (--)
<i>Df(3L)XS533</i> (5126)	76B4; 77B	NC
<i>Df(3L)ED4858</i> (8088)	76D3; 77C1	NC
<i>Df(3L)rdgC-co2</i> (2052)	77A1; 77D1	UM
<i>Df(3L)Exel6136</i> (7615)	77B2; 77C6	NC
<i>Df(3L)ri-79c</i> (3127)	77B-C; 77F-78A	NC
<i>Df(3L)ri-XT1</i> (5878)	77E2-4; 78A2-4	NC
<i>Df(3L)ME107</i> (4429)	77F3; 78C8-9	SU (-)
<i>Df(3L)Pc-2q</i> (4430)	78C5-6; 78E3-79A1	NC
<i>Df(3L)ED4978</i> (8101)	78D5; 79A2	NC

<i>Df(3L)Exel6137</i> (7616)	78F4; 79A4	NC
<i>Df(3L)BSC223</i> (9700)	79A3; 79B3	NC
<i>Df(3L)BSC249</i> (23149)	79B2; 79D1	NC
<i>Df(3L)ED230</i> (8089)	79C2; 80A4	NC
<i>Df(3L)ED5017</i> (8102)	80A4; 80C2	NC

Table D.4: Deficiency (3R) Stocks

Deficiency Name (Stock)	Cytology	Interaction (SU, EN, NR)*
<i>Df(3R)ME15</i> (1518)	81F3-6; 82F5-7	NC
<i>Df(3R)ED5046</i> (9197)	81F6; 82D2	NC
<i>Df(3R)3-4</i> (4787)	82F3-4; 82F10-11	NC
<i>Df(3R)ED5156</i> (8965)	82F8; 83A4	NC
<i>Df(3R)ED10257</i> (9159)	83A7; 83B4	NC
<i>Df(3R)ED5177</i> (8103)	83B4; 83B6	NC
<i>Df(3R)Exel6144</i> (7623)	83A6; 83B6	SU (-)
<i>Df(3R)ED5197</i> (9339)	83B7; 83D2	NC
<i>Df(3R)ED7665</i> (8685)	84B4; 84E11	EN (+)
<i>Df(3R)Exel6146</i> (7625)	84C8; 84D9	NC
<i>Df(3R)ED5223</i> (9076)	84D9; 84E11	NC
<i>Df(3R)ED5230</i> (8682)	84E6; 85A5	NC
<i>Df(3R)ED5296</i> (9338)	84F6; 85C3	EN (++)
<i>Df(3R)Exel8143</i> (7954)	85A5; 85B2-3	NC
<i>Df(3R)Exel6150</i> (7629)	85A5; 85B6	NC
<i>Df(3R)ED5330</i> (9077)	85A5; 85D1	EN (++)
<i>Df(3R)by10</i> (1931)	85D8-12; 85E7-F1	EN (++)
<i>Df(3R)ED5429</i> (8919)	85D19; 85F8	EN (++)
<i>Df(3R)ED5428</i> (9227)	85E1; 85F8	EN (+)

* All deficiencies were classified based on the criteria from Table 4.1. E (+) = Moderate Enhancer that is semi-lethal; E (++) = Strong Enhancer that is lethal; Su (-) = Moderate Suppressor; Su (--) = Strong Suppressor; UM = Undefined Modifier; NC = No Change.

<i>Df(3R)ED5454</i> (9080)	85E5; 85F12	NC
<i>Df(3R)ED5474</i> (9082)	85F11; 86B1	NC
<i>Df(3R)ED5495</i> (9215)	85F16; 86C7	E (++)
<i>Df(3R)Exel6159</i> (7638)	86C3; 86C7	NC
<i>Df(3R)ED5518</i> (9084)	86C7; 86E13	NC
<i>Df(3R)ED5559</i> (8920)	86E11; 87B11	NC
<i>Df(3R)Exel7314</i> (7969)	87B3; 87B8	NC
<i>Df(3R)ED5591</i> (9086)	87B7; 87C7	EN (++)
<i>Df(3R)Exel7315</i> (7931)	87B8; 87B9	UM
<i>Df(3R)Exel7316</i> (7970)	87B9; 87B11	UM
<i>Df(3R)Exel7317</i> (7932)	87B10; 87C3	NC
<i>Df(3R)Exel6166</i> (7645)	87C5; 87C7-8	UM
<i>Df(3R)ED5612</i> (9088)	87C7; 87F6	EN (+)
<i>Df(3R)Tp(3;Y)ry506-85C</i> (1534)	87D1-2; 88E5-6	EN (++)
<i>Df(3R)ED5623</i> (8921)	87E3; 88A4	EN (+)
<i>Df(3R)ED5644</i> (9090)	88A4; 88C9	NC
<i>Df(3R)Exel8160</i> (7978)	88C10; 88D6	NC
<i>Df(3R)Exel6173</i> (7652)	88D7; 88E1	EN (+)
<i>Df(3R)ea</i> (383)	88E7-13; 89A1	NC
<i>Df(3R)ED5705</i> (9152)	88E12; 89A5	NC
<i>Df(3R)Exel7326</i> (7980)	88F7; 89A5-6	NC
<i>Df(3R)sbd105</i> (756)	88F9-89A1; 89B9-10	<i>pannier</i> located here
<i>Df(3R)BSC569</i> (25670)	89A1; 89A5	NC

<i>Df(3R)Exel8162</i> (7981)	89A5; 89A8	NC
<i>Df(3R)Exel7327</i> (7982)	89A8; 89B1	<i>pannier</i> located here
<i>Df(3R)Exel7328</i> (7983)	89A12; 89B6	<i>pannier</i> located here
<i>Df(3R)sbd104</i> (1920)	89B5; 89C2-7	NC
<i>Df(3R)Exel7329</i> (7984)	89B9; 89B13	NC
<i>Df(3R)Exel6269</i> (7736)	89B12; 89B18	NC
<i>Df(3R)Exel6270</i> (7737)	89B18; 89D8	NC
<i>Df(3R)P115</i> (1467)	89B7-8; 89E7	NC
<i>Df(3R)DG2</i> (4431)	89E1-F4; 91B1-B2	NC
<i>Df(3R)Exel8165</i> (7988)	89E8; 89E11	NC
<i>Df(3R)ED5780</i> (8104)	89E11; 90C1	NC
<i>Df(3R)Exel6176</i> (7655)	89E11; 89F1	NC
<i>Df(3R)BSC684</i> (26536)	90A6; 90B7	NC
<i>Df(3R)ED5815</i> (9208)	90F4; 91B8	NC
<i>Df(3R)Cha7</i> (3011)	90F1-F4; 91F5	NC
<i>Df(3R)ED2</i> (6962)	91A5; 91F1	NC
<i>Df(3R)Exel6183</i> (7662)	91E4; 91F4	NC
<i>Df(3R)D1-BX12</i> (3012)	91F1-2; 92D3-6	NC
<i>Df(3R)Exel6184</i> (7663)	92A5; 92A11	NC
<i>Df(3R)ED6025</i> (8964)	92A11; 92E2	NC
<i>Df(3R)H-B79</i> (4962)	92B3; 92F13	SU (-)
<i>Df(3R)Exel6185</i> (7664)	92E2; 92F1	NC
<i>Df(3R)Exel6272</i> (7739)	93A4; 93B13	NC

<i>Df(3R)e-R1</i> (3340)	93B6-7; 93D2	EN (++)
<i>Df(3R)ED6076</i> (8962)	93E10; 94A1	NC
<i>Df(3R)ED6090</i> (9091)	94A1; 94C1	NC
<i>Df(3R)ED6096</i> (8684)	94B5; 94E7	NC
<i>Df(3R)BSC56</i> (8583)	94E1-2; 94F1-2	NC
<i>Df(3R)Exel6274</i> (7741)	94E4; 94E11	NC
<i>Df(3R)Exel9012</i> (7990)	94E9; 94E13	NC
<i>Df(3R)Exel6194</i> (7673)	94F1; 95A4	NC
<i>Df(3R)Exel6195</i> (7674)	95A4; 95B1	SU (-)
<i>Df(3R)Exel9013</i> (7991)	95B1; 95B5	SU (-)
<i>Df(3R)Exel9014</i> (7992)	95B1; 95D1	NC
<i>Df(3R)Exel6196</i> (7675)	95C12; 95D8	NC
<i>Df(3R)Exel6197</i> (7676)	95D8; 95E1	EN (++)
<i>Df(3R)ED6187</i> (9347)	95D10; 96A7	EN (++)
<i>Df(3R)crb87-5</i> (2363)	95F7; 96A17-18	EN (+)
<i>Df(3R)ED6220</i> (9211)	96A7; 96C3	NC
<i>Df(3R)Exel6202</i> (7681)	96D1; 96D1	EN (++)
<i>Df(3R)BSC522</i> (25050)	96D1; 96E3	EN (++)
<i>Df(3R)Exel6203</i> (7682)	96E2; 96E6	NC
<i>Df(3R)BSC140</i> (9500)	96F1; 96F10	NC
<i>Df(3R)Exel6204</i> (7683)	96F9; 97A6	NC
<i>Df(3R)ED6232</i> (8105)	96F10; 97D2	NC
<i>Df(3R)ED6255</i> (9210)	97D2; 97F1	NC

<i>Df(3R)ED6265</i> (8960)	97E2; 98A7	NC
<i>Df(3R)IR16</i> (9529)	97F1-2; 98A	NC
<i>Df(3R)BSC42</i> (7412)	98B1-2; 98B3-5	NC
<i>Df(3R)Exel6259</i> (7726)	98C4; 98D6	NC
<i>Df(3R)Exel6209</i> (7687)	98D6; 98E1	NC
<i>Df(3R)Exel6210</i> (7688)	98E1; 98F5	EN (+)
<i>Df(3R)Exel6211</i> (7689)	98F5; 98F6	NC
<i>Df(3R)3450</i> (430)	98E3; 99A6-8	EN (+)
<i>Df(3R)ED6310</i> (8961)	98F12; 99B2	EN (+)
<i>Df(3R)ED6316</i> (8925)	99A5; 99C1	EN (+)
<i>Df(3R)BSC547</i> (25075)	99B5; 99C2	NC
<i>Df(3R)Exel6213</i> (7691)	99C5; 99D1	NC
<i>Df(3R)B81</i> (3546)	99D3; 3Rt	NC
<i>Df(3R)Exel6214</i> (7692)	99D5; 99E2	NC
<i>Df(3R)Exel6215</i> (7693)	99F6-7; 99F8	EN (+)
<i>Df(3R)Exel7378</i> (7997)	99F8; 100A5	NC
<i>Df(3R)Exel8194</i> (7918)	100A4; 100A7	NC
<i>Df(3R)Exel7379</i> (7919)	100B2; 100B5-8	NC
<i>Df(3R)Exel6218</i> (7696)	100B5; 100C1	NC

Table D.5: Duplications Located On The 2nd Chromosome

Duplication Name (Stock)	Cytology	Interaction (SU, EN, NR)*
<i>Dp(2;2)Cam1</i> (3392)	21E2; 23D1-2	NC
<i>Dp(2;2)Cam2</i> (3394)	23D1-2; 26C1-2	EN (++)
<i>Dp(2;2)Cam3a</i> (8539)	26C; 27D	NC
<i>Dp(2;2)Cam3</i> (3401)	26C1-2; 29F	NC
<i>Dp(2;2)Cam3c</i> (8541)	27C; 27F	EN (+)
<i>Dp(2;2)Cam3b</i> (8540)	27F; 29F	NC
<i>Dp(2;2)Cam4</i> (3403)	29F; 32F	NC
<i>Dp(2;2)Cam5</i> (4521)	32E; 35B	NC
<i>Dp(2;2)Cam6</i> (4518)	35B; 36C	SU (-)
<i>Dp(2;2)Cam8</i> (2630)	36C; 40	NC
<i>Dp(2;2)Cam10</i> (4520)	41; 43B	NC
<i>Dp(2;2)Cam11</i> (2626)	43B3-C1; 47B10-14	SU (-)
<i>Dp(2;2)Cam13</i> (3391)	47B10-14; 48C6-8	NC
<i>Dp(2;2)Cam14T</i> (4519)	49A; 51EF	EN (++)
<i>Dp(2;2)Cam12a</i> (8542)	51F11-12; 52D5	NC
<i>Dp(2;2)Cam17</i> (4744)	52D10-E1; 53F	NC
<i>Dp(2;2)Cam18</i> (4745)	53F1-4; 57C4-6	NC
<i>Dp(2;2)Cam16</i> (2622)	57C4-6; 60E4	NC

* All duplications were classified based on the criteria from Table 4.1. E (+) = Moderate Enhancer that is semi-lethal; E (++) = Strong Enhancer that is lethal; Su (-) = Moderate Suppressor; Su (--) = Strong Suppressor; UM = Undefined Modifier; NC = No Change.

Table D.6: Duplications Located On The 3rd Chromosome

Duplication Name (Stock)	Cytology	Interaction (SU, EN, NR)*
<i>Dp(3;3)Cam31</i> (5743)	61F7-8; 64B10-12	UM
<i>Dp(3;3)Cam32</i> (5744)	64B10-12; 64E5-9	NC
<i>Dp(3;3)Cam34</i> (8543)	65C5-9; 67C5-11	NC
<i>Dp(3;3)Cam35</i> (5745)	67C5-11; 69A4-5	EN (++)
<i>Dp(3;3)Cam36</i> (5746)	69A4-5; 70F1-2	NC
<i>Dp(3;3)Cam37</i> (5747)	70F1-2; 73C3-D7	NC
<i>Dp(3;3)Cam30T</i> (5742)	90C; 93C	NC

* All duplications were classified based on the criteria from Table 4.1. E (+) = Moderate Enhancer that is semi-lethal; E (++) = Strong Enhancer that is lethal; Su (-) = Moderate Suppressor; Su (--) = Strong Suppressor; UM = Undefined Modifier; NC = No Change.

Appendix E. Letters of Copyright Permission

Appendix E. Letters of Copyright Permission

Dear, Dr. Daniel J. Klionsky

My name is Stephanie McMillan, and I am an author on a paper that has recently been published in *Autophagy*. As I am currently finishing my Masters, I would like to ask permission to publish some of the data from this paper, in particular the lysotracker data, in my Masters thesis. The reference from the paper is as follows:

Mohseni, N., McMillan, S.C., Chaudhary, R., Mok, J., Reed, B.H., 2009. Autophagy Promotes Caspase-Dependent Cell Death during *Drosophila* Development. *Autophagy* 5, 329-338.

Stephanie McMillan

Stephanie,

You have permission to publish these data. You simply need to cite the original article.

Dan

Dear, Dr. Daniel Klionsky,

Hello, my name is Stephanie McMillan, and I am an author on a paper that has recently been published in *Autophagy*. Recently I requested permission to publish some of my data (that has also been published in *Autophagy*) in my Masters thesis. Although I have received permission in the past, the journal should also be informed that I am signing a Theses Non-Exclusive License to publish my thesis in "Library and Archives Canada". Also, I must receive written acknowledgement from the editor that I have permission to do this.

Thank you for your time.

Stephanie McMillan

Dear Stephanie,

You have permission to publish your thesis containing the article from Autophagy in "Library and Archives Canada".

Sincerely,

Dan Klionsky

Editor-in-Chief

References

- Affolter, M., Marty, T., Vigano, M.A., Jazwinska, A., 2001. Nuclear Interpretation of Dpp Signaling in *Drosophila*. *EMBO J* 20, 3298-3305.
- Agnes, F., Suzanne, M., Noselli, S., 1999. The *Drosophila* JNK Pathway Controls the Morphogenesis of Imaginal Discs during Metamorphosis. *Development* 126, 5453-5462.
- Ahmed, Y., Hayashi, S., Levine, A., Wieschaus, E., 1998. Regulation of Armadillo by a *Drosophila* APC Inhibits Neuronal Apoptosis during Retinal Development. *Cell* 93, 1171-1182.
- Alberts, B., Johnson, A., Lewis, J., Raff, M., Roberts, K., Walter, P., 2008. *Molecular Biology of The Cell*. Fifth Ed. Garland Science. New York, NY. USA. 1115-1128.
- Armstrong, J.D., Edwards, C., Kaiser, K. (2006). Flytrap: The P[Gal4] enhancer-trap technique. October 4, 2006. <<http://www.flytrap.org/flytrap/html/docs/egal4.html>>
- Ashburner, M., 1989. *Drosophila: A Laboratory Handbook*. Cold Spring Laboratory Press. Cold Spring Harbour, NY. USA. 140, 187.
- Baehrecke, E.H., 2005. Autophagy: Dual Roles in Life and Death? *Nat Rev Mol Cell Biol* 6, 505-510.
- Bangs, P., Franc, N., White, K., 2000. Molecular Mechanisms of Cell Death and Phagocytosis in *Drosophila*. *Cell Death Differ* 7, 1027-1034.
- Bardet, P.L., Kolahgar, G., Mynett, A., Miguel-Aliaga, I., Briscoe, J., Meier, P., Vincent, J.P., 2008. A Fluorescent Reporter of Caspase Activity for Live Imaging. *Proc Natl Acad Sci U S A* 105, 13901-13905.
- Berry, D.L., Baehrecke, E.H., 2007. Growth Arrest and Autophagy are Required for Salivary Gland Cell Degradation in *Drosophila*. *Cell* 131, 1137-1148.
- Bloomington Stock Center, 2007. Bloomington Deficiency Kits. Indiana University, Bloomington, IN. USA. June 8, 2008. <http://flystocks.bio.indiana.edu/Browse/df-dp/dfextract.php?num=all&symbol=bloomdef>
- Clarke, P.G.H., *Developmental cell death: morphological diversity and multiple mechanisms*, *Anat. Embryol.* 181 (1990) 195-213.
- Debnath, J., Baehrecke, E.H., Kroemer, G., 2005. Does Autophagy Contribute to Cell Death? *Autophagy* 1, 66-74.
- Demerec, M., 1985. *Biology of Drosophila*. Harfner publishing company. New York. NY. USA. 276-283.

Drysdale, R.A., Crosby, M.A., FlyBase Consortium, 2005. FlyBase: Genes and Gene Models. *Nucleic Acids Res* 33, D390-5. April 14, 2008. (<http://flybase.bio.indiana.edu/>)

Franke, T.F., Hornik, C.P., Segev, L., Shostak, G.A. & Sugimoto, C. PI3K/Akt and apoptosis: size matters. *Oncogene* 22, 8983-8998 (2003).

Fristrom, D., Fristrom, J.W., 1993. The Development of *Drosophila melanogaster*: The Metamorphic Development of the Adult Epidermis. Cold Spring Harbour Laboratory Press. New York. 2. 843-897.

Gilbert, S.F., 2003. Developmental Biology. Seventh Edition. Sinauer Associates, Inc. Sunderland, Massachusetts. 585.

Hartwell, L., Hood, L., Goldberg, M., Reynolds, A., Silver, L., Veres, R., 2004. Genetics: From Genes to Genomes. 2nd Ed. New York: McGraw-Hill. 804-805.

Hou, Y.C., Chittaranjan, S., Barbosa, S.G., McCall, K., Gorski, S.M., 2008. Effector Caspase Dcp-1 and IAP Protein Bruce Regulate Starvation-Induced Autophagy during *Drosophila Melanogaster* Oogenesis. *J Cell Biol* 182, 1127-1139.

Jacinto, A., Martin, P., 2001. Morphogenesis: Unravelling the Cell Biology of Hole Closure. *Curr Biol* 11, R705-7.

Jacinto, A., Wood, W., Woolner, S., Hiley, C., Turner, L., Wilson, C., Martinez-Arias, A., Martin, P., 2002. Dynamic Analysis of Actin Cable Function during *Drosophila* Dorsal Closure. *Curr Biol* 12, 1245-1250.

Jiang, C., Baehrecke, E.H., Thummel, C.S., 1997. Steroid Regulated Programmed Cell Death during *Drosophila* Metamorphosis. *Development* 124, 4673-4683.

Jiang, Z., Wu, X.L., Michal, J.J., McNamara, J.P., 2005. Pattern Profiling and Mapping of the Fat Body Transcriptome in *Drosophila Melanogaster*. *Obes Res* 13, 1898-1904.

Johnson, S.A., Milner, M.J., 1990. Cuticle Secretion in *Drosophila* Wing Imaginal Discs in Vitro: Parameters of Exposure to 20-Hydroxy Ecdysone. *Int J Dev Biol* 34, 299-307.

Klionsky, D.J., 2007. Autophagy: From Phenomenology to Molecular Understanding in Less than a Decade. *Nat Rev Mol Cell Biol* 8, 931-937.

Klionsky, D.J., 2004. Cell Biology: Regulated Self-Cannibalism. *Nature* 431, 31-32.

Klionsky, D.J., Emr, S.D., 2000. Autophagy as a Regulated Pathway of Cellular Degradation. *Science* 290, 1717-1721.

- Kozlova, T., Thummel, C.S., 2003. Essential Roles for Ecdysone Signaling during *Drosophila* Mid-Embryonic Development. *Science* 301, 1911-1914.
- Lee, C.Y., Baehrecke, E.H., 2001. Steroid Regulation of Autophagic Programmed Cell Death during Development. *Development* 128, 1443-1455.
- Lee, C.Y., Baehrecke, E.H., 2000. Genetic Regulation of Programmed Cell Death in *Drosophila*. *Cell Res* 10, 193-204.
- Levine, B., Yuan, J., 2005. Autophagy in Cell Death: An Innocent Convict? *J Clin Invest* 115, 2679-2688.
- Levine, B., Klionsky, D.J., 2004. Development by Self-Digestion: Molecular Mechanisms and Biological Functions of Autophagy. *Dev Cell* 6, 463-477.
- Lockshin, R.A., Zakeri, Z., 2004. Apoptosis, Autophagy, and More. *Int J Biochem Cell Biol* 36, 2405-2419.
- Lum, J.J., DeBerardinis, R.J., Thompson, C.B., 2005. Autophagy in Metazoans: Cell Survival in the Land of Plenty. *Nat Rev Mol Cell Biol* 6, 439-448.
- Luo, X., Puig, O., Hyun, J., Bohmann, D., Jasper, H., 2007. Foxo and Fos Regulate the Decision between Cell Death and Survival in Response to UV Irradiation. *EMBO J* 26, 380-390.
- Madhavan, M.M., Madhavan, K., 1980. Morphogenesis of the Epidermis of Adult Abdomen of *Drosophila*. *J Embryol Exp Morphol* 60, 1-31.
- Martin, D.N., Baehrecke, E.H., 2004. Caspases Function in Autophagic Programmed Cell Death in *Drosophila*. *Development* 131, 275-284.
- McGuire, S.E., Le, P.T., Osborn, A.J., Matsumoto, K., Davis, R.L., 2003. Spatiotemporal Rescue of Memory Dysfunction in *Drosophila*. *Science* 302, 1765-1768.
- McPhee, C.K., Baehrecke, E.H., 2009. Autophagy in *Drosophila Melanogaster*. *Biochim Biophys Acta* .
- Mélendez, A., Neufeld, T.P., 2008. The Cell Biology of Autophagy in Metazoans: A Developing Story. *Development* 135, 2347-2360.
- Mohseni, N., McMillan, S.C., Chaudhary, R., Mok, J., Reed, B.H., 2009. Autophagy Promotes Caspase-Dependent Cell Death during *Drosophila* Development. *Autophagy* 5, 329-338.
- Neufeld, T.P., Baehrecke, E.H., 2008. Eating on the Fly: Function and Regulation of Autophagy during Cell Growth, Survival and Death in *Drosophila*. *Autophagy* 4, .

Neufeld, T.P., 2007. Contribution of Atg1-Dependent Autophagy to TOR-Mediated Cell Growth and Survival. *Autophagy* 3, 477-479.

Nezis, I.P., Lamark, T., Velentzas, A.D., Rusten, T.E., Bjorkoy, G., Johansen, T., Papassideri, I.S., Stravopodis, D.J., Margaritis, L.H., Stenmark, H., Brech, A., 2009. Cell Death during *Drosophila Melanogaster* Early Oogenesis is Mediated through Autophagy. *Autophagy* 5, 298-302.

Ninov, N., Chiarelli, D.A., Martin-Blanco, E., 2007. Extrinsic and Intrinsic Mechanisms Directing Epithelial Cell Sheet Replacement during *Drosophila* Metamorphosis. *Development* 134, 367-379.

Pattingre, S., Espert, L., Biard-Piechaczyk, M., Codogno, P., 2008. Regulation of Macroautophagy by mTOR and Beclin 1 Complexes. *Biochimie* 90, 313-323.

Peña-Rangel, M.T., Rodriguez, I., Riesgo-Escovar, J.R., 2002. A Misexpression Study Examining Dorsal Thorax Formation in *Drosophila Melanogaster*. *Genetics* 160, 1035-1050.

Pérez-Garijo, A., Martin, F.A., Morata, G., 2004. Caspase Inhibition during Apoptosis Causes Abnormal Signalling and Developmental Aberrations in *Drosophila*. *Development* 131, 5591-5598

Purves, D.C., Brachmann, C., 2007. Dissection of Imaginal Discs from 3rd Instar *Drosophila* Larvae. *J Vis Exp* (2), 140.

Reed, B.H., McMillan, S.C., Chaudhary, R., 2009. The Preparation of *Drosophila* Embryos for Live-Imaging using the Hanging Drop Protocol. *J Vis Exp* (25). pii: 1206. doi, 10.3791/1206.

Reed, B.H., Wilk, R., Schock, F., Lipshitz, H.D., 2004. Integrin-Dependent Apposition of *Drosophila* Extraembryonic Membranes Promotes Morphogenesis and Prevents Anoikis. *Curr Biol* 14, 372-380.

Reggiori, F., Shintani, T., Nair, U., Klionsky, D.J., 2005. Atg9 Cycles between Mitochondria and the Pre-Autophagosomal Structure in Yeasts. *Autophagy* 1, 101-109.

Rusten, T.E., Lindmo, K., Juhasz, G., Sass, M., Seglen, P.O., Brech, A., Stenmark, H., 2004. Programmed Autophagy in the *Drosophila* Fat Body is Induced by Ecdysone through Regulation of the PI3K Pathway. *Dev Cell* 7, 179-192.

Sarkar, S., Krishna, G., Imarisio, S., Saiki, S., O'Kane, C.J., Rubinsztein, D.C., 2008. A Rational Mechanism for Combination Treatment of Huntington's Disease using Lithium and Rapamycin. *Hum Mol Genet* 17, 170-178.

Scott, R.C., Juhasz, G., Neufeld, T.P., 2007. Direct Induction of Autophagy by Atg1 Inhibits Cell Growth and Induces Apoptotic Cell Death. *Curr Biol* 17, 1-11.

Shimizu, S., Kanaseki, T., Mizushima, N., Mizuta, T., Arakawa-Kobayashi, S., Thompson, C.B., Tsujimoto, Y., 2004. Role of Bcl-2 Family Proteins in a Non-Apoptotic Programmed Cell Death Dependent on Autophagy Genes. *Nat Cell Biol* 6, 1221-1228.

Stephan, J.S., Herman, P.K., 2006. The Regulation of Autophagy in Eukaryotic Cells: Do all Roads Pass through Atg1? *Autophagy* 2, 146-148.

Su, H., Yang, J.R., Xu, T., Huang, J., Xu, L., Yuan, Y., Zhuang, S.M., 2009. MicroRNA-101, Down-Regulated in Hepatocellular Carcinoma, Promotes Apoptosis and Suppresses Tumorigenicity. *Cancer Res* 69, 1135-1142.

Tschopp, J., Thome, M., Hofmann, K., Meinel, E., 1998. The Fight of Viruses Against Apoptosis. *Curr Opin Genet Dev* 8, 82-87.

Tsujimoto, Y., Shimizu, S., 2005. Another Way to Die: Autophagic Programmed Cell Death. *Cell Death Differ* 12 Suppl 2, 1528-1534.

Van Cruchten, S., and Van Den Broeck, W. , 2002. Morphological and biochemical aspects of apoptosis, oncosis and necrosis. *Anat. Histol. Embryol.* 4, 214-223.

Vellai, T., Bicsak, B., Toth, M.L., Takacs-Vellai, K., Kovacs, A.L., 2008. Regulation of Cell Growth by Autophagy. *Autophagy* 4, 507-509

White, K., Grether, M.E., Abrams, J.M., Young, L., Farrell, K., Steller, H., 1994. Genetic Control of Programmed Cell Death in *Drosophila*. *Science* 264, 677-683.

Wieschaus, E., and Nüsslein-Volhard., 1986. Looking At Embryos. In *Drosophila: A Practical Approach* (ed. D.B. Roberts), pp 199-228. IRL Press, Washing DC.

Wieschaus, E., Sweeton, D., and M. Costa. 1991 Convergence and extension during germ band elongation in *Drosophila* embryos. In *Gastrulations: Movements, patterns, and molecules* (ed. R. Keller *et al.*), pp.213-223. Plenum Press, New York.

Yin, V.P., Thummel, C.S., 2004. A Balance between the diap1 Death Inhibitor and Reaper and Hid Death Inducers Controls Steroid-Triggered Cell Death in *Drosophila*. *Proc Natl Acad Sci U S A* 101, 8022-8027.

Yu, L., Alva, A., Su, H., Dutt, P., Freundt, E., Welsh, S., Baehrecke, E.H., Lenardo, M.J., 2004. Regulation of an ATG7-Beclin 1 Program of Autophagic Cell Death by Caspase-8. *Science* 304, 1500-1502.

Zeitlinger, J., Bohmann, D., 1999. Thorax Closure in *Drosophila*: Involvement of Fos and the JNK Pathway. *Development* 126, 3947-3956.